

216  
11-25-79

DR. 2482

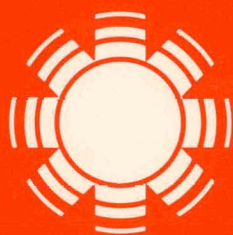
SERI/TR-32-150

February 1979

# Photovoltaics Research Annual Report - FY78

## For Period October 1, 1977 - September 30, 1978

L.L. Kazmerski



# SERI

**Solar Energy Research Institute**

A Division of Midwest Research Institute

1536 Cole Boulevard  
Golden, Colorado 80401

Operated for the  
**U.S. Department of Energy**  
under Contract No. EG-77-C-01-4042



**MASTER**

## DISCLAIMER

**This report was prepared as an account of work sponsored by an agency of the United States Government. Neither the United States Government nor any agency Thereof, nor any of their employees, makes any warranty, express or implied, or assumes any legal liability or responsibility for the accuracy, completeness, or usefulness of any information, apparatus, product, or process disclosed, or represents that its use would not infringe privately owned rights. Reference herein to any specific commercial product, process, or service by trade name, trademark, manufacturer, or otherwise does not necessarily constitute or imply its endorsement, recommendation, or favoring by the United States Government or any agency thereof. The views and opinions of authors expressed herein do not necessarily state or reflect those of the United States Government or any agency thereof.**

## **DISCLAIMER**

**Portions of this document may be illegible in electronic image products. Images are produced from the best available original document.**

Printed in the United States of America  
Available from:  
National Technical Information Service  
U.S. Department of Commerce  
5285 Port Royal Road  
Springfield, VA 22161  
Price:  
Microfiche \$3.00  
Printed Copy \$5.25 8, 2

#### NOTICE

This report was prepared as an account of work sponsored by the United States Government. Neither the United States nor the United States Department of Energy, nor any of their employees, nor any of their contractors, subcontractors, or their employees, makes any warranty, express or implied, or assumes any legal liability or responsibility for the accuracy, completeness or usefulness of any information, apparatus, product or process disclosed, or represents that its use would not infringe privately owned rights.

SERI/TR-32-150  
UC CATEGORY: UC-63

PHOTOVOLTAICS RESEARCH  
ANNUAL REPORT - FY78

(TASK 3210)

FOR PERIOD  
OCTOBER 1, 1977- SEPTEMBER 30, 1978

L. L. KAZMERSKI

FEBRUARY 1979

NOTICE

This report was prepared as an account of work sponsored by the United States Government. Neither the United States nor the United States Department of Energy, nor any of their employees, nor any of their contractors, subcontractors, or their employees, makes any warranty, express or implied, or assumes any legal liability or responsibility for the accuracy, completeness or usefulness of any information, apparatus, product or process disclosed, or represents that its use would not infringe privately owned rights.


**Solar Energy Research Institute**

1536 Cole Boulevard  
Golden, Colorado 80401

A Division of Midwest Research Institute

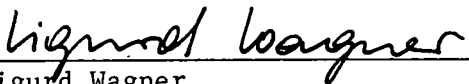
Prepared for the  
U.S. Department of Energy  
Contract No. EG-77-C-01-4042

**DISTRIBUTION OF THIS DOCUMENT IS UNLIMITED**



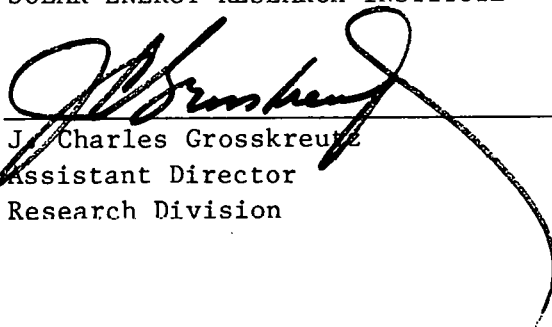
## FOREWORD

This document summarizes the SERI Photovoltaics Branch research efforts performed under SERI Task 3210 during fiscal year 1978. The SERI Photovoltaics Research and Development Program is a major portion of the Photovoltaics Branch Program Plan. It has as its long term objectives significant contributions to: (1) the development and demonstration of intermediate efficiency (greater than 10%) amorphous or polycrystalline thin-film solar cells; and, (2) the development and demonstration of high efficiency (greater than 30%) photovoltaic devices. These have been identified as major high-risk, high-payoff research areas that can provide significant contributions to the overall goal of the National Photovoltaics Program - the establishment of technical and economic feasibility of photovoltaic systems.

  
\_\_\_\_\_  
Sigurd Wagner  
Branch Chief, Photovoltaics Branch  
Principal Investigator

Approved for:

SOLAR ENERGY RESEARCH INSTITUTE

  
\_\_\_\_\_  
J. Charles Grosskreutz  
Assistant Director  
Research Division

## TABLE OF CONTENTS

	<u>Page</u>
Foreword.....	ii
Summary.....	1
1.0 Introduction and Task Objectives.....	3
2.0 Research Staff and Activities - FY78.....	5
2.1 Solid State and Device Theory.....	5
2.2 Amorphous Semiconductors.....	5
2.3 Silicon Crystallization and Growth.....	6
2.4 Silicon Purification and Characterization.....	6
2.5 Ellipsometry Studies of Multicrystalline Silicon.....	7
2.6 Photovoltaic Surfaces and Interfaces.....	7
2.7 Spectral Irradiance: Photovoltaic Applications.....	8
2.8 Measurement Development.....	8
2.9 Molecular Beam Epitaxy.....	8
3.0 Anthology of SERI Photovoltaic Publications - FY78.....	11
3.1 Grain Boundary and Interdiffusion Studies in Compound Semiconductor Thin Films and Devices Utilizing AES and SIMS.....	12
3.2 Auger Electron Spectroscopy Studies of I-III-VI <sub>2</sub> Chalcopyrite Compounds.....	25
3.3 The Effects of Grain Boundary and Interface Recombina- tion on the Performance of Thin-Film Solar Cells.....	37
3.4 The Performance of Copper-Ternary Based Thin-Film Solar Cells.....	55
3.5 Fabrication and Characterization of ITO/CuInSe <sub>2</sub> Photovoltaic Heterojunctions.....	67
3.6 Effects of Grain Boundaries on the Performance of Thin-Film Photovoltaic Devices.....	79
3.7 Attainable Efficiencies with Thin-Film Heterojunction Solar Cells.....	89
3.8 Stability and Ternary Chalcopyrite Photovoltaic Devices.....	91
3.9 Interdiffusion and Interface Problems Relating to Thin-Film Photovoltaic Devices.....	107
3.10 Report on the Stability of CdS and Amorphous Based Thin Film Solar Cells.....	127
3.11 Growth of CuInSe <sub>2</sub> on CdS Using Molecular Beam Epitaxy.....	137
3.12 Absorption Coefficient Measurements for Vacuum - Deposited Cu-Ternary Thin Films.....	141
3.13 A Combined Irradiance - Transmittance Solar Spectrum and Its Application to Photovoltaic Efficiency Calculations.....	143

**TABLE OF CONTENTS (continued)**

	<u>Page</u>
4.0 Conference Presentations.....	159
Appendix A Staff Summary.....	A1
Appendix B FY78 Contracted Facilities/Research.....	B1



## SUMMARY

SERI Photovoltaics Task 3210, "Photovoltaics Research" was initiated as a part of the Fiscal Year 1978 Annual Operating Plan. This task covers the research activities which form a major portion of the Photovoltaics Branch Program Plan. The objectives include contributions to: (1) the development and demonstration of intermediate efficiency (greater than 10%) amorphous or polycrystalline thin-film solar cells; and, (2) the development and demonstration of high efficiency (greater than 30%) photovoltaic devices. Nine program areas have been identified both as integral parts of the FY78 research plan for Task 3210 and as a basis for building FY79 and subsequent research programs. These areas include:

- solid-state and device theory,
- very high efficiency cells (e.g., III-V, single crystal semiconductor devices),
- intermediate efficiency thin-film cells (e.g., amorphous silicon devices),
- silicon purification,
- silicon crystallization,
- device processing,
- advanced II-VI technologies (e.g., spray and paste techniques);
- surface and interface analysis, and
- measurement development.

Due to delays in staffing, on-site laboratory completion and capital equipment acquisition, research activities could not be initiated in all nine of these areas during FY78. While research planning and experiment design were undertaken for all nine of these areas, surface and interface analysis, silicon crystallization and characterization, and measurement development provided the primary results during FY78.

Accomplishments included:

- growth of the first ternary semiconductor by molecular beam epitaxy (MBE) and the fabrication of the first MBE  $\text{CuInSe}_2/\text{CdS}$  heterodiode for photovoltaic investigations;
- development of an accurate solar spectrum (SOLTRAN) for photovoltaic applications and dissemination to DOE Advanced R&D contractors;
- modeling of polycrystalline heterojunction solar cells, emphasizing grain boundary and interface mechanisms;
- prediction of heterojunction and multijunction solar cell performance based upon SOLTRAN;

- characterization of semiconductor thin films on conductive substrates;
- AES/SIMS evaluation of impurity segregation in multicrystalline silicon;
- AES/SIMS investigation of interdiffusion, especially grain boundary diffusion, in Cu-ternary thin-film solar cells; and
- acoustic microscopy studies of multigrained silicon.

Overall during FY78, Task 3210 provided the basis for the future branch research by initiating research efforts which were defined and identified in other branch tasks; coordinating research activities with the SERI in-house (interim) laboratory design and development; and identifying feasible cooperative and contractual research efforts with local or other laboratory facilities. Descriptions and the status of those photovoltaics research areas which have been activated under SERI Task 3210 during FY78 are summarized in this report. Also included is an anthology of scientific publications and presentations which resulted as a part of that task effort. It should be stressed that for SERI and for the Photovoltaics Branch, FY78 was marked as a period of growth, program definition, and facility design. Therefore, this report encompasses results which have been produced in that environment rather than emerging from full-scale R&D activity.

## SECTION 1.0

### INTRODUCTION AND TASK OBJECTIVES

The SERI Photovoltaics Program is a multiyear effort which encompasses several complementary activities, each of which is designed to contribute to the overall objective of the National Photovoltaic Program. That is, its intention is to establish technical and economic feasibility of photovoltaic systems. Major among the SERI activities is the in-house research and development effort which has as its long-term objectives significant contributions to: (1) the development and demonstration of intermediate efficiency (greater than 10%) amorphous or polycrystalline thin-film solar cells; and (2) the development and demonstration of high efficiency (greater than 30%) photovoltaic devices. In each of these cases, establishment of device stability and reliability are equally important.

Several R&D efforts directed toward the long-range objectives were initiated in the FY78 period. Specifically, the SERI Photovoltaics Task 3210, "Photovoltaics Research", was introduced on January 3, 1978, as part of the FY78 AOP. The objectives of this task included:

- Photovoltaic Program Assessment and Research Plan (3202); Monitoring of DOE Photovoltaics Research Efforts (3203); Photovoltaic Manufacturing Technology Assessment (3204); and Critical Status Review (3206).
- Coordination of research activities with the SERI in-house (interim) laboratory design and development.
- Identification and initiation of feasible, cooperative, and contractual research efforts with local or other critical facilities.

Nine program areas have been identified as both integral parts of the FY78 R&D plan for Task 3210 and as a basis for FY79 and subsequent research programs. These areas include:

- solid-state and device theory;
- very high efficiency cells (e.g., III-V, single crystal semiconductor devices);
- intermediate efficiency thin-film cells (e.g., amorphous silicon devices);
- silicon purification;
- silicon crystallization;
- device processing;
- advanced II-VI technologies (e.g., spray and paste techniques);
- surface and interface analysis; and
- measurement development.

Three major problems inhibited the progress and/or initiation of R&D efforts in all nine of these areas, most of which are highly experimental. First, staffing and research program definition were delayed until the Photovoltaics Branch Chief reported on February 1, 1978. As a result, the majority of the Photovoltaics Branch senior staff joined SERI after May 1978. (See Appendix A for a summary). Second, a freeze in capital research equipment expenditures was imposed in April 1978. Some capital items were later ordered, but not until late summer. Third, several delays and uncertainties were experienced in completion of the on-site laboratory. Although the laboratory was originally to be ready in early summer, a FY79 occupation date was finally determined. The uncertainty in laboratory readiness also affected the start of some projects in leased or contracted area facilities. A listing of contracted facilities and cooperative research programs is given in Appendix B.

## SECTION 2.0

## RESEARCH STAFF AND ACTIVITIES - FY78

The FY78 research staff of the Photovoltaics Branch reached five senior level personnel (including the Branch Chief), one staff scientist, four associate scientists, one faculty associate/consultant, and two research associates (coop students). The staff and their starting dates are listed in Appendix A. This section summarizes the research, activities, and associated photovoltaic staff relating to this FY78 task.

## 2.1 SOLID STATE AND DEVICE THEORY (A. Zunger)

The major problem addressed has been the definition and application of first principle pseudopotentials to selected photovoltaic material and device problems. As both empirical and semiempirical atomic pseudopotentials have previously proved to provide a simple and accurate method of describing electronic properties of semiconducting materials, the extension and expansion of the theoretical understanding of these two photovoltaic applications have been started.

Investigative areas initiated:

- new methods of pseudopotential construction directly from the density functional one-particle equation (i.e., nonempirical-based approach);
- phase separation predictions for binary alloys; and
- theoretical investigation of Schottky-barrier formation in III-V semiconductors.

## 2.2 AMORPHOUS SEMICONDUCTORS (R. C. Kerns)

The future development of the amorphous silicon (i.e., hydrogenated amorphous silicon) solar cell depends upon the better understanding and documentation of the basic electronic and optical properties of the material itself. Research is underway on the structure and basic properties of amorphous semiconductors. In particular, research plans have been formulated for the application of very sensitive spectroscopic techniques to the identification of the local chemical and structural environment of plasma discharge-grown amorphous silicon.

Investigative areas initiated:

- initial design of chemical vapor decomposition system for depositing hydrogenated amorphous silicon; and

- preliminary design of electron nuclear resonance experiments to identify unpaired electrons.

### 2.3 SILICON CRYSTALLIZATION AND GROWTH (T. Cizek, J. Hurd)

This program focuses on one major problem that is limiting the deployment of silicon solar cells - the relatively high cost of producing quality silicon substrates. Several crystallization techniques are being investigated (ribbon, directional solidification, etc.) for both single crystal and multigrained silicon production. Crystallographic studies of multigrained material have been started. A primary goal of this work is to achieve crystallization techniques that are simple, continuous, and low-cost while retaining adequate photovoltaic characteristics.

Investigative areas initiated:

- design and fabrication of temporary growth apparatus;
- preliminary experimental research at Colorado School of Mines;
- acoustic microscopy studies of multigrained silicon (with Stanford University);
- meniscus height calculations for silicon ribbon growth; and
- identification of cooperative efforts for solar cell processing on experimental silicon material.

### 2.4 SILICON PURIFICATION AND CHARACTERIZATION (J. Olson, N. Meyer)

The initial emphasis of this program has been directed toward two areas: (1) the investigation of the reduction - purification process compared to current silicon purification schemes with the goals of studying the practical limitations of the process and to develop a kinetic model of the growth process itself; and (2) the fabrication and characterization of Schottky barrier devices, based on multigrained silicon substrates (in cooperation with T. Cizek) in order to determine the effects of impurities and defects on the electrical characteristics of these devices.

Investigative areas initiated:

- initial design of reduction - purification apparatus;
- fabrication of multigrained silicon Schottky barrier devices (at the University of Colorado);
- design of deep-level transient spectroscopy experiments; and
- modeling of reduction processes.

## 2.5 ELLIPSOMETRY STUDIES OF MULTICRYSTALLINE SILICON (S. Wagner, D. Burleigh†)

A study of the differences in oxides which grow on multi versus single crystal silicon was undertaken. Both native oxides and those grown by the wet process were investigated using ellipsometry techniques. These studies have important implications for device processing and MIS structure device production.

Investigative areas initiated:

- studies of effects of surface roughness; and
- determination of oxide growth differences on multicrystalline substrates.

## 2.6 PHOTOVOLTAIC SURFACES AND INTERFACES (L. L. Kazmerski, P. J. Ireland, P. Sheldon††)

The program has been directed toward two areas: (1) Interrelationships between surfaces, interfaces, and the performance of solar cells. This includes the effects of grain boundaries (including effects on transport properties of thin films, recombination, carrier lifetime, passivation, and the correlation of those parameters with device performance); interfaces (especially heterodiodes), and surfaces (scattering theory, impurity segregation); and (2) Structural/chemical/compositional characteristics, including the application of surface analysis techniques (Auger electron spectroscopy-AES, secondary ion mass spectroscopy-SIMS) to interdiffusion, grain boundary diffusion, chemical reactions, impurity diagnosis, and impurity segregation.

Investigative areas initiated:

- modeling of polycrystalline CdS heterodiodes ( $\text{CuInSe}_2$ ,  $\text{CuInS}_2$ , InP) and solar cells;
- AES/SIMS investigation of interdiffusion, especially grain boundary diffusion, in Cu-ternary thin-film solar cells; and
- AES/SIMS analysis of impurity segregation in multicrystalline silicon.

---

†Summer research associate

††Coop Research Associate

## 2.7 SPECTRAL IRRADIANCE: PHOTOVOLTAIC APPLICATIONS (P. J. Ireland, S. Wagner, L. L. Kazmerski, and R. J. Hulstrom†)

A reliable, accurate solar spectrum has been developed as a joint effort between the SERI Photovoltaics and Resource Assessment Branches. This spectral irradiance program, called SOLTRAN, is capable of providing spectra under a variety of air mass and aerosol conditions. It has been made available to all DOE photovoltaics advanced materials contractors and has demonstrated usefulness in predicting the performances of single heterodiodes and multijunction devices.

Investigative areas initiated:

- development of SOLTRAN and dissemination to contractors;
- prediction of performances of heterojunction and multijunction solar cells based upon SOLTRAN; and
- incorporation of SOLTRAN into the highly accurate quantum efficiency spectrometer.

## 2.8 MEASUREMENT DEVELOPMENT (S. Hogan, S. Wagner, F. Barnes,†† P. Sheldon, T. Cizek, J. Olson, and L. L. Kazmerski)

The development of special measurement techniques which are important to both the in-house R&D effort and to eventual utilization in the National Measurement Facility have been initiated. These measurements relate to material properties and device characterization.

Techniques:

- quantum efficiency spectroscopy using SOLTRAN;
- characterization of semiconductor thin films on conductive substrates (in cooperation with the University of Colorado); and
- deep level transient spectroscopy (DLTS) of polycrystalline layers.

## 2.9 MOLECULAR BEAM EPITAXY (L. L. Kazmerski, in cooperation with the University of Maine)

Molecular beam epitaxy (MBE) has been utilized to fabricate single crystal  $\text{CuInSe}_2/\text{CdS}$  heterodiodes. This method of film growth, which essentially

---

†Resource Assessment Branch

††Summer Faculty Associate/Consultant



deposits a single layer of atoms at a time, is a highly sensitive and controllable technique to produce optimum layers. The fabrication system has been developed at the University of Maine due to the unavailability of laboratory space at SERI. This joint effort has led to the growth of the first ternary film by MBE. The work will continue on a contract basis in FY79.

Major Results:

- growth of first true ternary thin film by MBE; and
- fabrication of first  $\text{CuInSe}_2/\text{CdS}$  heterodiode (single crystal) by MBE.

THIS PAGE INTENTIONALLY LEFT BLANK

**SECTION 3.0****ANTHOLOGY OF SERI PHOTOVOLTAICS PUBLICATIONS-FY78**

For SERI and the Photovoltaics Branch, FY78 was marked as a period of growth, program definition, and facility design rather than a period of full-scale R&D activity. Thus, the formal research reported in this section reflects those efforts initiated early in Task 3210. The collection of articles contained herein either have appeared or have been accepted for publication in the refereed scientific literature and/or have resulted from presentations at scientific meetings.

Because SERI's laboratory facility was not operational in FY78, these publications are the result of in-house modeling studies or experimental efforts conducted at other laboratories by SERI staff. They primarily concern activities in the surfaces and interfaces, device modeling, and solar irradiance areas which had research staff available early in FY78.

### 3.1 GRAIN BOUNDARY AND INTERDIFFUSION STUDIES IN COMPOUND SEMICONDUCTOR THIN FILM AND DEVICES UTILIZING AES AND SIMS

SERI AUTHOR: L. L. Kazmerski

JOURNAL: Thin Solid Films (To appear)

CONFERENCE: 4th International Thin Films Congress  
Loughborough, UK  
September 11-15, 1978

#### ABSTRACT

Interdiffusion problems in polycrystalline thin film and thin-film heterojunctions are investigated. Depth-compositional profiling using Auger electron spectroscopy (AES) and secondary ion mass spectroscopy (SIMS) is employed to determine both grain boundary diffusion and interdiffusion coefficients in thin films and devices involving CdS, CuInSe<sub>2</sub> and CuInS<sub>2</sub>. Specifically, the temperature dependencies of the diffusion coefficients of Cd from CdS and from elemental films into the Cu-ternaries are experimentally determined. The effects of grain boundary type and the effects of these diffusion processes on thin-film device stability are discussed.

### 3.1.1 Introduction

Solar conversion efficiency inevitably receives the primary attention in photovoltaic device research. Initially, the demonstration of a high-efficiency solar cell is mandatory since it is a justification that the particular device is worthy of some further investigation. However, an equally important factor which eventually determines deployment and must be addressed in the development phase is that of device stability. This is particularly true in the case of the thin-film solar cell which has both its performance and potential lifetime complicated by its inherent structural features, especially grain boundaries and interfaces. Thin films and thin-film devices have large surface-to-volume ratios and, as a result, possess characteristics which are greatly surface and interface dependent. As a result, the problem of interdiffusion is a dominant degradation mechanism for such devices. In the case of photovoltaics, this mechanism is not only enhanced owing to structural features (grain boundaries, dislocations, etc.) but is accelerated due to environmental effects including intense and changing illumination, varying electrical and thermal stresses, elevated temperatures, and, in fact, the ensemble of processing steps encountered in device fabrication. This paper examines the interdiffusion problem in thin-film polycrystalline heterojunctions, emphasizing important grain boundary contributions to this phenomenon.

Interdiffusion mechanisms have been indicated in several device types.<sup>1-6</sup> In the present study, depth-compositional profiling using Auger electron spectroscopy (AES) and secondary ion mass spectroscopy (SIMS) are employed to investigate the interdiffusion mechanisms in  $\text{CuInSe}_2$  and  $\text{CuInSe}_2$  films and heterodiodes with CdS. Specifically, the temperature dependence of the bulk and grain boundary diffusion coefficients of Cd, from both CdS and elemental sources, into the Cu-ternaries are experimentally determined and compared using these surface analysis techniques.

### 3.1.2 Experimental Details

The Cu-ternary thin films for the AES studies were grown by the two-source technique reported previously.<sup>7</sup> Grain sizes were  $0.8\text{-}1.2\ \mu\text{m}$  for the  $\text{CuInS}_2$  and  $1.8\text{-}2.4\ \mu\text{m}$  (see Fig. 1) for  $\text{CuInSe}_2$ , with thicknesses of  $0.8\text{-}2.0\ \mu\text{m}$ .<sup>8</sup> These p-type films had a preferential (112) growth.<sup>8</sup> The p-type single crystal samples were prepared by the Bridgman technique and had the identical (112) orientation. For the SIMS studies, single crystal films ( $1.4\ \mu\text{m}$  thickness) were grown by MBE<sup>9</sup> on single crystal CdS substrates in order to avoid grain boundary complications. The ternary film was ion etched (2 kV, 2 min.) immediately prior to the deposition of the diffusing layer.

### 3.1.3 Results and Discussion

Two basic configurations were used in these diffusion studies. The first, shown in Fig. 2, has the diffusing species, indicated as region A, deposited upon the ternary surface (indicated at B in Fig. 2). After annealing, interdiffusion can occur, shown by the shaded region, and is usually enhanced at the grain boundary. Since the entire structure is deposited on a substrate, D, it is very difficult to examine the back surface directly. Therefore, in this configuration, the diffusion determination method involves careful depth-compositional analysis followed by an analytical modeling of the data to a diffusion profile from which the pertinent parameters can be extracted.<sup>10</sup> This technique is better applied to single crystal or very large grain polycrystalline layers. The second approach involves the initial deposition of the diffusion species onto which the ternary film is grown (i.e., the reverse of the first configuration). Thus, techniques involving the measurement of the "first arrival" of the diffusing species at the front surface can be utilized.<sup>11-12</sup> Such techniques (e.g. the formalism developed by Hall and Morabito<sup>11</sup>) are better suited for deducing grain boundary diffusion mechanisms in polycrystalline layers which can be diluted in the averaging processes involved in the in-depth profiling measurements.

#### 3.1.3.1 AES Studies

Interdiffusion coefficients ( $D$ ) and grain boundary diffusion coefficients ( $D'$ ) can be measured for either of the two cases mentioned in the previous section using AES techniques. For the grain boundary mechanism, the Hall-Morabito formalism is a particularly useful and simple method.<sup>11</sup> The "first appearance" of the diffusing species is noted at the opposite surface of the layer being analyzed, using the detectability limits ( $\sim 0.1$  atomic %) of AES. If the grains are columnar (as for the ternary films) and if the diffusion coefficient within the grain is much less than in the grain boundary, the value of  $D'$  can be obtained in a straightforward manner. This method has been applied to the CdS/CuInSe<sub>2</sub> thin-film solar cell.<sup>12</sup> In the investigation of the stability of these photovoltaic devices, which have measured solar conversion efficiencies to 6.6% under AM1 conditions, the problem of Cd diffusion from the CdS layer into the ternary film was demonstrated as a potential degradation mechanism. The grain boundary diffusion coefficient for Cd from the CdS film into the CuInSe<sub>2</sub> was found to follow the relationship:<sup>11,6</sup>

$$D' = D_0 \exp(-E_a/kT) \quad (1)$$

where  $D_0 = 10.6 \text{ cm}^2/\text{s}$  and  $E_a = 1.5 \text{ eV}$ . These data are shown in Fig. 3d. The diffusion of Cu into the CdS is minimal and is discernible by AES only at temperatures exceeding 650 K.

Diffusion related problems in the Cu-ternaries have been reported by Tomlinson et al.,<sup>13</sup> who reported rapid degradation due to Cu diffusion at room temperature for his Cu-CuInSe<sub>2</sub> diodes. Tell et al.,<sup>14</sup> examined the diffusion of elemental Cd into CuInSe<sub>2</sub> crystals. Their results, using conventional angle lapping techniques, reported the bulk diffusion coefficient dependence<sup>14</sup>

$$D = 164 \exp(-1.19\text{eV}/kT) \quad (2)$$

which is quite different than the result measured using the CdS source (Eq. 1).

In the present investigation, studies related to those of Tell et al.,<sup>14</sup> have been performed using AES and an elemental Cd film diffusion source for both single crystal and thin-film CuInSe<sub>2</sub> and CuInS<sub>2</sub>. A representative AES spectrum is presented in Fig. 4. The total spectrum is shown for the CuInS<sub>2</sub> control (prediffusion) sample. The energy region 340-390eV is expanded in the insert. The spectrum portion indicated in (a) is that for In, before annealing the film. The portion (b) shows the appearance of several Cd-peaks after the 0.8 μm film had been annealed for 40 min at 600 K. Quantitatively, the Cd concentration is calculated to be approximately 1.2 at-%. Fig. 3 summarizes the measured dependence of D and D' upon temperature for several CuInSe<sub>2</sub> cases, indicating the following relationships:

(a) Thin film, bulk diffusion within the grain, elemental Cd-source:

$$D = 154 \exp(-1.25\text{eV}/kT) \quad (3)$$

(a') Thin film, grain boundary diffusion, elemental Cd-source:

$$D = 8.4 \times 10^3 \exp(-1.15\text{eV}/kT) \quad (4)$$

(b) Single crystal, bulk diffusion, elemental Cd-source:

$$D = 160 \exp(-1.22\text{eV}/kT) \quad (5)$$

For purposes of comparison, the data of Tell et al. is presented in Fig. 3c.

The agreement of the Cd-source data for both the single crystal (Fig. 3b) and the thin film (Fig. 3a) with that of Tell et al. (Fig. 3c) is remarkable considering the difference in the analysis techniques. The similarity in results between these and other studies using a variety of metal diffusing species support the proposition that these Cu-ternary compounds have high vacancy populations which dominate the diffusion process.

For CuInS<sub>2</sub> thin films, this AES technique yields the grain boundary terms: (i) CdS-source -  $D'_0 = 13.8 \text{ cm}^2/\text{s}$ ,  $E_a = 1.7\text{eV}$ ; (ii) Cd-source -  $D'_0 = 6.2 \times 10^4 \text{ cm}^2/\text{s}$ ,  $E_a = 1.1\text{eV}$ . The relatively large differences between the diffusion coeffi-

coefficients of the Cd and CdS diffusion sources are attributed to: (i) the differences in concentrations of Cd in each of the sources and the concentration gradients at the interface. Excess concentrations are expected to yield enhanced diffusion processes;<sup>15</sup> (ii) possible stress differences at the interface. The lattice match between CdS and CuInSe<sub>2</sub> is 1.16%, while that between this ternary and elemental Cd, about 7%. The differences are similar for CuInS<sub>2</sub> and a higher diffusion coefficient is expected for the higher stress case;<sup>15</sup> and, (iii) the activation process in each case is expected to be quite different. In the case of the CdS source, the Cd must be activated from the CdS lattice before the diffusion into the ternary commences. The contribution of each of these three components is presently being investigated, but it appears that the activation difference might be the major cause.

A final comparison is that of the grain boundary diffusion from the elemental Cd source into CuInS<sub>2</sub> and CuInSe<sub>2</sub>. The grain sizes in the CuInSe<sub>2</sub> films are about twice those in the CuInS<sub>2</sub>. Electron diffraction data have indicated a large concentration of medium angle grain boundaries in the CuInSe<sub>2</sub> films compared to almost exclusively high angle boundaries in the CuInS<sub>2</sub>.<sup>8</sup> Higher D<sub>0</sub> values and lower activation energies are expected for large angle grain boundaries and these data reflect this qualitative assessment.

Fig. 5 shows the ratio of the AES Cd, 376eV, peak-to-peak amplitude to the In, 400eV, p-p amplitude as a function of annealing time measured at the arriving (front) surface. Data for elemental source Cd into (a) CuInS<sub>2</sub> and (b) CuInSe<sub>2</sub>, as well as for CdS into (c) CuInSe<sub>2</sub> films are shown. This ratio, from an examination of Fig. 4, is representative of the detected concentration of Cd at the surface. After diffusing up the grain boundaries, the Cd tends to migrate or pool across the ternary surface. After long annealing times, the surface can have a thin, continuous Cd film especially if the grain sizes are small - while the interior of the grains themselves are Cd-free. The differences in the slopes of the lines in Fig. 5 are indicative of differences in the activity of the diffusion mechanism in each case.

### 3.1.3.2 SIMS Evaluations

Fig. 6 presents depth profile data for the interface between the Cd-film and the MBE grown CuInSe<sub>2</sub> layer. Several portions of this sample were annealed in vacuo at 640 K for various times. Fig. 6a shows the control (unannealed) sample; Fig. 6b, an identical sample annealed for 8 min; and Fig. 6c, annealed for 15 min. The diffusion coefficients of the Cd into the ternary film were estimated by subtracting the control profile from each of the annealed profiles, and fitting these data to the expression:

$$C(x,t) = (C_0/2) \operatorname{erfc}(x/4Dt) \quad (6)$$



where  $x$  is the distance from the interface and  $t$ , the pertinent annealing time. The diffusion coefficient dependence upon temperature was then determined by repeating this procedure at  $T = 500$  K,  $560$  K and  $680$  K and fitting the data to the relationship given in Eq. 1. The result is:

$$D = 138 \exp(-1.3\text{eV}/kT) \quad (7)$$

This compares quite well with the corresponding AES results (Eqs. 3 and 5).

### 3.1.4 Conclusions

1. The diffusion of Cd from CdS into the Cu-ternary films represents a potential, serious degradation mechanism for CdS/Cu-ternary thin-film solar cells, especially for  $T > 600$  K.
2. Rapid diffusion of elemental Cd occurs in the Cu-ternary materials and is likely due to large vacancy concentrations in these compounds.
3. The diffusion coefficient-temperature dependences measured with AES and SIMS compare well with those measured by other techniques.
4. Differences exist in the magnitudes of  $D$  and  $D'$  between CdS and Cd sources due to stress, concentration and activation processes. As expected,  $D'$  magnitudes are an order of magnitude higher than  $D$  values for comparable cases.

### 3.1.5 References

1. C. M. Garner, Y. D. Shen, J. S. Kim, G. L. Pearson, W. E. Spicer, J. S. Harris, D. D. Edwall and R. Sahai, *J. Vac. Sci. Technol.* 14 (1977) 985.
2. H. B. Kim, A. F. Lovas, G. G. Sweeney and T. M. S. Heng, in L. F. Eastman (ed.), *Gallium Arsenide and Related Compounds*, Vol. 33a, *Instit. of Phys. Conf. Series*, London, 1976, Chap. 3, p. 145.
3. H. M. Day, A. Christou and A. C. Macpherson, *J. Vac. Sci. Technol.* 14 (1977) 939.
4. H. J. Mathieu, K. K. Reinhartz and H. Rickert, *Proc. IEEE Photovoltaics Spec. Conf.*, IEEE, New York, 1973, p. 93.
5. D. E. Carlson and C. W. Magee, *Appl. Phys. Lett.* 33 (1978) 81.
6. L. L. Kazmerski, R. B. Cooper, F. R. White and A. J. Merrill, *IEEE Trans. Electron Dev.* ED24 (1977) 496.

7. L. L. Kazmerski, in G. D. Holah (ed.), Ternary Compounds 1977, Vol. 35, Instit. of Phys. Conf. Series, London, 1977, p. 217.
8. L. L. Kazmerski, M. S. Ayyagari, G. A. Sanborn, F. R. White and A. J. Merrill, Thin Solid Films 37 (1976) 323.
9. F. R. White, A. H. Clark, M. C. Graf and L. L. Kazmerski, Appl. Phys. Lett. (in press) (1978).
10. P. M. Hall and J. M. Morabito, Surface Sci. 54 (1976) 79.
11. P. M. Hall and J. M. Morabito, Surface Sci. 59 (1976) 624.
12. D. Gupta, in J. M. Poate, K. M. Tu and J. W. Mayer (eds.), Thin Films: Interdiffusion and Reactions, Wiley Interscience, New York, 1978, p. 161.
13. R. D. Tomlinson, E. Elliott, J. Parkes and M. J. Hampshire, Thin Solid Films 26 (1975) 383.
14. B. Tell, S. Wagner and P. M. Bridenbaugh, Appl. Phys. Lett. 28 (1976) 454.
15. See, for example, D. Shaw, Atomic Diffusion in Semiconductors, Plenum Press, London, 1973, pp 432-596.

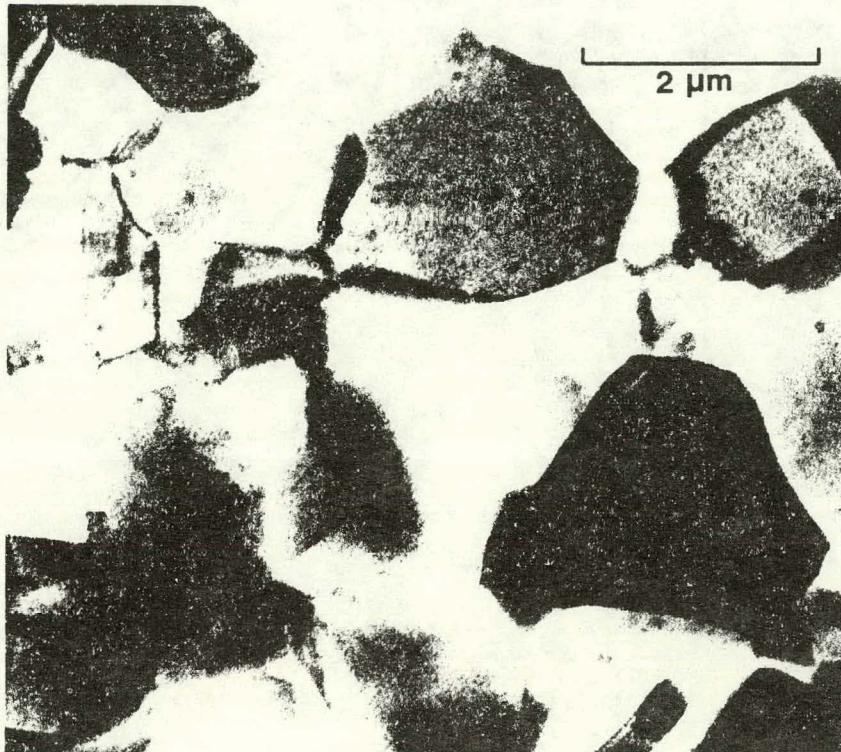


Fig. 1 Transmission electron micrograph of CuInSe<sub>2</sub> thin film indicating grain sizes.

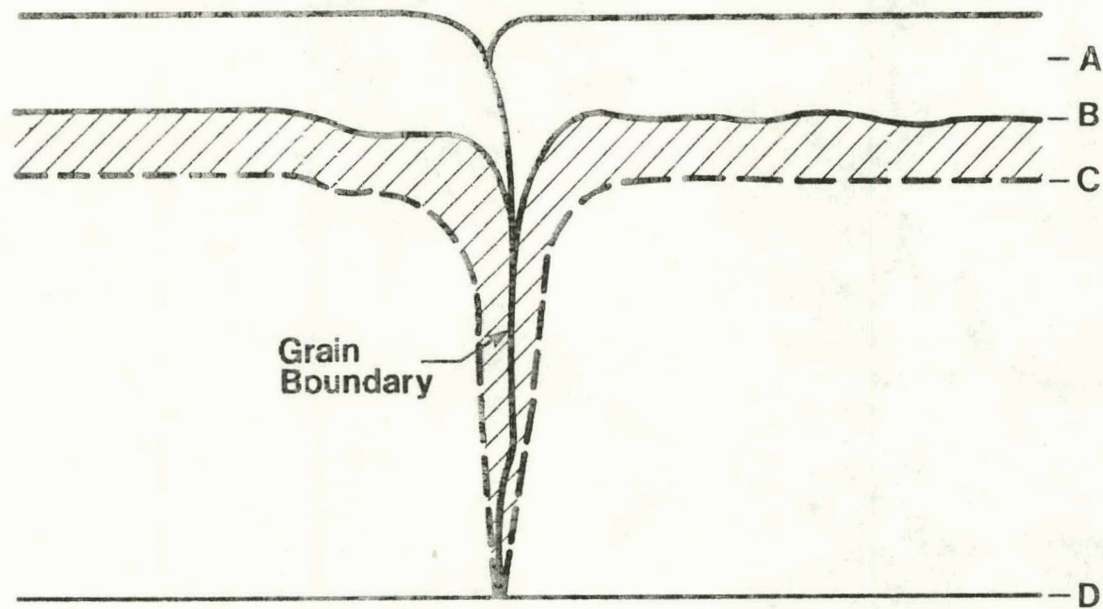


Fig. 2 Representation of diffusion process in polycrystalline thin film. Diffusing species in this case is deposited at A with the original film interface at B. The shaded region to C indicates diffused region after annealing. D is the substrate surface.

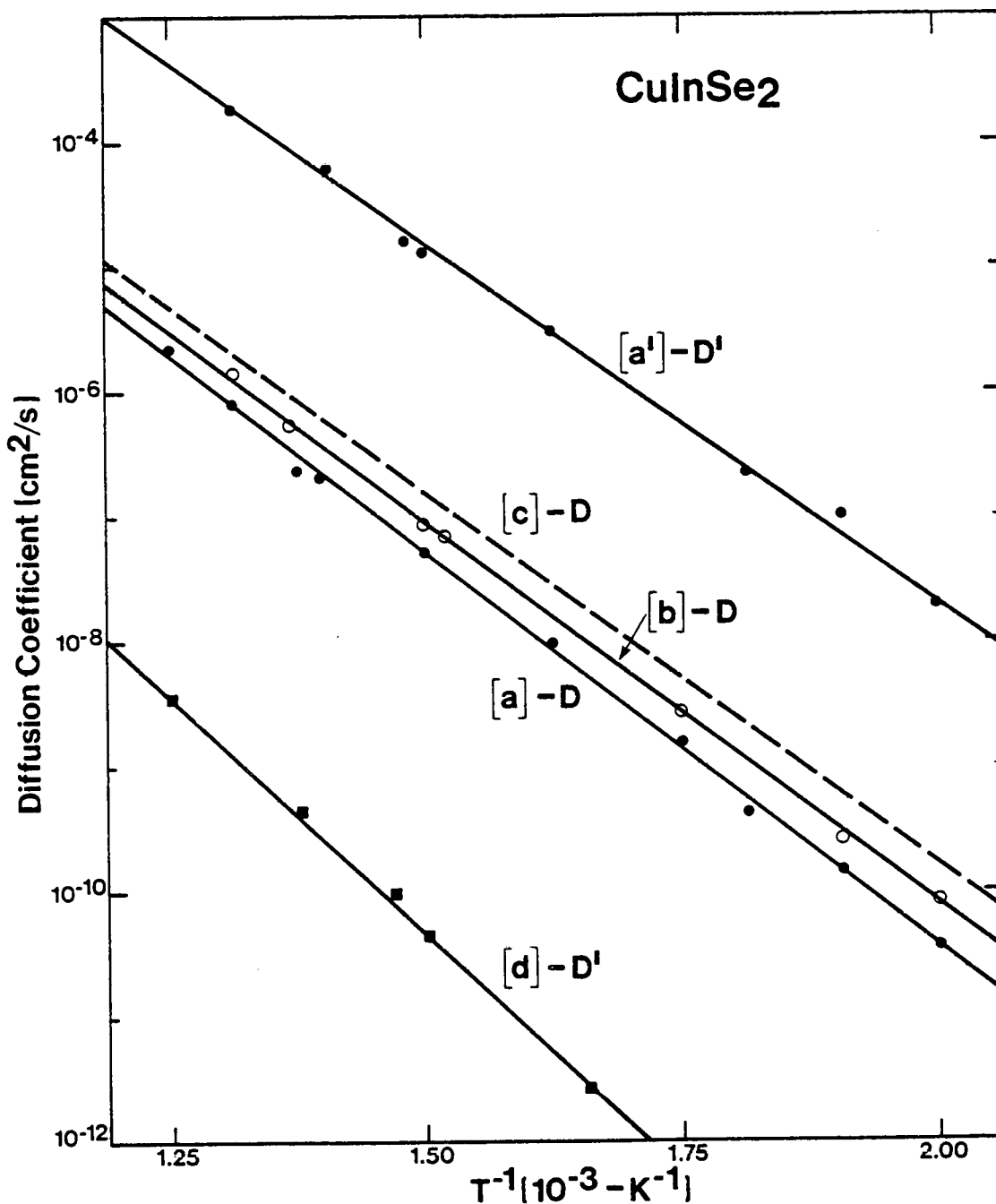


Fig. 3 Diffusion coefficient ( $D$ -interdiffusion;  $D'$ -grain boundary) dependences upon inverse temperature for (a) and (a') thin-film  $\text{CuInSe}_2$ , elemental Cd-source; (b) single crystal  $\text{CuInSe}_2$ , elemental Cd-source; (c) single crystal  $\text{CuInSe}_2$ , elemental Cd-source (Tell et al.<sup>14</sup>); and (d) thin-film  $\text{CuInSe}_2$ , CdS-source.

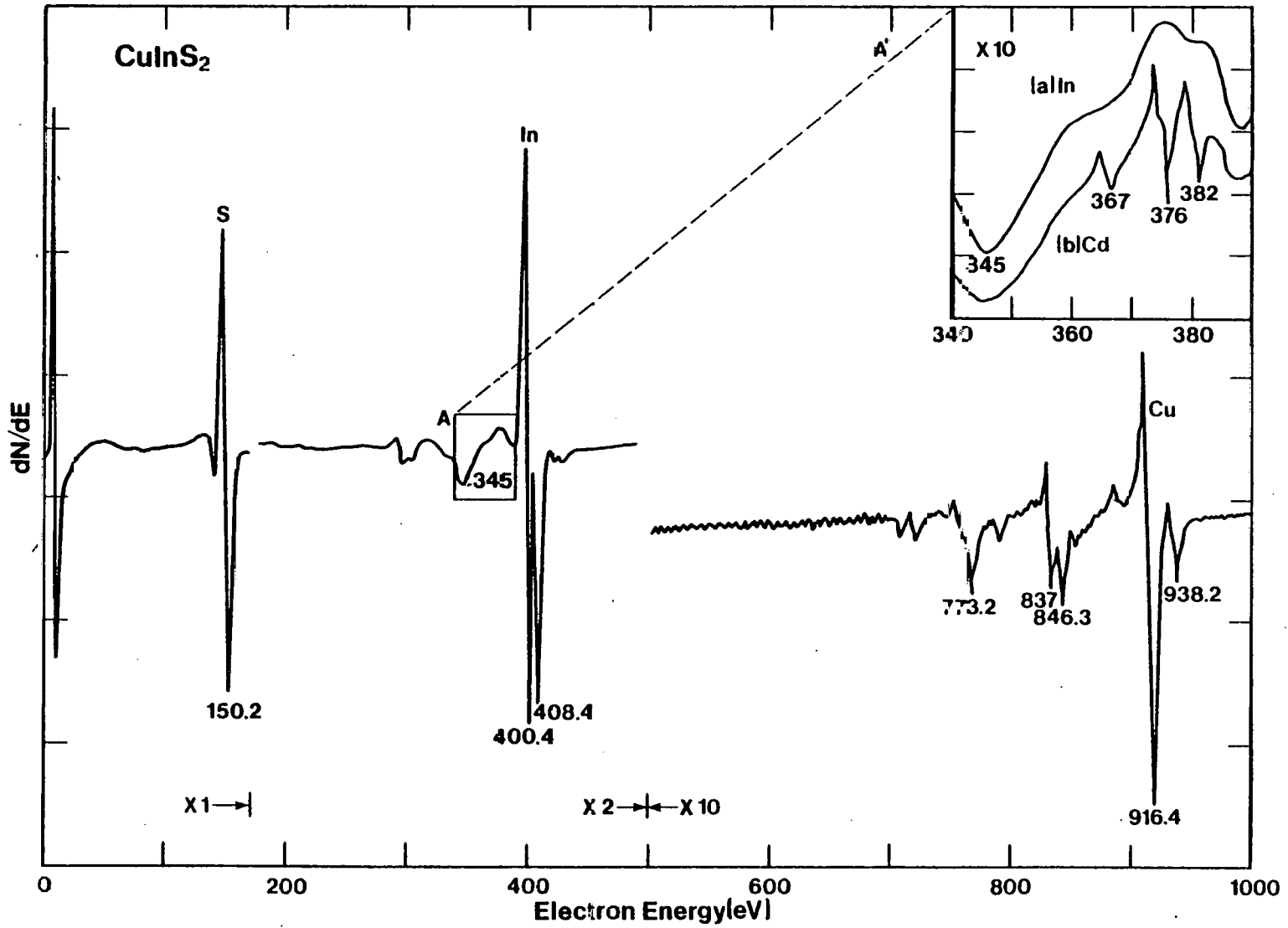


Fig. 4 Scanning Auger (AES) spectrum of  $\text{CuInS}_2$  thin film. Insert indicates expanded region 340-390eV for (a) control (unannealed) sample; (b) annealed sample with appearance of Cd-peaks.  $E_p = 3 \text{ kV}$ ,  $I_p = 4.4 \mu\text{A}$ .

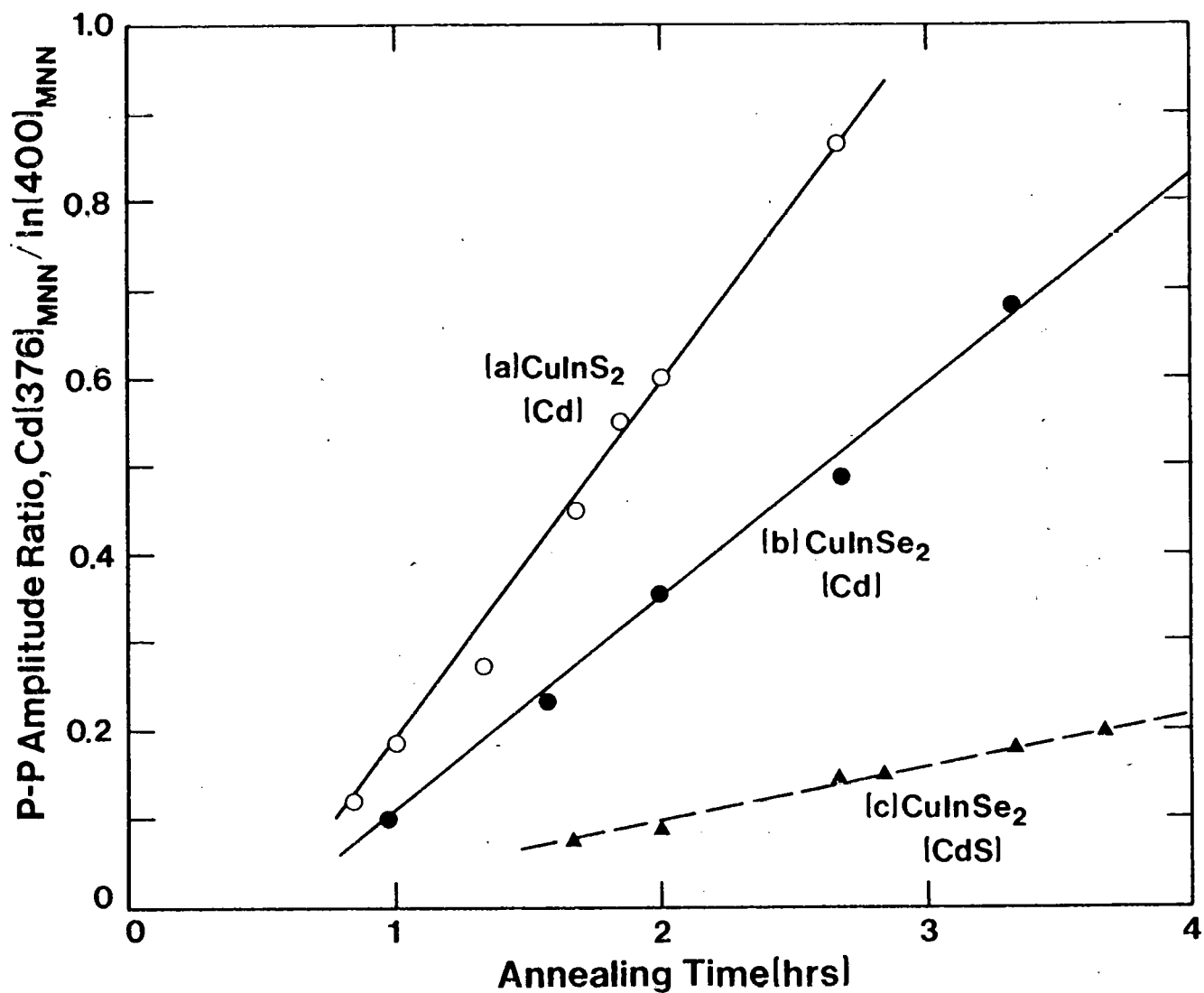


Fig. 5 Ratio of peak-to-peak amplitudes of Cd to In AES signals as functions of annealing times for (a)  $\text{CuInS}_2$  thin film, Cd-source, ( $T = 640 \text{ K}$ ); (b)  $\text{CuInSe}_2$  thin film, Cd-source ( $T = 640 \text{ K}$ ); (c)  $\text{CuInSe}_2$  thin film, CdS-source ( $T = 700 \text{ K}$ ).

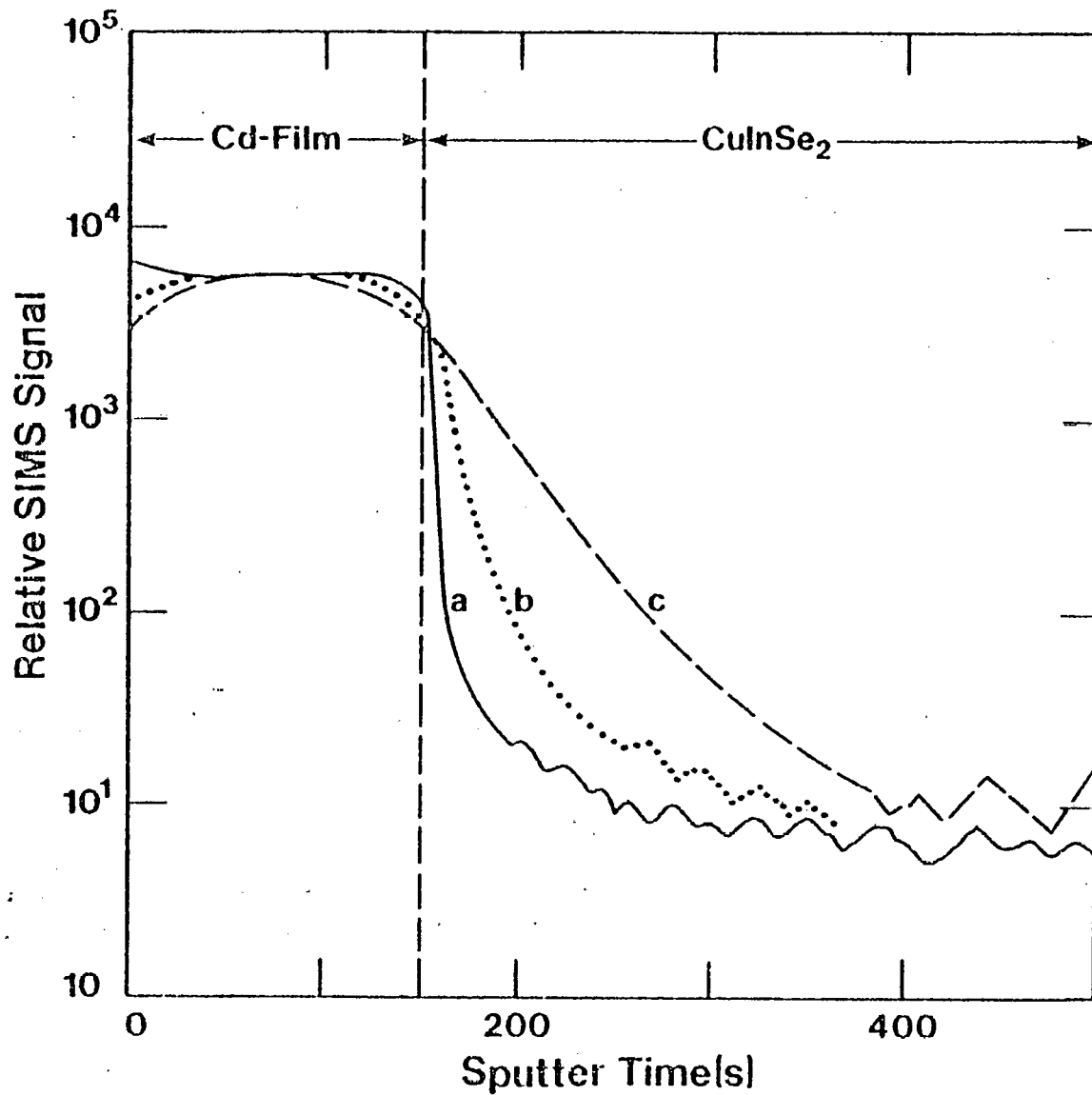


Fig. 6 SIMS depth profile showing Cd distribution in MBE grown CuInSe<sub>2</sub> thin film for: (a) control (unannealed) sample; (b) sample after 8 min., 640K anneal; (c) sample after 15 min., 640 K anneal.



### 3.2 AUGER ELECTRON SPECTROSCOPY STUDIES OF I-III-VI<sub>2</sub> CHALCOPYRITE COMPOUNDS

SERI AUTHOR: L. L. Kazmerski

OTHER AUTHORS: D. L. Sprague and R. B. Cooper (University of Maine)

JOURNAL: Journal of Vacuum Science and Technology  
Vol. 15(2), pp. 249-253 (March-April, 1978)

CONFERENCE: 24th Annual AVS Symposium  
Boston, MA.  
November 8-11, 1977

#### ABSTRACT

Auger electron spectroscopy (AES) spectra are presented for Cu ternary chalcopyrite compounds. CuInS<sub>2</sub>, CuInSe<sub>2</sub>, and CuInTe<sub>2</sub> thin films, bulk polycrystalline, and single-cell samples are examined and their AES spectra are compared. The validity of quantitative analysis methods [(1) calibration with Ag-standard, (2) utilization of sensitivity factors, and (3) calibration with specific ternary standards] is examined and the results are compared. Consistent results are obtained for polycrystalline (bulk and thin film) samples, but not for the single-crystal cases. It is found that peak width variations must be considered in the single-crystal data which vary due to diffraction channeling effects. Calculations taking these variations into account yield the expected results.

### 3.2.1 Introduction

Due to the recent demonstrations of their device-application potential, several I-III-VI<sub>2</sub> chalcopyrite semiconductor compounds have been receiving considerable attention.<sup>1-7</sup> This has been particularly the case in the photovoltaics area, in which solar cell homojunctions and heterostructure involving CuInS<sub>2</sub>,<sup>3</sup> CuInSe<sub>2</sub>,<sup>4,5</sup> and CuInTe<sub>2</sub><sup>5</sup> have shown some initial promise. However, the electrical, optical, and device characteristics of these ternaries have been reported to depend critically upon the stoichiometry of these materials.<sup>7-10</sup> Therefore, the identification and control of the composition and related characteristics of the Cu ternaries are important. The purpose of this paper is to provide such information on CuInX<sub>2</sub> (X = S, Se, Te) using Auger electron spectroscopy (AES). In addition, a comparison of several AES quantitative analysis methods applied to both polycrystalline and single crystal materials is presented for the purpose of determining the viability of these techniques in compositional determinations for the Cu ternaries.

### 3.2.2 Experiment Details

The ternary films in this study were grown using the previously reported dual-source deposition technique in which one source contained single-phase ternary powder and the other, the pertinent chalcogen (i.e., S, Se or Te).<sup>8-10</sup> The purpose of this second source is to control the chalcogen content of the films and the resulting majority carrier type and film electrical properties. Films with excess Se, S, or Te are p-type and films with chalcogen deficiencies, n-type.<sup>8-10</sup> Grain sizes are typically CuInS<sub>2</sub>, 0.8-1.2 μm; CuInSe<sub>2</sub>, 1.2-2.0 μm; and CuInTe<sub>2</sub>, 0.2-0.6 μm. The films were deposited onto fused silica substrates at deposition rates ranging from 30 to 50 Å/s in a diffusion-pump vacuum system with base pressure ≈10<sup>-5</sup> Pa. Film thicknesses were in the range 1.0-2.5 μm.

Bulk, polycrystalline samples were produced directly from stoichiometric melts, with resulting grain sizes CuInS<sub>2</sub> and CuInTe<sub>2</sub>, 1.5-6.0 μm, and CuInSe<sub>2</sub>, 2.0-10.0 μm. This material, determined to be single phase by x-ray analysis, was also used (after grinding) for the thin-film deposition source powder. The crystals were grown by the Bridgman method,<sup>7</sup> with as-grown crystals, p-type. By annealing these crystals in a minimum chalcogenide pressure, n-type samples were produced.<sup>7</sup>

The AES studies were performed on a Physical Electronics Industries PHI 545 Scanning Auger Microprobe with minimum electron beam diameter 2.8 μm. Data were taken at 3- and 5-keV electron gun energies, with 0.1-eV energy resolution and 3-eV modulation energy. Ion etching and depth profiling were accomplished with a variable (0-5 kV) ion gun. Sample surfaces were cleaned by ion etching with argon at 2 kV for 0.5 min to remove surface contamination (generally only carbon).

### 3.2.3 Results and Discussion

#### 3.2.3.1 AES Studies

Measured AES spectra for  $\text{CuInS}_2$  and  $\text{CuInSe}_2$  thin films are presented in Figs. 1 and 2, respectively. The quality of these films have been independently monitored using the following techniques: (1) transmission electron microscopy (TEM) electron diffraction which indicates that the films have the chalcopyrite structure with the preferred (221) orientation<sup>11</sup>, (2) Electrical measurements using Hall techniques showing that the p-type films had reasonable mobilities and carrier concentrations ( $\mu_p = 6.6 \text{ cm}^2/\text{V-s}$  and  $p = 2.2 \times 10^{17}/\text{cm}^3$  for  $\text{CuInS}_2$ , and  $\mu_p = 9.2 \text{ cm}^2/\text{V-s}$  and  $p = 4.7 \times 10^{16}/\text{cm}^3$  for  $\text{CuInSe}_2$ );<sup>8-10</sup> (3) optical absorption coefficient spectra measurements showing the films to have the proper absorption edges corresponding to band-to-band transitions ( $\lambda = 0.8 \mu\text{m}$  for  $\text{CuInS}_2$ ) and  $\lambda = 1.2 \mu\text{m}$  for  $\text{CuInSe}_2$ . In addition, the p-type  $\text{CuInS}_2$  film's absorption spectrum contained an additional edge at  $\lambda = 0.88 \mu\text{m}$  ( $E = 1.41 \text{ eV}$ ) corresponding to an expected Cu-vacancy level to conduction band transition.<sup>12</sup>

Several methods for quantitative Auger analysis have been reported, and four of these have been utilized comparatively in this study:<sup>13,14</sup> (1) calibration with ternary standards, (2) calibration with an Ag standard, (3) utilization of published relative sensitivity factors, and (4) calculation of sensitivity factor including matrix effects. Of these methods, the calibration to an "identical" standard (method 1) is the most desirable.<sup>14</sup> In this method, the peak-to-peak heights of the differentiated Auger spectra are compared. The accuracy of this method is limited primarily by the accuracy of the material standard that is used. Another calibration method is to use a material standard of another type (e.g., silver, as in method 2) and to compare the relative peak-to-peak intensities and relative sensitivities of the element under consideration to that of the standard.<sup>13</sup> Problems arise with this method, as well as with all quantitative methods which do not employ an identical standard, and errors result due to:<sup>14,17</sup> (a) the effects of the material environmental (matrix effects) on the escape depth of the Auger electrons and the backscattered electron contribution to the Auger yield, (b) possible chemical effects on peak shape, especially peak width, and (c) possible differences in surface morphology and microstructure.

In the absence of standards, the composition of the sample can be determined by making use of published relative sensitivity factors for each element (method 3).<sup>13</sup> These are usually referenced to the sensitivity for pure silver. The atomic concentration  $C$  of any element "i" in a material containing "j" elements can be calculated from<sup>13,17,18</sup>

$$C_i = (I_i/S_i) / (\sum_j I_j/S_j), \quad (1)$$

where  $S_j$  is the relative sensitivity factor of the pertinent element and  $I$  is the normalized peak-to-peak differential Auger intensity. This method is also limited by the matrix, chemical, and morphological effects summarized previously. However, since the sensitivity factors in Eq. (1) appear as ratios among the elements (i.e.,  $S_i/S_j$ ), the errors are minimized since the limiting effects tend to influence the sensitivity factors in the same manner. Application of these three quantitative AES techniques to polycrystalline--both thin-film and bulk--samples yields consistent results. Table 1 summarizes the data, presented in terms of atomic percentages. It is observed that for these polycrystalline samples the expected 25:25:50 ratios are closely approached for  $\text{CuInS}_2$ ,  $\text{CuInSe}_2$  and  $\text{CuInTe}_2$ . The consistency in the AES technique is enhanced by comparing n-type and p-type forms of identical type samples (e.g., n-type and p-type thin films). In every case, the p-type film exhibits a greater chalcogen concentration, as expected.<sup>7-10</sup> It should be noted that the material standard in each case was a bulk polycrystalline sample determined to be of 99.999% purity.

Several  $\text{CuInS}_2$  and  $\text{CuInSe}_2$  single crystals were also examined by AES. However, the expected atomic concentrations were not obtained when relative sensitivity factor based quantitative analysis techniques were utilized. Fig. 3 shows the major peaks for a  $\text{CuInS}_2$  single crystal on an expanded energy scale, and compares the expanded spectra for this  $\text{CuInS}_2$  crystal with a thin film which was compositionally correct using the three methods of quantitative analysis. Two differences are apparent: (1) The peak-to-peak heights are different, although the spectra were obtained under identical conditions, and (2) the peak widths are different. In fact, the peak widths for the thin film are nearly the same for Cu, In, and S, but vary for the crystal case. Using the difference between the maximum and the minimum ( $\equiv \delta$ ) of the differentiated Auger signal as a measure of the peak width:  $\delta_S = 6.6\text{eV}$ ,  $\delta_{\text{In}} = 6.5\text{ eV}$  and  $\delta_{\text{Cu}} = 6.6\text{eV}$  for the thin polycrystalline film; and  $\delta_S = 5.6\text{ eV}$ ,  $\delta_{\text{In}} = 4.6\text{ eV}$  and  $\delta_{\text{Cu}} = 6.6\text{eV}$  for the single crystal. It is thought that the differences in peak width can be attributed to the differences between the more randomly oriented, fine-grained structure of the film and the ordered structure of the crystal. Specifically, diffraction effects (channeling) in the single crystal can influence the peak height and width.<sup>15</sup>

If the peak width and height vary, but the peaks (i.e.,  $N(E)$  vs  $E$  spectrum) are essentially Gaussian, the sensitivity factor of one element (m) relative to another element (n) can be approximated by<sup>14,18</sup>

$$\begin{aligned} P_{\text{rel}} &= (P_n/P_m) \\ &= (E_m/E_n)^{1/2} (\delta_m/\delta_n)^2 (1+r_n)/(1+r_m), \end{aligned} \quad (2)$$

where  $E$  is the energy of the pertinent peak,  $\delta$  the separation between the maximum and minimum of the differential peak, and  $r$  is the backscattering factor.

The backscattering factors can be calculated in principle for the elements Cu, In, and Se using the method of Bishop and Riviere.<sup>16</sup> However, estimations could only be made since the dependences of the ionizing cross sections and backscattering currents are not known exactly. Therefore, backscattering effects have been neglected. Extracting the peak widths and peak energies from the expanded spectra, the concentrations can be calculated by combining Eqs. (1) and (2). An example, for the single-crystal sample in Fig. 3, the sensitivity factor ratios are calculated from Eq. (2):

$$P_{\text{Cu}}/P_{\text{In}} = 0.335$$

and;

$$P_{\text{Cu}}/P_{\text{In}} = 0.292,$$

where the values of  $\delta$  have been previously stated and E's are found on Fig. 3. The concentration of any element can now be calculated using Eq. 1 and measuring the peak-to-peak heights on Fig. 3. Thus (for  $I_{\text{Cu}} = 23.9$  mm,  $I_{\text{In}} = 71.4$  mm, and  $I_{\text{s}} = 163.9$  mm, unexpanded, on the original spectrum).

$$C_{\text{Cu}} = \frac{I_{\text{Cu}}}{I_{\text{Cu}} + I_{\text{In}}(P_{\text{Cu}}/P_{\text{In}}) + I_{\text{s}}(P_{\text{Cu}}/P_{\text{In}})}$$

$$= 0.249.$$

Similar calculations can be carried out on the remaining elements. Results are summarized in Table 1 in the column labeled "calculated." The results for the thin films and bulk polycrystalline samples are consistent with those obtained by the other three methods. In addition, the calculated single-crystal values are now close to the expected atomic percentages. The differences in peak widths had led to different results than those using sensitivity factor-based quantitative methods.

### 3.2.4 Conclusion

AES spectra for Cu-ternary thin films, bulk polycrystalline, and single-crystal samples have been compared. Quantitative analysis methods (calibration with Ag standard, utilization of published sensitivity factors, and calibration with ternary standards) yield consistent results for the polycrystalline and thin-film samples, but not for the single-crystal cases. However, calculation of the atomic percentages, taking peak width changes due to diffraction effects into account, provides expected values in all cases.

### 3.2.5 Acknowledgements

This work was supported in part by the National Science Foundation (RANN) and the U.S. Energy Research and Development Administration.

### 3.2.6 References

- a NSF Undergraduate Research Participant.
1. S. Wagner, L.J. Shay, P. Migliorato, and H.M. Kasper, Appl. Phys. Lett. 25, (1974) 434.
  2. Y. Kokubun and M. Wada, Jpn. J. Appl. Phys. 16, 579 (1977).
  3. L. L. Kazmerski and G. A. Sanborn, J. Appl. Phys. 48, 3178 (1977).
  4. L. L. Kazmerski, F. R. White, G. K. Morgan, Appl. Phys. Lett. 29, 268 (1976).
  5. L. L. Kazmerski, J. Phys. C 10, (1977).
  6. L. L. Kazmerski, F. R. White, M. S. Ayyagari, Y. J. Juang, and R. P. Patterson, J. Vac. Sci. Technol. 14, 65 (1977).
  7. J. L. Shay and J. H. Wernick, Ternary Chalopyrite Semiconductors: Growth, Electronic Properties and Applications (Pergamon, New York, 1975), pp.- 175-214.
  8. L. L. Kazmerski, M. S. Ayyagari, and G. A. Sanborn, J. Appl. Phys. 46, 4685 (1975).
  9. L. L. Kazmerski, M. S. Ayyagari, F. R. White and G. A. Sanborn, J. Vac. Sci. Technol. 13, 139 (1976).
  10. L. L. Kazmerski and Y. J. Juang, J. Vac. Sci. Technol. 14, 769 (1977).
  11. L. L. Kazmerski, M. S. Ayyagari, F. R. White and A. J. Merrill, Thin Solid Films 37,323 (1976).
  12. L. Y. Sun, L. L. Kazmerski, A. H. Clark, P. J. Ireland, and D. W. Morton, J. Vac. Sci. Technol. 15, 265 (1978).
  13. P. W. Palmberg, G. E. Raich, R. E. Weber, and N. C. MacDonald, Handbook of Auger Electron Spectroscopy (Physical Electronics Industries, Eden Prairie, MN, 1975). pp. 1-16.
  14. J. M. Morabito and P. M. Hall, Proceedings 9th Annual Scanning Electron Microscopy Symposium, Chicago (ITT Press, Chicago, 1976), pp. 221-230.
  15. C. C. Chang, Appl. Phys. Lett. 31, 304 (1977).
  16. H. E. Bishop and J. C. Riviere, J. Appl. Phys. 40, 1740 (1969).

17. P. W. Palmberg, *Anal. Chem.* 45, 549A, (1973).
18. J. M. Morabito, *Surf., Sci.* 49, 318 (1975).

Table I. Compositional measurements of various Cu-ternary materials by several quantitative methods indicating Cu:In:X (X=S,Se or Te) atomic percentages.

Material and Form	Method of Quantitative Analysis (a)			
	Ag-Standard	Relative	Material Ternary Standard	Calculated
CuInS <sub>2</sub> : Thin Film- p-type n-type Polycrystalline (bulk) Single Crystal- p-type n-type	24.3: 25.1: 50.6	24.2: 25.4: 50.4	24.4: 25.2: 50.4	24.4: 25.3: 50.3
	24.8: 25.4: 49.8	24.8: 25.6: 49.6	24.6: 25.6: 49.8	24.7: 25.5: 49.8
	24.7: 24.8: 50.5	24.7: 24.7: 50.6		24.9: 24.9: 50.2
	28.4: 19.4: 52.2	28.2: 19.5: 52.3		24.9: 25.0: 50.1
	29.1: 19.8: 51.1	29.0: 19.9: 51.1		25.2: 25.0: 49.8
CuInSe <sub>2</sub> : Thin Film- p-type n-type Polycrystalline (bulk) Single Crystal- p-type n-type	24.8: 24.8: 50.4	24.6: 24.7: 50.7	24.9: 25.0: 50.1	24.9: 24.9: 50.2
	25.0: 25.2: 49.8	24.7: 25.5: 49.8	24.8: 25.4: 48.8	24.9: 25.2: 49.9
	24.7: 24.7: 50.6	24.5: 24.6: 50.9		24.9: 24.9: 50.2
	30.5: 21.4: 48.1	30.2: 21.5: 48.3		25.0: 24.9: 50.1
	30.4: 21.9: 47.7	31.5: 20.6: 47.9		25.0: 25.1: 49.9
CuInTe <sub>2</sub> : Thin Film- p-type n-type Polycrystalline (bulk)	24.6: 25.2: 50.2	24.2: 25.8: 50.0	24.4: 25.4: 50.2	24.3: 25.6: 50.1
	25.1: 25.5: 49.4	25.0: 25.3: 49.7	24.6: 26.0: 49.4	27.7: 26.2: 49.1
	24.7: 24.7: 50.6	24.7: 24.4: 50.9		24.8: 24.7: 50.5

(a) Each set of data represents the average of 8 measurements taken on a single sample at 3 and 5 KV acceleration potentials.



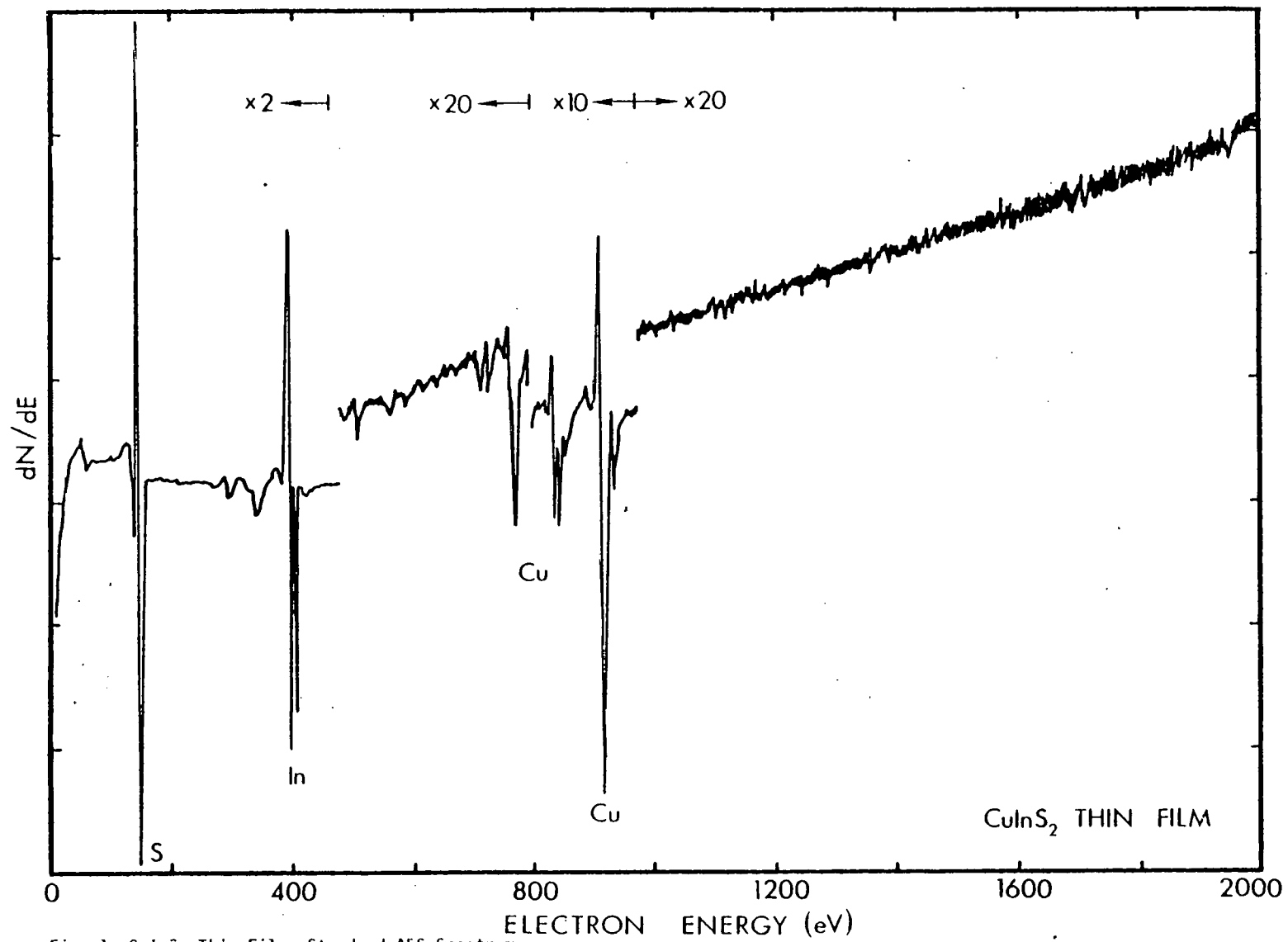


Fig. 1. CuInS<sub>2</sub> Thin Film, Standard AES Spectrum.

$E_p = 3$  KV,  $I_p = 6.4$   $\mu$ A.

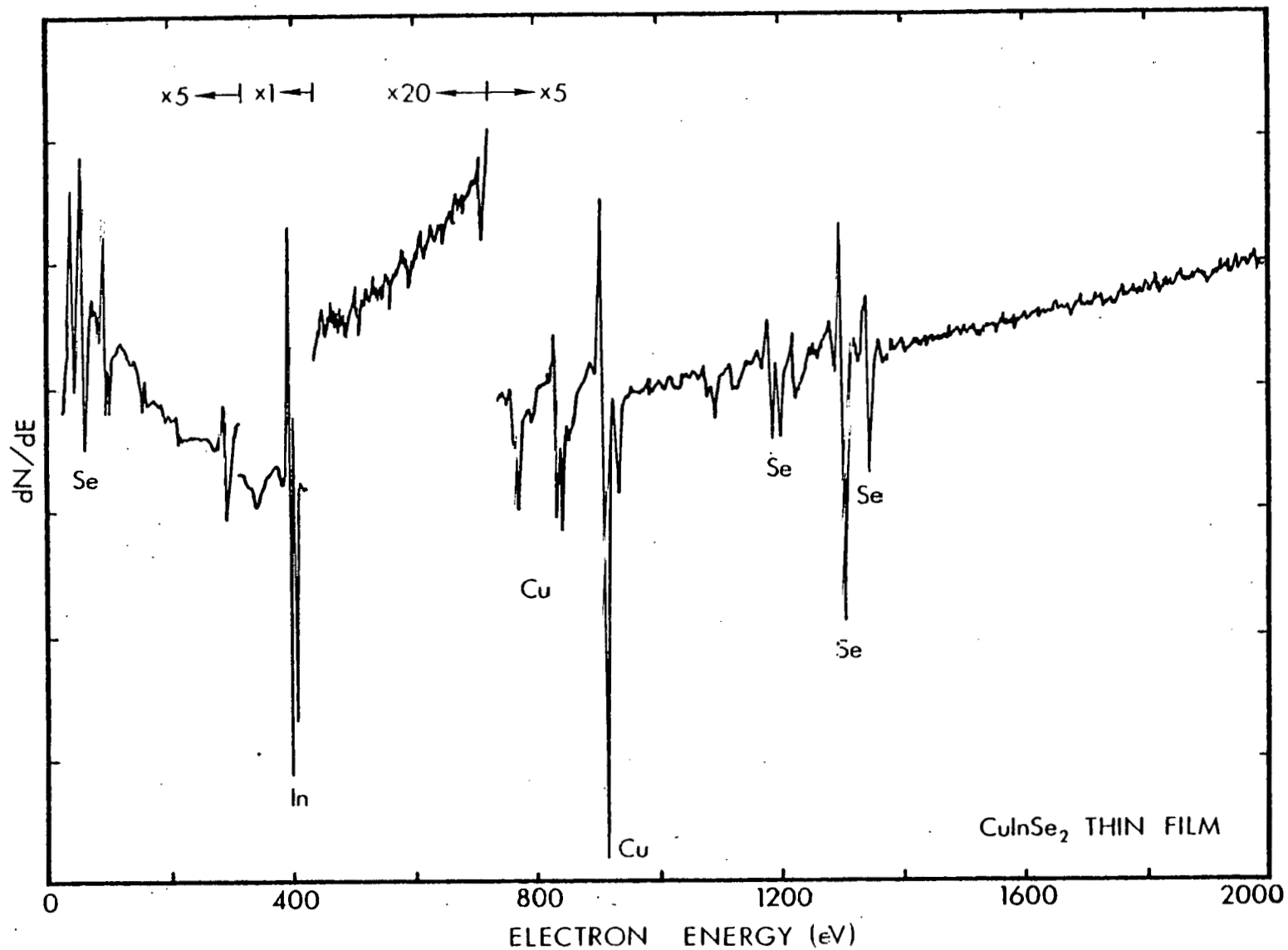


Fig. 2.  $\text{CuInSe}_2$  Thin Film, Standard AES Spectrum.  
 $E_p = 3^c \text{KV}$ ,  $I_p = 6.6 \mu\text{A}$ .

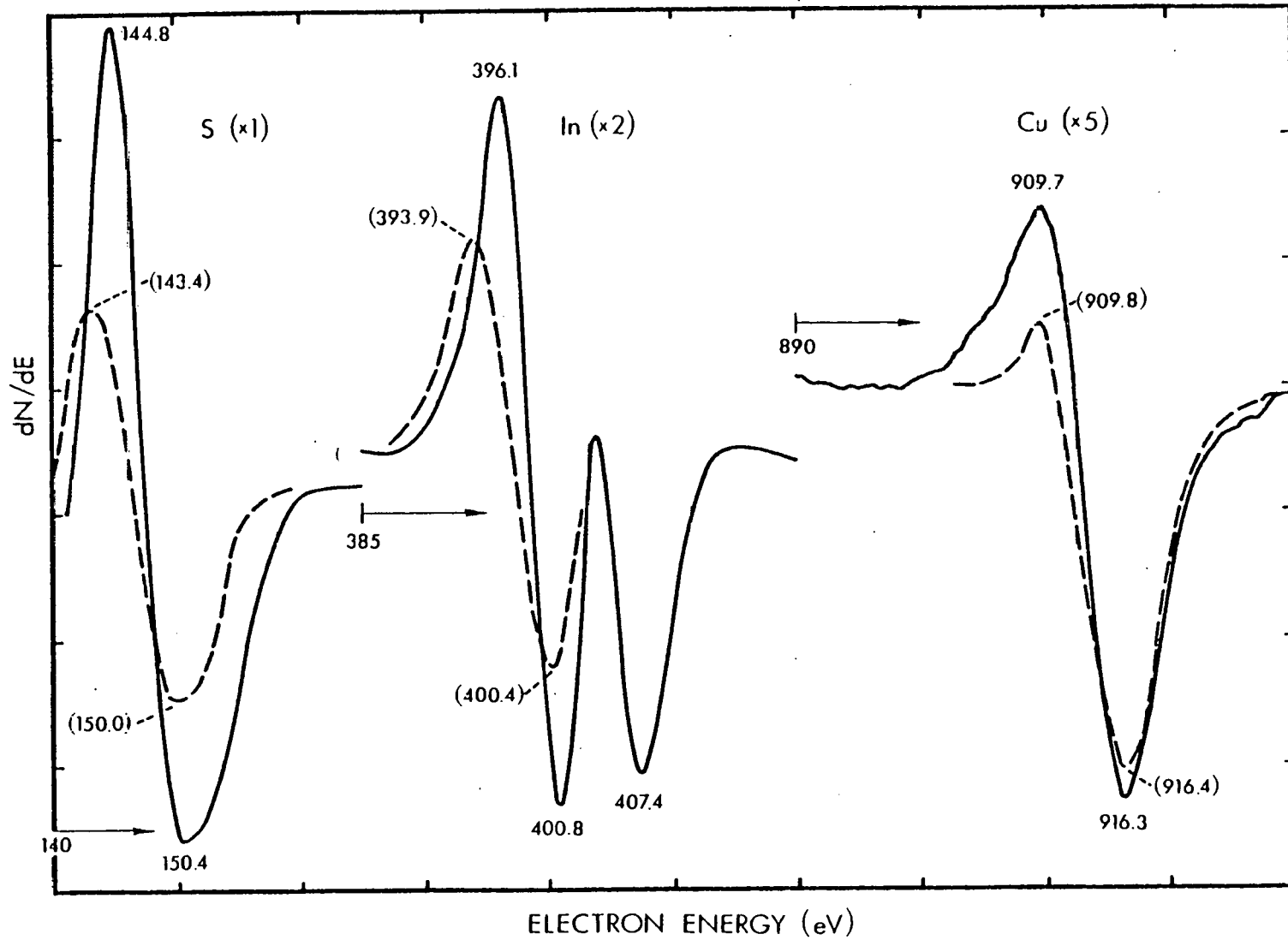


Fig. 3. CuInS<sub>2</sub> Expanded Spectra. Solid Lines Indicate Single Crystal Data, Dashed Lines, Thin Film Data.

THIS PAGE INTENTIONALLY LEFT BLANK

### 3.3 THE EFFECTS OF GRAIN BOUNDARY AND INTERFACE RECOMBINATION ON THE PERFORMANCE OF THIN-FILM SOLAR CELLS

SERI AUTHOR: L. L. Kazmerski

JOURNAL: Solid State Electronics (to appear)

CONFERENCE: International Conference on Recombination in  
Semiconductors  
Southampton, U.K.  
August 30 - September 1, 1978

#### ABSTRACT

The effects of grain boundary and interface carrier recombination on polycrystalline thin-film photovoltaic heterojunctions are presented. The grain boundary is modeled accounting for interface states due to low, medium and high-angle grain boundaries. The dark and illuminated diffusion potentials are calculated as functions of interface state densities and carrier concentrations. These are used to estimate the recombination functions of interface state densities and carrier concentrations. These are used to estimate the recombination velocities and minority carrier lifetimes. These parameters are, in turn, correlated with the short-circuit currents and open-circuit voltages. The dependence of  $V_{oc}$  on the recombination velocity effected primarily through dark reverse current, is indicated. The combined effects of grain boundary and interface recombination mechanisms of  $J_{sc}$  are discussed. Data are presented to verify the model based upon the CdS/CuInSe<sub>2</sub> photovoltaic heterojunction.

### 3.3.1 Introduction

Two proposed long-range, economically viable options for the large-scale deployment of solar cells are: (i) high conversion efficiency (>30%), single-crystal, concentrator-type devices and (ii) intermediate efficiency (>10%), thin-film devices (1). Prominent among the approaches considered in the latter case is the thin film, polycrystalline photovoltaic cell. To date, however, the intermediate efficiency goal has not been demonstrated, even in research or laboratory devices. Several factors contribute to the degradation in performance of these polycrystalline devices (compared to their single-crystal analogues). This paper focuses on the predominant, structural features of these semiconductor devices, namely the grain boundary and the pn junction. In particular, the effects of minority carrier recombination at these grain boundaries and junction interfaces on the electrical characteristics of polycrystalline heterojunctions are examined.

In the initial considerations of the performance of polycrystalline solar cells, it was predicted that under illumination: (i) short-circuit current densities ( $J_{sc}$ ) would be significantly lower than for an equivalent single-crystal device. This decrease in  $J_{sc}$  would result from recombination of carriers at the grain boundary and interfacial defects. And, (ii) the open-circuit voltages ( $V_{oc}$ ) would be comparable to the single crystal case. However in the accumulated experiences in the fabrication and characterization of several thin-film devices, the effects have been notably different than those logically predicted (2-6). In general, the decrease in  $J_{sc}$  has not been as drastic as predicted, but  $V_{oc}$  has been limited to values significantly below those expected.

In this paper, the relationships between the solar cell device parameters ( $J_{sc}$ ,  $V_{oc}$ ) and minority carrier recombination in the thin films are modeled in an attempt to explain polycrystalline solar cell performance. The effects of recombination are considered at (i) grain boundaries, and (ii) interface (junction) regions for several photovoltaic heterostructure types. Specific parameters of devices and materials are summarized in Table 1.

### 3.3.2 Grain Boundary Effects

The relationship between grain boundary defects and the electrical properties of semiconductor thin films has been considered in several investigations (7-9). Card and Yang discussed the effects of grain boundary recombination on the dark current and open-circuit voltage for silicon Schottky barrier and  $p^+n$  junction solar cells (10). Fraas presented a qualitative model describing grain boundary effects in polycrystalline heterostructure solar cells (11). This model treats the grain boundary analogously to a surface which can be in an accumulated, depleted, or inverted condition. This qualitative model, which represents six grain boundary types, explains grain boundary

behavior in selected heterojunction cells quite well. However, the quantitative treatment of grain boundary recombination mechanisms in such compound semiconductor thin-film solar cells, and the effects of such minority carrier recombination on device parameters have not been reported.

In this section, a relationship between the open-circuit voltage of a heterojunction solar cell and grain size is derived. The method starts by modeling the grain boundary in dark and illuminated conditions and determining the resulting diffusion potentials. From these, the recombination velocity and minority carrier lifetimes are calculated as functions of several parameters, including diffusion potential, interface state density, effective carrier concentration and grain size,  $\delta$ . These data are then combined with the open circuit voltage model for the heterostructure to find  $V_{oc}(\delta)$ .

### 3.3.2.1 Grain Boundary Model and Diffusion Potential

Fig. 1 represents the band diagram of the region surrounding a grain boundary in a n-type semiconductor. For the dark case (Fig. 1a), the states are filled (in equilibrium) to the Fermi level, and the band bending results in order to preserve charge neutrality. In the usual case, the width of the grain boundary ( $w$ ) is much less than the width of the depleted region ( $2d$ ). Thus balancing the charge:

$$Q_i = Q_d \quad (1)$$

where  $Q_i$  is the net negative charge contained in the interface states and  $Q_d$  the net positive charge in the depletion region. Letting  $E_v(0) = 0$ , these charge densities are expressed:

$$\begin{aligned} Q_d &= qN_d(2d) \\ &= 8q \epsilon_s N_d (q \phi_b) \end{aligned} \quad (2)$$

and

$$Q_i = qN_i(2E_f/3q - E_v/q) \quad (3)$$

where  $\epsilon_s$  is the semiconductor permittivity;  $\phi_b$ , the diffusion potential;  $N_d$ , the density of states (i.e., doping concentration); and,  $N_i$ , the grain boundary interface state density, which has the units  $\text{cm}^{-2}\text{eV}^{-1}$ . The diffusion potential,  $\phi_b$ , can then be calculated using these relationships in Eq. 1. A similar relationship can be obtained using a model for a p-type  $\text{CuInSe}_2$  as a function of the grain boundary interface density for various carrier concentrations. The interface state densities correspond roughly to the following grain boundary types:

1.  $N_i > 10^{13}/\text{cm}^2\text{-eV}$  High-angle grain boundaries

2.  $10^{11} < N_i < 10^{13} / \text{cm}^2 - \text{eV}$  Medium-angle grain boundaries
3.  $N_i < 10^{11} / \text{cm}^2 - \text{eV}$  Low-angle grain boundaries

For a solar cell under illumination, the interface states adjust their charge by an initial net capture of holes (n-type semiconductor) or electrons (p-type). This, in turn, reduces the diffusion potential to a value  $q \phi'_b$  which is  $\sim 0.1 q \phi_b$  and results in the maximum recombination rate. The grain boundary region under illumination is shown in Fig. 1b.

### 3.3.2.2 Recombination Velocity and Minority Carrier Lifetime

In the case of a solar cell material under illumination, the recombination velocity,  $S$ , of the minority carriers at the grain boundary can be estimated in a straightforward manner. The recombination current is defined (12)

$$J_r = q S_o p'_o \approx q S_o p_o \quad (4)$$

where the subscript "o" indicates  $x=0$ ,  $p'_o$  is the excess concentration, and  $p_o$  is the equilibrium concentration, and can be expressed  $p_o = p(d) \exp(q \phi'_b / kt)$  from Fig. 1b. If  $p_o \approx n_o$ , the recombination current is given by (13)

$$J_r = \frac{q}{2} N_i \sigma v (E_{fn} - E_{fp}) \quad (5)$$

where  $\sigma$  is the capture cross section and  $v$ , the thermal velocity of carriers. The recombination current at the edge of the edge of the depletion region has been calculated (10)

$$J_r \sim q S_p(d) \quad (6)$$

and, combining Eq. 6 with Eqs. 4 and 5

$$S \sim 1/4 \sigma v (E_{fn} - E_{fp}) N_i \exp(q \phi'_b / kT) \quad (7)$$

Thus, the diffusion potential,  $\phi'_b$  enhances the recombination at the grain boundary.

The dependence of  $S$  upon  $q \phi'_b$  for various  $N_i$  is presented in Fig. 3 for  $\text{CuInSe}_2$  ( $\sigma = 2 \times 10^{-15} \text{cm}^2$ ,  $v = 10^7 \text{cm/s}$ ,  $E_{fn} - E_{fp} \sim 0.5 \text{eV}$ ). For  $N_a \sim 10^{16} / \text{cm}^3$ ,  $q \phi'_b \sim 0.13 \text{eV}$ . Thus, for high angle grain boundaries ( $N_i > 10^{13} / \text{cm}^2 - \text{eV}$ ), recombination velocities in excess of  $10^6 \text{cm/s}$  are expected.



The minority carrier lifetime can be calculated for a film with columnar grain geometry. In this case, the volume recombination center density is (11).

$$N_r = 4N/\delta \quad (8)$$

where  $N$  is the surface density at  $x=d$  (i.e., from examination of Eq. 7,  $S = N\sigma v$  or  $N = 1/4 (E_{fn} - E_{fp}) N_i \exp(q\phi'_b/kT)$ ). Therefore,

$$N_r = (E_{fn} - E_{fp}) (N_i/\delta) \exp(q\phi'_b/kT) \quad (9)$$

Therefore, for a p-type semiconductor, the minority carrier lifetime is (12)

$$\begin{aligned} \tau_n &= 1/\sigma v N_r \\ &= \delta \exp(-q\phi'_b/kT) / \sigma v N_i (E_{fn} - E_{fp}) \end{aligned} \quad (10)$$

This dependence is shown in Fig. 4 for  $\text{CuInSe}_2$ . For the high angle grain boundary case, with typical  $10^{-4}$  cm grain size, the minority carrier lifetime is in the  $10^{-9}$ - $10^{-10}$  s range which is more than one order of magnitude lower than that reported for the corresponding single crystal.

### 3.3.2.3 Device Parameter Effects

The correlation between grain boundary minority carrier recombination and the short-circuit current of a heterojunction solar cell has been discussed and reported previously (14). Of interest to this paper is the effect of the grain boundary on the open-circuit voltage of the photovoltaic device. In modeling the photovoltaic heterojunction, the open circuit voltage can be expressed (for a planar junction) (14)

$$V_{oc} = E_g - \Delta X + kT \ln[f(j_{sc}(\tau), j_o(\tau))] - kT \ln(qN_c S_I) \quad (11)$$

Thus, since the functional relationship combining the minority carrier lifetime dependence in the third term of this equation has been determined, the dependence of  $V_{oc}$  upon the minority carrier lifetime incorporating grain boundary recombination can be found. Fig. 5 presents the analytical dependence of the change in  $V_{oc}$  (i.e.,  $V'_{oc} - V_{oc}$ ) as a function of the lifetime ratio,  $\tau'/\tau$ , for the  $\text{CdS/CuInSe}_2$  device. By combining Eq. 11 with the dependence of  $\tau$  upon  $\delta$  (Fig. 4), the relationship between  $V_{oc}$  and grain size can be predicted. This is shown in Fig. 6 for both high angle grain boundary ( $N_i = 10^{13}/\text{cm}^2\text{-eV}$ ) and low angle grain boundary ( $N_i = 10^{10}/\text{cm}^2\text{-eV}$ ) cases. For each case, the calculated value at which the  $\text{CdS/CuInSe}_2$  open circuit voltage will saturate is indicated at A and B. For reference, the measured  $V_{oc}$  for a  $\text{CdS/CuInSe}_2$  device with  $\delta = 2.5 \times 10^{-4}$  cm was reported to be 0.49 V, and this

is predicted quite well in Fig. 6 for the high angle grain boundary condition expected for the thin film grown by vacuum deposition (6).

### 3.3.3 Interface Effects

For the interface between two semiconductors in a heterojunction solar cell, two major characteristics are considered in the selection of the materials; (i) electron affinity matches for the semiconductors; and (ii) lattice matches (6). The former factor can cause severe spikes in the conduction band at the junction, both lowering  $V_{oc}$  and limiting current transport. This phenomenon has been covered previously (14) for the heterostructures considered in this paper. This section focuses on the effects of heterointerface recombination, especially on the short-circuit currents and open-circuit voltages of those photovoltaic devices.

#### 3.3.3.1 Interface Parameters

In order to compensate for the mismatch in lattice constants between two semiconductors used in a heterojunction, dislocations occur at the interface. The density of these dislocations, which are recombination sites, can be calculated. The density of interface states is (13,15)

$$N_i = \frac{2}{a_1 a_2} (\Delta a / a_2) \quad (12)$$

where  $a_1$  and  $a_2$  are the lattice constants and  $\Delta a / a_2$  represents the mismatch. Fig. 7 shows the dependence of  $N_i$  upon  $\Delta a / a_2$  for semiconductor /CdS heterojunctions. Using the value of  $N_i$ , the interface recombination velocity,  $S_I$ , can be determined:

$$S_I = v \sigma N_i \quad (13)$$

From Eq. 13,  $S_I$  lies in the range  $10^5$ - $10^6$  cm/s for the CdS/CuInSe<sub>2</sub> device.

The value of  $S_I$  can be experimentally determined by determining the  $kT^{-1} = 0$  intercept of the  $\ln j_0$  vs  $kT^{-1}$  dependence. This is shown in Fig. 8 for a 6.6% efficient CdS/CuInSe<sub>2</sub> device. The intercept indicates  $S_I = 2.4 \times 10^5$  cm/s. The value of  $S_I$  is important in determining  $J_{sc}$ , since (14, 15)

$$J_{sc} = \mu F(\phi') / (S_I + \mu F(\phi')).$$

$$\int_{\lambda} \phi \sigma T_g R'(\lambda) A'(\lambda) \eta_{coll}(\lambda, \tau) d\lambda \quad (14)$$

where  $\mu$  is the mobility;  $F$ , the electric field at the junction;  $\phi'$ , the photon flux at the junction;  $\phi_{\sigma}$ , the incident photon flux;  $T_g$ , the optical transmis-

sion of the top contact;  $R'(\lambda)$  and  $A'(\lambda)$  functions of reflection and absorption coefficients; and,  $\eta_{coll}$ , the collection efficiency. The value of  $S_I$  also enters importantly into determining  $V_{oc}$  through the dark saturation current,  $j_0$ .

### 3.3.3.2 Illuminated Current, Voltage

The effect of  $S_I$  upon the open circuit voltage can be illustrated through Eq. 11. The change in  $V_{oc}$  (i.e.,  $V_{oc} - V'_{oc}$ ) as a function of recombination velocity ratio,  $S_I/S_I'$ , is shown in Fig. 5b. Small changes in  $V_{oc}$  (approximately 10 mV) occur for large changes in  $S/S_I$  (two orders of magnitude). This effect seems less important than the grain size effect discussed in the previous section.

The combined effects of grain boundary and interface effects on short circuit current is presented in Fig. 9. The solid line represents the model (Eq. 14) with the grain boundary recombination velocity and lifetime, as well as the interface contributions included. Good agreement is observed for several data points representing CdS/CuInSe<sub>2</sub> devices having different grain sizes.

### 3.3.4 Summary and Conclusions

Minority carrier recombination has been investigated in polycrystalline semiconductor thin-film photovoltaic devices. Two regimes were considered:

#### 1. Grain Boundary Effects

- a. A grain boundary model was developed and the associated diffusion potential was found to increase with increasing interface state density (i.e., higher angle grain boundaries had higher  $\phi_b$  and  $\phi'_b$ ).
- b. The minority carrier lifetime was found to increase with grain diameter and decrease non-linearly with increasing interface state density (higher angle grain boundaries).
- c. The change in  $V_{oc}$  was found to depend non-linearly on the change in minority carrier lifetime.
- d. The open circuit voltage increased non-linearly with increasing grain diameter. This model predicts well the behavior of the CdS/CuInSe<sub>2</sub> photovoltaic heterojunction.

#### 2. Interface (Junction) Effects

- a. The change in  $V_{oc}$  dependence on the recombination velocity ratio was estimated, and found to increase non-linearly with this parameter. The change in  $V_{oc}$  was not sufficient to fully account for differences in polycrystalline devices.

The combined effects of the above mechanisms predicted the behavior of the CdS/CuInSe<sub>2</sub> polycrystalline solar cell.

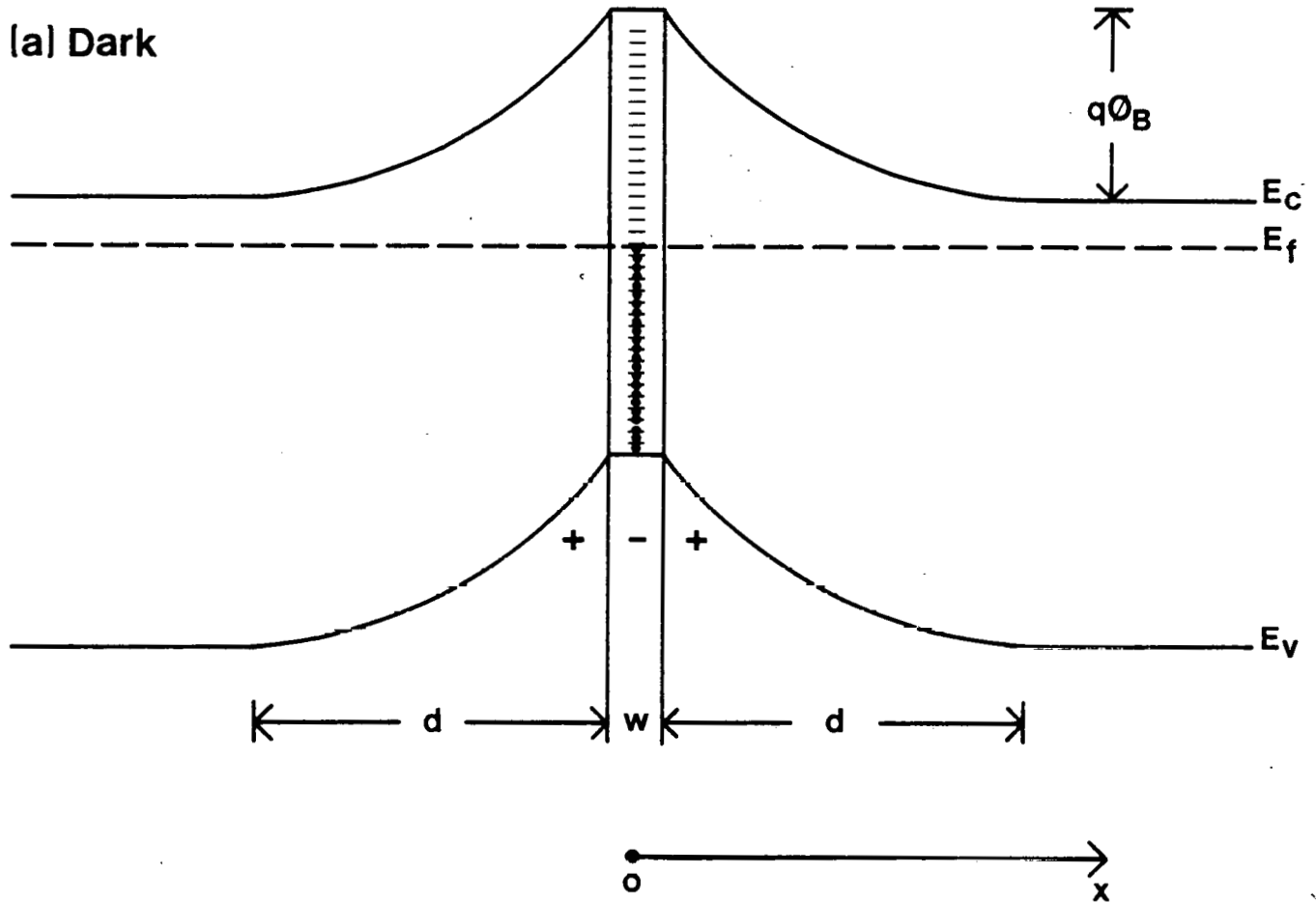
### 3.3.5 References

1. E. A. DeMeo and P. B. Bos, Perspectives on Utility Central Station Photovoltaic Applications (EPRI Rpt. ER-589-SR; Jan. 1978).
2. J. L. Shay, S. Wagner and J. C. Phillips, Appl. Phys. Lett. 28, 31 (1976).
3. N. Nakayama, H. Matsumoto, K. Yamaguchi, S. Ikegami and Y. Hioki. Jap. J. Appl. Phys. 15, 2281 (1976).
4. A. G. Stanley, Applied Solid State Science, Vol. 5 (Academic Press, New York; 1975) pp. 251-366.
5. L. L. Kazmerski, F. R. White, M. S. Ayyagari, Y. J. Juang and R. P. Patterson, J. Vac. Sci. Technol. 14, 65 (1977).
6. L. L. Kazmerski, in Ternary Compounds 1977 (Instit. Phys. Conf. Series, Number 35, 1977) pp. 217-228.
7. H. F. Matare, Defect Electronics in Semiconductors (Wiley Interscience, New York; 1971) pp. 222-234.
8. R. L. Petritz, Phys. Rev. 104, 1508 (1956).
9. T. H. DiStefano and J. J. Cuomo, Appl. Phys. Lett. 30, 351 (1977).
10. H. C. Card and E. S. Yang, IEEE Trans. Electron Dev. ED-24, 397 (1977).
11. L. M. Fraas, J. Appl. Phys. 49, 871 (1978).
12. S. M. Sze, Physics of Semiconductor Devices (J. Wiley and Sons, New York; 1969) pp. 22-149, 640-653.
13. A. G. Milnes and D. L. Feucht, Heterojunctions and Metal-Semiconductor Junctions, (Academic Press, New York, 1972) pp. 3-29, 51-57, 125-142.
14. L. L. Kazmerski, P. J. Ireland, F. R. White and R. B. Cooper, Proc. 13th IEEE Photovoltaics Spec. Conf. Washington, D.C. (IEEE New York; 1978), (in press).
15. A. Rothwarf and A. M. Barnett, Proc. IEEE Trans. Electron Dev. ED-24.

Table 1. PROPERTIES OF HETEROJUNCTION MATERIALS

Material	E <sub>g</sub> (eV)	Lattice Constants (Å)		Mismatch with CdS(%)
		a	c	
CdS	2.42	4.136	6.716	---
Cu <sub>2</sub> S	1.2	11.881	13.491	3.6-4.2
InP	1.34	6.869	---	0.32
CuInSe <sub>2</sub>	1.02	5.782	11.62	1.16
CuInS <sub>2</sub>	1.55	5.523	11.12	5.56

(a) Dark



(b) Illuminated

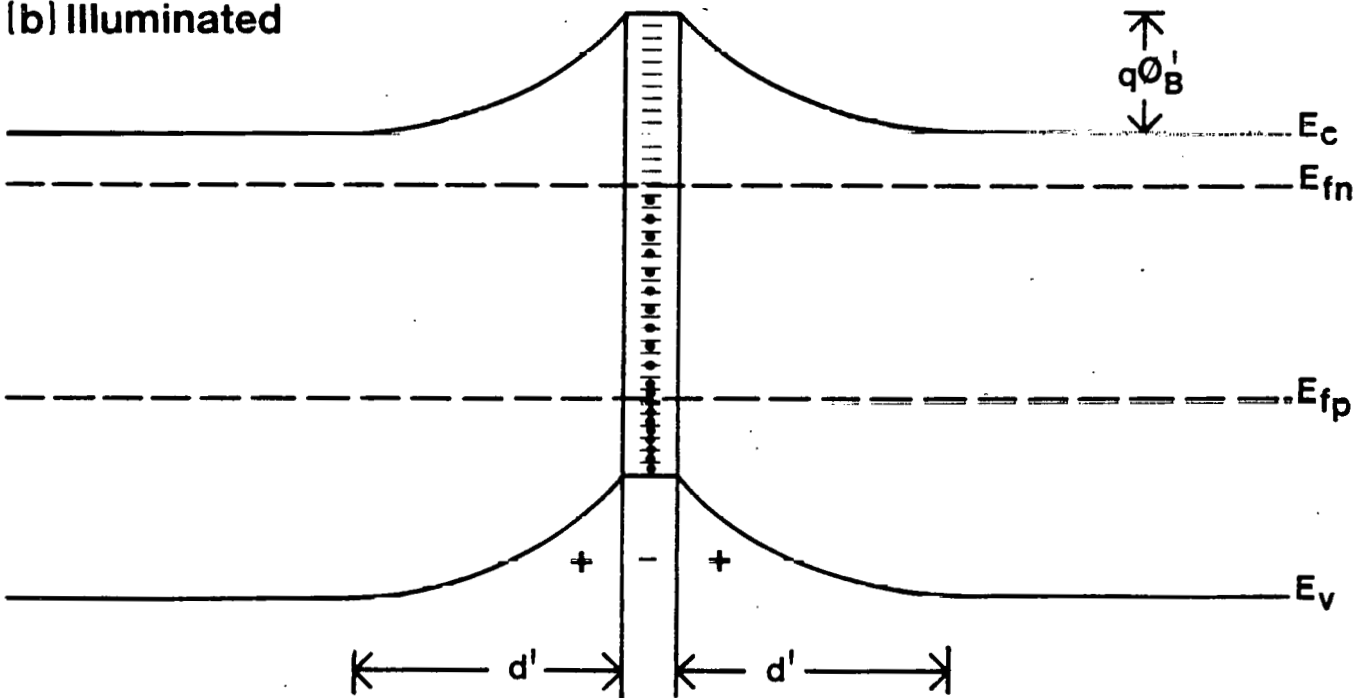


Fig. 1. Energy band diagram of the grain boundary region for a n-type semiconductor. (a) Dark case; (b) Illuminated case.  $q\phi_b$  and  $q\phi'_b$  are the dark and light diffusion potentials, respectively.

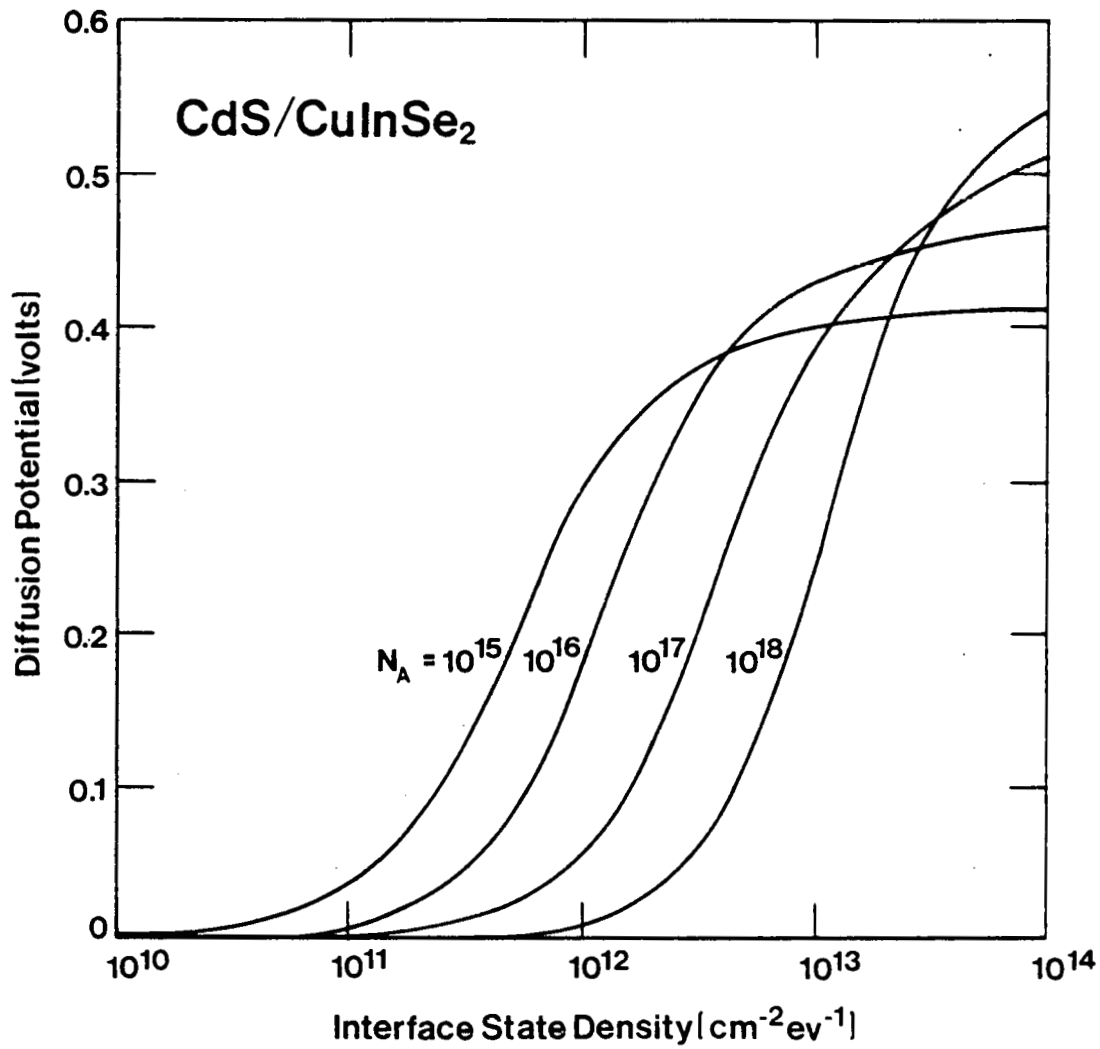


Fig. 2. Dark diffusion potential dependence on interface state density for various carrier concentrations in p-type CuInSe<sub>2</sub>.

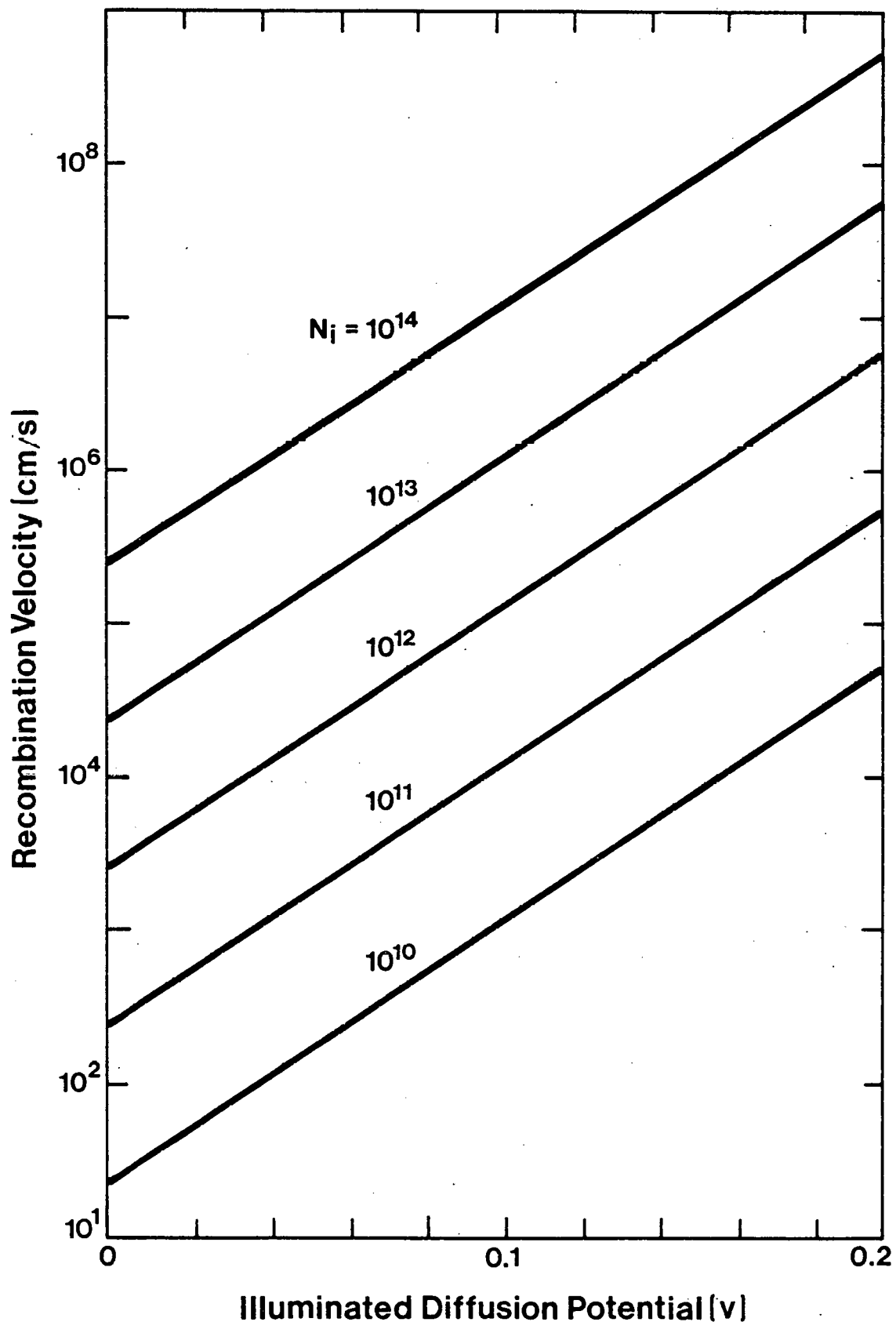


Fig. 3. Dependence of the recombination velocity upon the illuminated diffusion potential and interface state density in CuInSe<sub>2</sub> under 100 mW/cm<sup>2</sup> illumination.



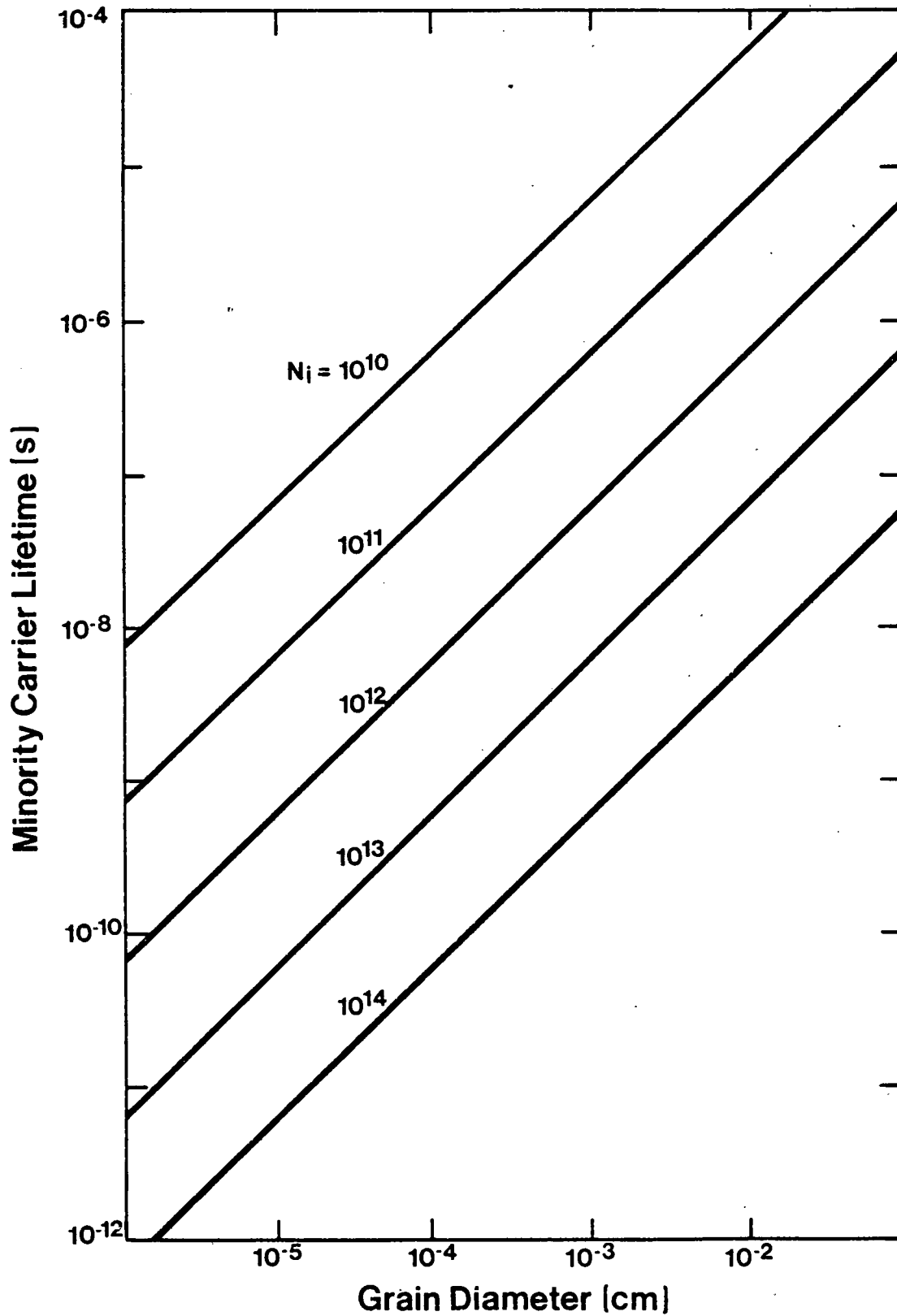


Fig. 4. Dependence of the minority carrier lifetime on grain diameter for various interface state densities in  $\text{CuInSe}_2$ .

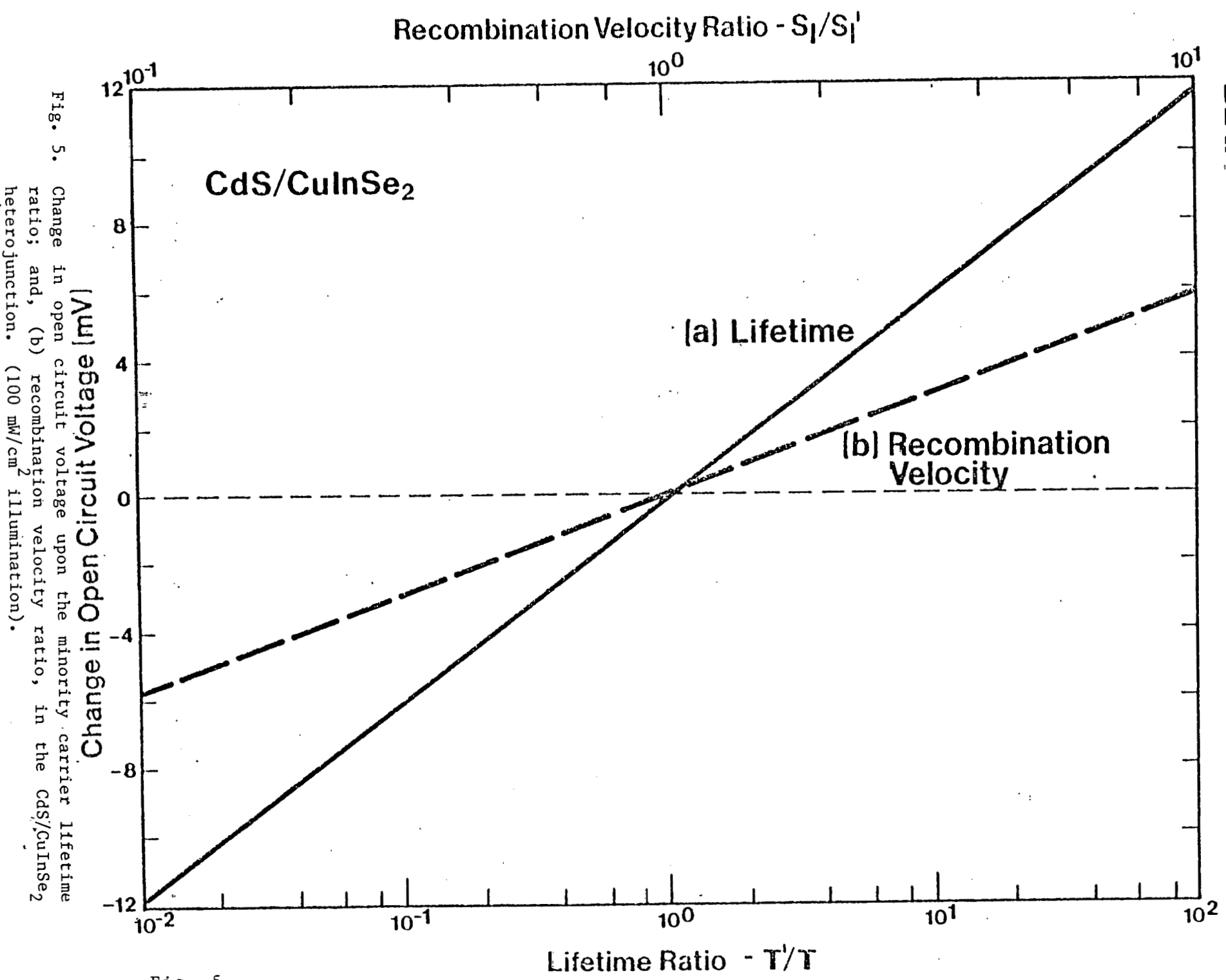


Fig. 5.

Fig. 5. Change in open circuit voltage upon the minority carrier lifetime ratio; and, (b) recombination velocity ratio, in the CdS/CuInSe<sub>2</sub> heterojunction. (100 mW/cm<sup>2</sup> illumination).

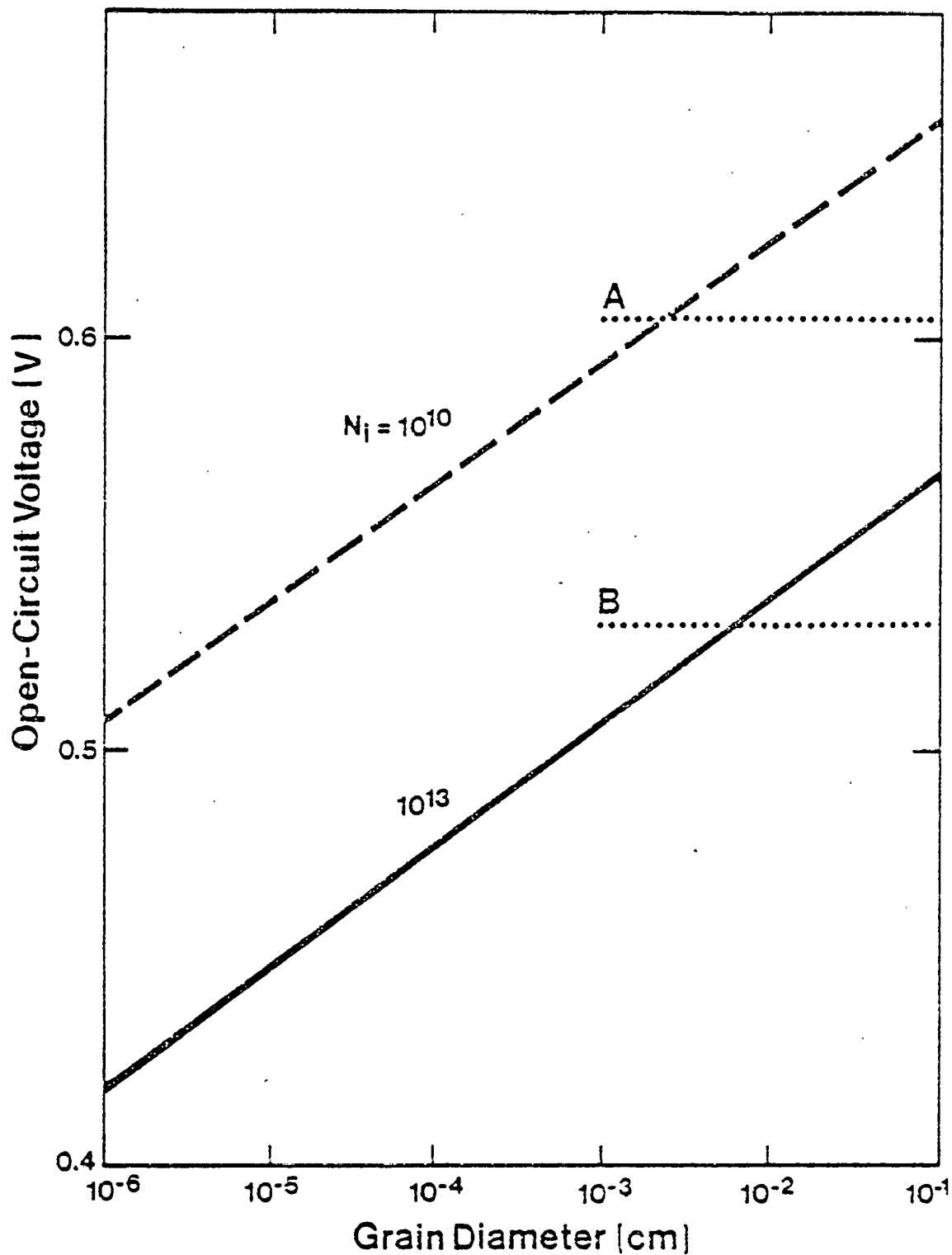


Fig. 6. Open circuit voltage dependence on grain size for CdS/CuInSe<sub>2</sub> device. Dotted line at A indicates calculated saturated value for  $N_i = 10^{10}/\text{cm}^2\text{-eV}$ ; and B, for  $N_i = 10^{13}\text{cm}^2\text{-eV}$ .

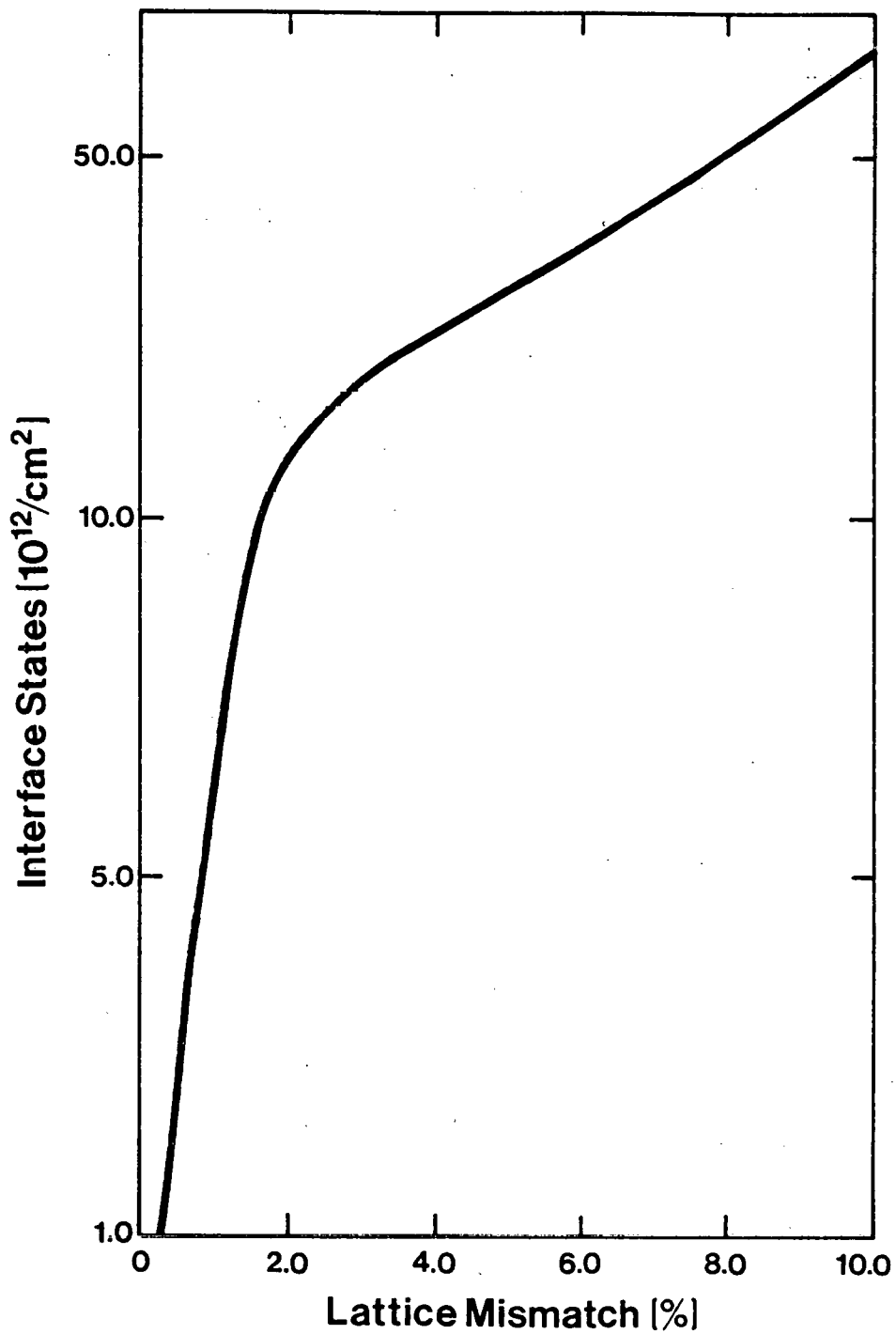


Fig. 7. Junction interface state density as a function of lattice mismatch for CdS-based heterostructures.

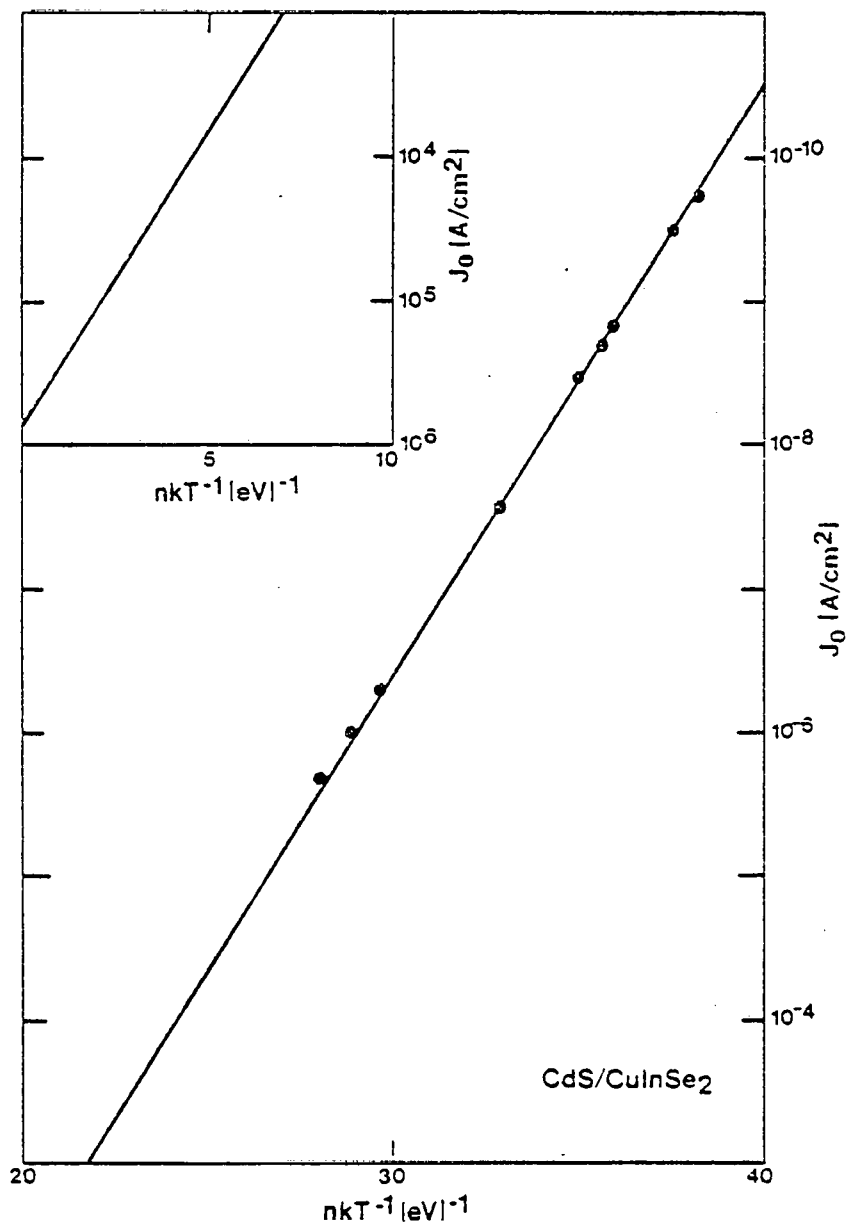


Fig. 8. Reverse, dark saturation current dependence on inverse temperature. Insert shows  $T^{-1} = 0$  intercept indicating  $S_I = 2.4 \times 10^6 \text{ cm/s}$  for CdS/CuInSe<sub>2</sub> heterojunction.

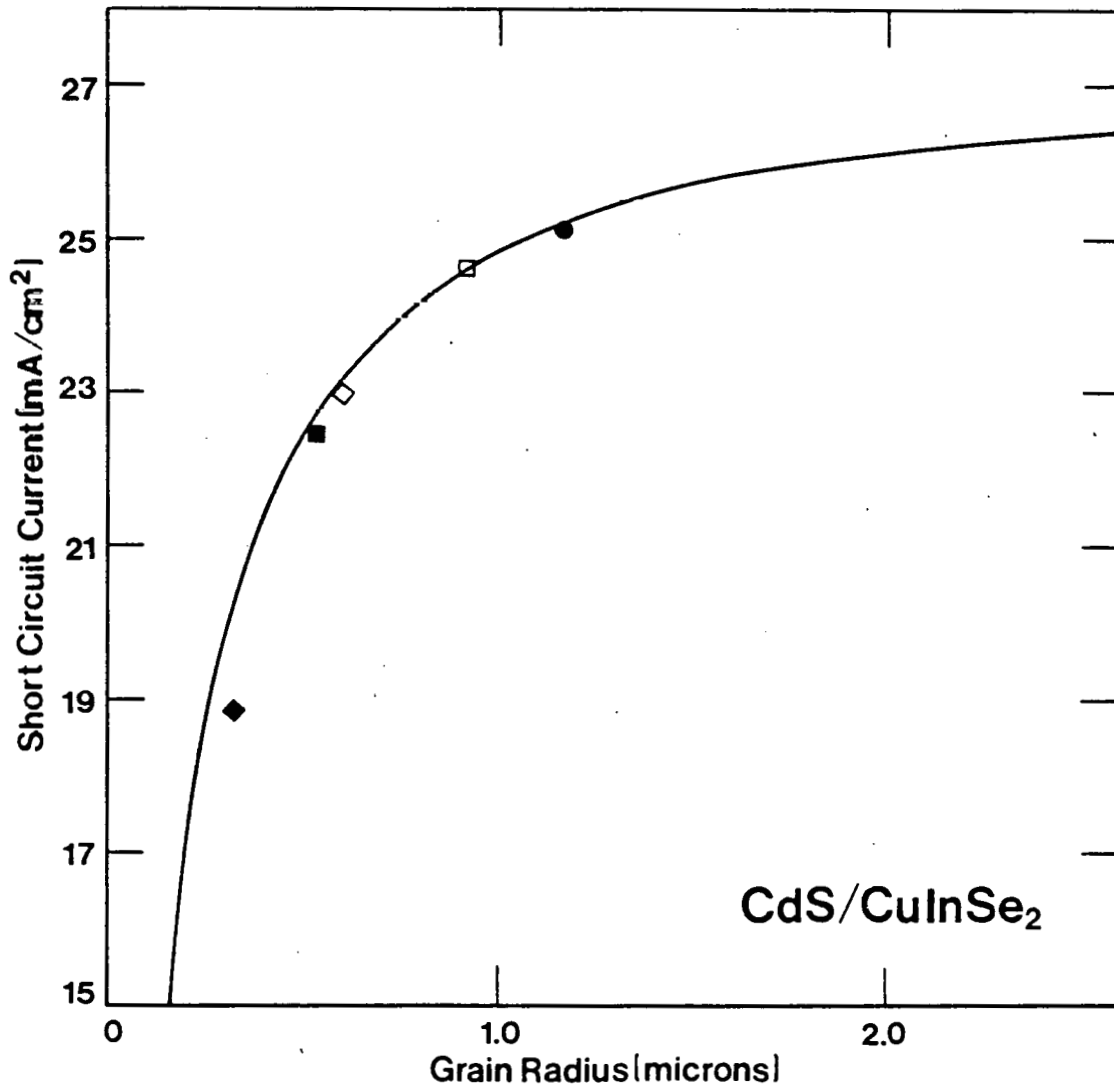


Fig. 9. Dependence of short circuit current upon grain radius. Solid line indicates model calculation. Symbols indicate device data: ● - 6.6% efficient thin-film device; □ - 6.1% device; ■ - 5.2% device; ◇ - 5.4% device; and, ◆ - 4.0% device.

### 3.4 THE PERFORMANCE OF COPPER-TERNARY BASED THIN-FILM SOLAR CELLS

SERI AUTHORS: L. L. Kazmerski, and P. J. Ireland

OTHER AUTHORS: F. R. White, and R. B. Cooper (University of Maine)

PROCEEDINGS: Proceedings of the 13th IEEE Photovoltaics Specialists Conference (IEEE New York) pp. 184-189.

CONFERENCE: 13th IEEE Photovoltaics Specialists Conference  
Washington, D.C.  
June 5-8, 1978

#### ABSTRACT

The performance of the Cu-ternary thin-film photovoltaic device; with some emphasis on the CdS/CuInSe<sub>2</sub> solar cell, is examined. A model for this heterostructure is presented and correlated with reported device performances. Attainable efficiencies based upon obtainable materials properties and producible electrical, optical, and structural characteristics are predicted. Temperature dependences of  $V_{oc}$  and  $j_0$  are used to determine electron affinity difference and interface recombination velocity, respectively. Dark capacitance-voltage data are presented for the CdS/CuInSe<sub>2</sub> device and diffusion voltages are reported. Heterojunction band diagrams are given for present and optimized device situations.

### 3.4.1 Introduction

Accompanying the recent surge in interest in the terrestrial utilization of photovoltaic conversion has been the intensification of research efforts aimed at the identification and development of more suitable solar cell materials and devices. Research activity in developing intermediate efficiency ( $10 < \eta < 15\%$ ) thin-film solar cells has led to the demonstration of the photovoltaic effect in several Cu-ternary based devices. The work in this area was initially spurred by the report of a 12% efficient, epitaxially grown CdS/single-crystal CuInSe<sub>2</sub> device by Wagner *et al.* (1). Following this disclosure, a variety of thin-film ternary solar cells has been reported, including: homojunctions - (i) n,p CuInS<sub>2</sub>, 3.6% efficiency, 0.124 cm<sup>2</sup> area (2); (ii) n,p CuInSe<sub>2</sub>, 3.0% efficiency, 0.25 cm<sup>2</sup> area (3); and heterojunctions - (i) CdS/CuInS<sub>2</sub>, 3.25% efficiency, 0.25 cm<sup>2</sup> area (3); (ii) CdS/CuInSe<sub>2</sub>, 6.6% efficiency, 1.2 cm<sup>2</sup> area (3,4).

Based upon their exceptional electrical, structural, and optical properties, it can be predicted that Cu-ternaries might be excellent candidates for photovoltaic application. The potential of CuInS<sub>2</sub>, CuInSe<sub>2</sub>, and CuInTe<sub>2</sub> is indicated by: (i) their band gaps are near optimum for terrestrial conversion in homojunction (5) and heterojunction (6) device configurations; (ii) these ternaries are direct bandgap types with high absorption coefficients (7,8), minimizing the volume of material needed for large scale deployment; (iii) both n- and p-type films have been produced, permitting homojunction formation and increasing the number of heterojunction possibilities (3); and (iv) for heterostructures, the electron affinities of these ternary compounds are compatible (i.e., no interfacial conduction band spikes) with CdS (9) and the lattice matches with CdS are acceptable, minimizing interface recombination problems (3,9).

This paper examines the performance of the Cu-ternary devices, emphasizing that of the CdS/CuInSe<sub>2</sub> heterostructure. This device has been modeled, based upon the methods of Rothwarf and Barnett (10), and attainable efficiencies using obtainable materials' properties and producible electrical, optical, and structural characteristics, are predicted. Measurements of  $V_{oc}$  and  $j_0$ , as functions of temperature are used to reduce electron affinity and interface recombination information, respectively. Capacitance-voltage data are introduced for the CdS/CuInSe<sub>2</sub> device, and heterojunction band diagrams are deduced for the present and optimized cases.

### 3.4.2 Experimental Details

The techniques and parameters used in fabricating these thin-film devices have been reported previously (2-4). The devices were produced completely in situ in order to minimize contamination, especially at the junction interfaces. A dual-source deposition method was utilized to grow the ternary films (3).



Basically, this technique employs a resistive-heated crucible for the single-phase ternary powder and a Ta boat for either the S or Se. This second source is used to alter the chalcogen content of the film during growth, and hence, to control the carrier type (3).

### 3.4.3 Modeling Techniques

The basic analysis approach used by Rothwarf and Barnett (10) is followed in modeling the performance of the CdS/CuInSe<sub>2</sub> heterostructure. In this analysis method, the device conversion efficiency ( $\eta$ ) is determined by considering the four specific factors--short circuit current ( $J_{sc}$ ), open circuit voltage ( $V_{oc}$ ), fill-factor (FF), and solar power input density ( $P_i$ )--which are used to calculate  $\eta$  through the relationship

$$\eta = J_{sc} V_{oc} FF/P_i \quad (1)$$

Each of these four factors can be determined in terms of the properties of the materials used, the characteristics of the junction produced, and the spectral content and intensity of the illumination. For example, the short circuit current density of a heterojunction can be expressed (10):

$$J_{sc} = \mu F (\phi') / [S_I + \mu F (\phi')] \cdot \int_{\lambda} \phi_o (\lambda) T_g R' (\lambda) A' (\lambda) \eta_{coll} (\lambda) d\lambda \quad (2)$$

where  $\mu$  is the effective mobility of the active material;  $F$ , the electric field at the junction,  $\phi'$  the total photon flux;  $S_I$ , the interface recombination velocity,  $\phi_o$ , the incident photon-flux density;  $T_g$ , the optical transmission of the top (grid) electrode;  $R'(\lambda)$  and  $A'(\lambda)$ , factors and absorption losses of the cell; and  $\eta_{coll}$  is the collection efficiency, which depends upon the absorption coefficient, the diffusion length, the layer thickness, the drift field, the grain size and grain boundary recombination, the surface recombination velocity and the mode of operation of the cell (i.e., front or backwall). Depending on the model of the cell, analytical relationships expressing  $V_{oc}$  and FF to fundamental parameters can be found (10), in which:

$$V_{oc} = V_{oc} (E_g, \Delta X, N_c, S_I, A') \quad (3)$$

and

$$FF = FF (R_s, J_{sc}, V_a, C) \quad (4)$$

where  $E_g$  is the energy bandgap of the absorbing layer;  $\Delta X$ , the electron affinity difference;  $N_c$ , the effective density of states at the band edge to planar junction area;  $R_s$ , the cell series resistance; and,  $C$ , a multiplicative factor (10). If the cell is dominated by interface recombination, Eq. 3 becomes:

$$V_{oc} = E_g - \Delta X + nkT \ln (J_{sc}) - nkT \ln (qN_c S_I) \quad (5)$$

for a planar junction, where  $n$  is the diode factor.

### 3.4.4 Results and Discussion

In this section, the performance of the Cu-ternary heterojunction solar cells is discussed. The reported device efficiencies and related parameters are compared to calculated values and some prediction of device performance is deduced. Examples of the experimental determination of some model parameters are presented. Finally, the band diagram of the CdS/CuInSe<sub>2</sub> heterojunction is concluded, based upon the experimental evidence.

#### 3.4.4.1 Determination of Basic Performance

Of fundamental importance to the determination of any device parameter which depends upon the solar irradiance or spectral content is a reliable, accurate representation of the solar spectrum. For the calculations in this paper, the SERI SOLTRAN solar spectra are used (1). This computer simulation has been verified against weather/insolation data and several independent measurements. The program allows the selection of any relative or absolute air mass conditions, including the selective addition of aerosols or pollutants into the atmosphere. Fig. 1 shows the AM1 and AM2 solar spectra for sea level, mid-latitude (i.e., Boston, Mass.) during mid-summer. Included is the AM0 spectrum for comparison. In this paper, the AM1 spectrum for Denver, Colorado is utilized since its total irradiance is close to the 100 mW/cm<sup>2</sup> used in the measurement of the ternary heterodiodes. A comparison of device performance for the Boston and Denver insolation cases is presented later.

Most of the basic parameters necessary for the analytical evaluation have been measured during the normal characterization of the device. Table 1 summarizes these parameters for the reported 6.6% CdS/CuInSe<sub>2</sub> thin-film device (3). The absorption coefficient dependence of the CuInSe<sub>2</sub> film upon  $\lambda$  has been measured (8) and these data are used in the short circuit current determination. Two important quantities which can be evaluated from relatively simple measurements are the electron affinity difference ( $\Delta X$ ) and the product  $N_c S_I$ . Fig. 2 shows the dependence of  $V_{oc}$  on  $nkT$ . From Eq. 5, the  $T=0$  intercept gives the value of  $(E_g - \Delta X)$ , indicating the electron affinity difference to be 0.08 eV for the CdS/CuInSe<sub>2</sub> heterodiode, in which  $E_g(\text{CuInSe}_2) = 1.02$  eV (300 K). Measurements on several devices have shown the electron affinity difference to lie in the range of  $0.08 < \Delta X < 0.10$  eV, which affirms the compatibility of the electron affinities for those materials (3,9). The dependence of  $J_o$  on inverse temperature is shown in Fig. 3 for the same device. The intercept of the  $J_o$  line at  $(kT)^{-1} = 0$  yields the quantity  $qA N_c S_I$ , where  $A$  is the junction area. For a planar junction, the product

$N_c S_I = 8 \times 10^{23}/\text{cm} \cdot \text{s}$  for an estimated typical value for  $N_c = 2 \times 10^{18}/\text{cm}^2$ ,  $S_I = 4 \times 10^5 \text{ cm/s}$ . This is consistent with a calculated value of  $S_I$  which is based upon the lattice matches of the materials at the interface (10).

#### 3.4.4.2 Performance of the CdS/CuInSe<sub>2</sub> Heterojunction

The analytical model allows the adjustment of a number of parameters. Only a few important ones are represented herein in order to illustrate the directions for device improvements.

The dependence of the short circuit current density upon grain radius is presented in Fig. 4. The model calculation is represented by the solid line, and good agreement is indicated for the several experimental points which are included. Since the thickness of the ternary film is in the same range as the grain size, the value of  $J_{so}$  is expected to depend critically on this parameter (10). It should be noted that the parameters for the solid line in Fig. 4 have been established for the 6.6% device and some variation is expected for the other devices, especially at lower grain sizes where these parameters can vary significantly.

Two important limiting factors in the performance of the CdS/CuInSe<sub>2</sub> device have been the series resistance of the back contact and relatively high resistivity (6-12  $\Omega$ -cm) of the CdS layer which tends to spread out the effective length of the junction. Fig. 5 shows the dependence of the efficiency upon the CdS resistivity. The solid line represents the model calculation with a 1.0  $\Omega$  /cm<sup>2</sup> back contact. The efficiencies of the measured devices correspond well to this dependence, indicating the limitation of the high CdS resistivity. Lowering  $\rho < 1 \Omega$ -cm can yield a 9% device, keeping the other parameters constant. If the back contact can be lowered to 0.25  $\Omega$  /cm<sup>2</sup>, the dashed-curve results. Thus, a 10% efficient device can be approached by both lowering  $\rho$ (CdS) and minimizing the back contact resistance. Once again, this assumes no change or optimization of the other parameters.

Some dependence of device performance on geographic location is indicated in Fig. 6. Curve A shows the dependence of  $J_{sc}$  upon solar irradiance (i.e., relative air mass conditions) for Denver and curve B, for Boston. The fact that the two curves do not intersect is a result of a slight difference in spectral content between the two sites.

A comparison of reported device parameters with the model calculation is presented in Table 2 for thin-film and single crystal devices. Good correlation is noted. The model can be used to predict attainable device performance for this heterostructure. With  $\rho$ (CdS) = 0.1  $\Omega$ -cm, grain radius = 1.2  $\mu\text{m}$ ,  $R$ (back contact) = 0.25  $\Omega$  /cm<sup>2</sup>,  $d(\text{CuInSe}_2) = 0.8 \mu\text{m}$ ,  $d(\text{CdS}) = 4.0 \mu\text{m}$  and  $N_c = 2 \times 10^{18}/\text{cm}^2$ , the following performance parameters could be obtained:

$$V_{oc} = 0.55 \text{ V}$$

$$J_{sc} = 27.6 \text{ mA/cm}^2$$

$$FF = 0.74$$

and

$$\eta = 11.1\%$$

### 3.4.4.3 Band Diagram of the Heterojunction

Typical dark C - V data for the CdS/CuInSe<sub>2</sub> heterodiode are presented in Fig. 7. The slope of  $(C/A)^{-2}$  vs V line indicates  $N_a = 2.5 \times 10^{16}/\text{cm}^3$  which is in agreement with that determined by Hall measurements (2-4). The intercept at C = 0 indicates a diffusion voltage of 0.78 V. Incorporating these data with that previously measured, the band diagram for the CdS/CuInSe<sub>2</sub> device, shown in Fig. 8, can be constructed. For the 6.6% efficient device,  $\Delta\chi = 0.08$  eV and  $qV_{oc} = 0.49$  eV. The value of the diffusion voltage is

$$V_D = \phi_1 + \phi_2 \quad (6)$$

where  $\phi_1$  = magnitude of  $E_v$  banding from CuInSe<sub>2</sub> bulk to  $\Delta E_v$  spike (0.49 eV) and  $\phi_2$  = magnitude of  $E_c$  banding from CdS bulk to  $\Delta E_c$  spike (0.29 V).

The band diagram of Fig. 8 represents the worst possible case for this heterojunction. In order to improve device performance, two alternatives can be proposed: (1) lower the CuInSe<sub>2</sub> resistivity significantly and keep  $\rho(\text{CdS})$  high; or (2) lower the resistivity of the CdS. From the experimental evidence, it is not feasible to lower the ternary into the degenerate state and keep single phase material (12). Thus, the latter case, as described in the calculations in the previous section, is the better alternative. The band diagram for this case is represented in Fig. 9. A higher  $V_{oc}$  can be realized by not spreading the junction field region into the CdS, without significant loss in  $J_{sc}$ .

### 3.4.5 Summary and Conclusions

The primary reason for investigating the application of the Cu-ternaries for photovoltaic devices is their potential in providing an intermediate efficiency thin-film solar cell. Device performance has been limited by:

1. The control of the physical, electrical, and optical properties of the ternary layer and;

2. The inability to produce low resistivity ( $< 1\Omega\text{-cm}$ ) CdS films on the  $\text{CuInSe}_2$ .

It is to be expected that controlling the properties of a thin film composed of multiple elemental species would be difficult. It is hoped that the ongoing research programs can find solutions to the inconsistencies encountered in grain size, resistivity, and compositional quality. The problem with CdS resistivity may be major. It may be that some interdiffusion of trace impurities from the  $\text{CuInSe}_2$  layer at the necessary elevated substrate temperatures occurs, compensating the properties of the CdS. The predicted efficiencies for the CdS/ $\text{CuInSe}_2$  heterojunction cannot be reached unless the band diagram of Fig. 9 can be realized.

The wide-scale deployment of photovoltaic devices will require a substantial amount of material availability. A final caveat for these ternary devices lies in the consideration of the availability of substantial quantities of indium. This potential materials limitation must be carefully examined to ensure commercial feasibility.

#### 3.4.6 Acknowledgements

The authors wish to acknowledge the assistance and encouragement of Dr. Sigurd Wagner, SERI, as well as his suggestions in the preparation of this manuscript. Sincere appreciation is expressed to Dr. A. Rothwarf, University of Delaware, for his helpful technical discussions and advice. The cooperation of Dr. Roland Hulstrom, SERI, in the generation of the spectral data is gratefully acknowledged.

#### 3.4.7 References

1. S. Wagner, J. L. Shay, P. Migliorato, and H. M. Kasper, Appl. Phys. Lett. 25, 434 (1974).
2. L. L. Kazmerski and G. A. Sanborn, J. Appl. Phys. 48, 3178 (1977).
3. L. L. Kazmerski, in Ternary Compounds 1977, Institute of Phys. Conf. Series, 35, pp. 217-228 (1977).
4. L. L. Kazmerski, F. R. White and G. K. Morgan, Appl. Phys. Lett. 29, 268 (1976).
5. J. J. Loferski, J. Appl. Phys. 27, 777, (1956).
6. P. J. Ireland, L. L. Kazmerski and S. Wagner (to be published).

7. J. L. Shay and J. H. Wernick, Ternary Chalcopyrite Semiconductors: Growth Properties and Applications (Pergamon Press, New York; 1975) pp. 1-2, 175-214.
8. L. Y. Sun, L. L. Kazmerski, A. H. Clark, P. J. Ireland and D. W. Morton, J. Vac. Sci. Technol. (to appear March-April 1978 issue).
9. K. J. Bachman, E. Buehler, J. L. Shay and S. Wagner, Appl. Phys. Lett. 29, 121 (1976).
10. A. Rothwarf and A. M. Barnett, IEEE Trans. Electron Dev. ED-24 381 (1977).
11. R. Hulstrom (SERI program, to be published).
12. L. L. Kazmerski, M. S. Ayyagari, G. A. Sanborn, F. R. White and A. J. Merrill, Thin Solid Films, 37, 323 (1976).

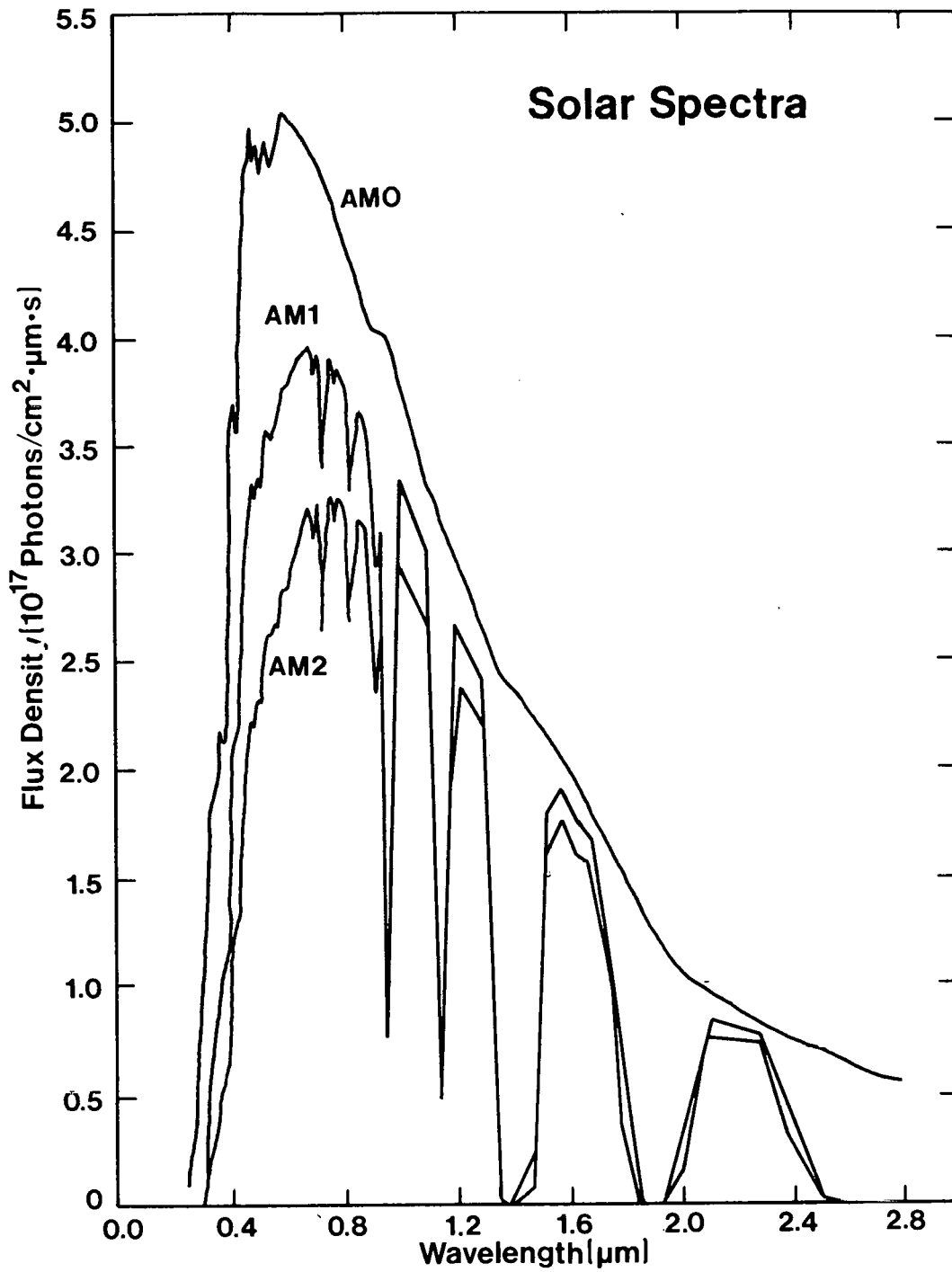


Fig. 1. AMO, AM1 and AM2 Solar Spectra Based Upon SERI SOLTRAN Program.

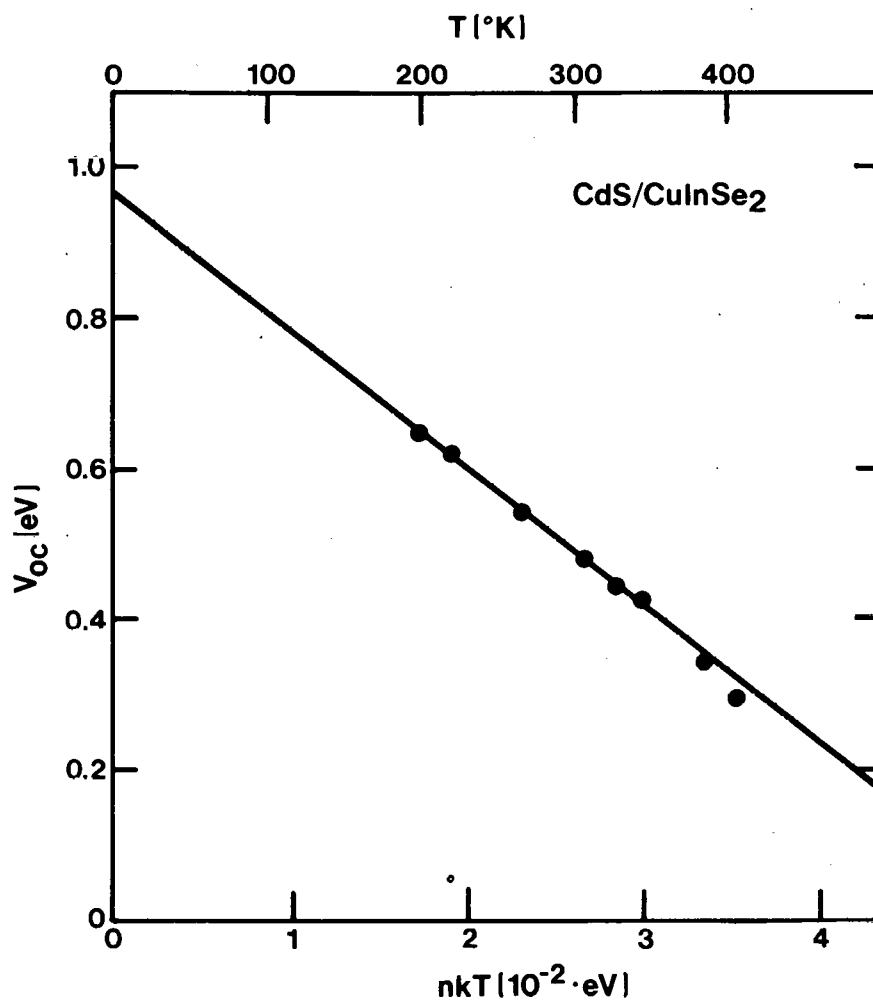


Fig. 2. Dependence of  $V_{oc}$  upon Temperature for CdS/CuInSe<sub>2</sub> Device. Intercept at  $T=0$  Indicates  $E_g - \Delta\chi = 0.08$  eV.



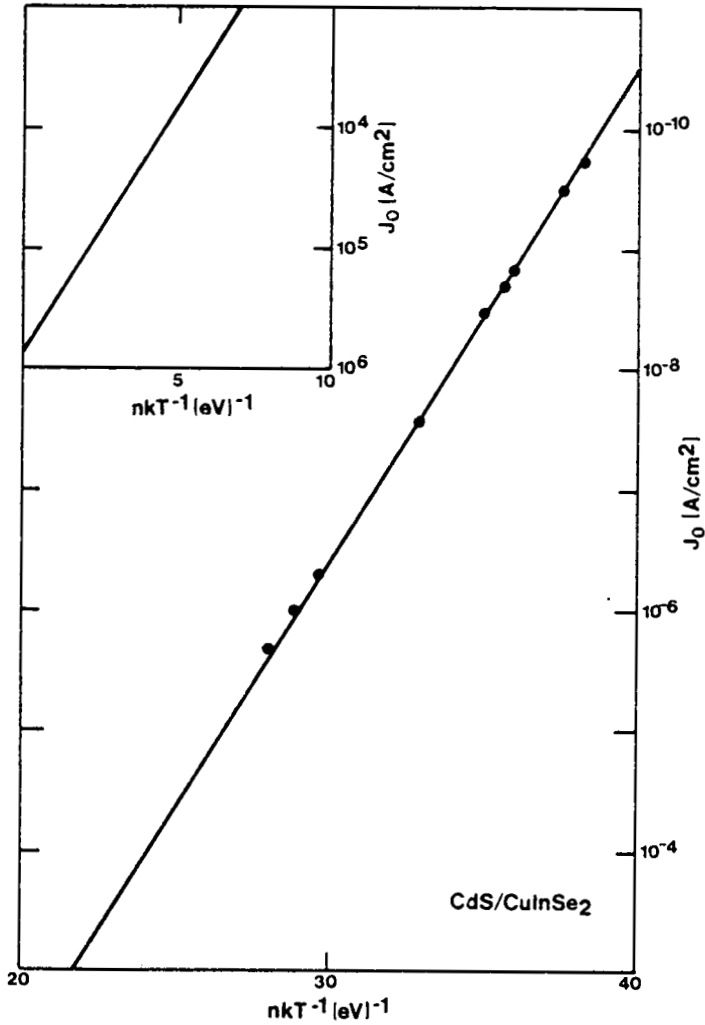


Fig. 3.  $J_0$  as a function of Inverse Temperature for CdS/CuInSe<sub>2</sub> Thin Film Device. Inset Indicates  $(nkT)^{-1} = 0$  Intercept.

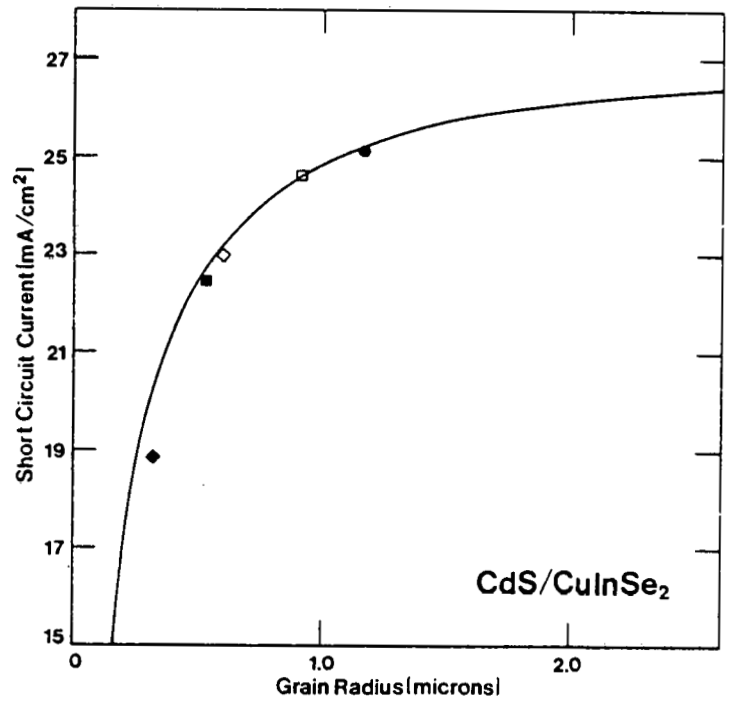


Fig. 4. Dependence of  $J_{SC}$  upon Grain Radius. Solid Line Indicates Model Calculation. Symbols Indicate Device Data: ●-6.6% Efficient Thin Film Device; □-6.1% Device; ■-5.2% Device; ◇-5.4% Device; and, ◆-4.0% Device.

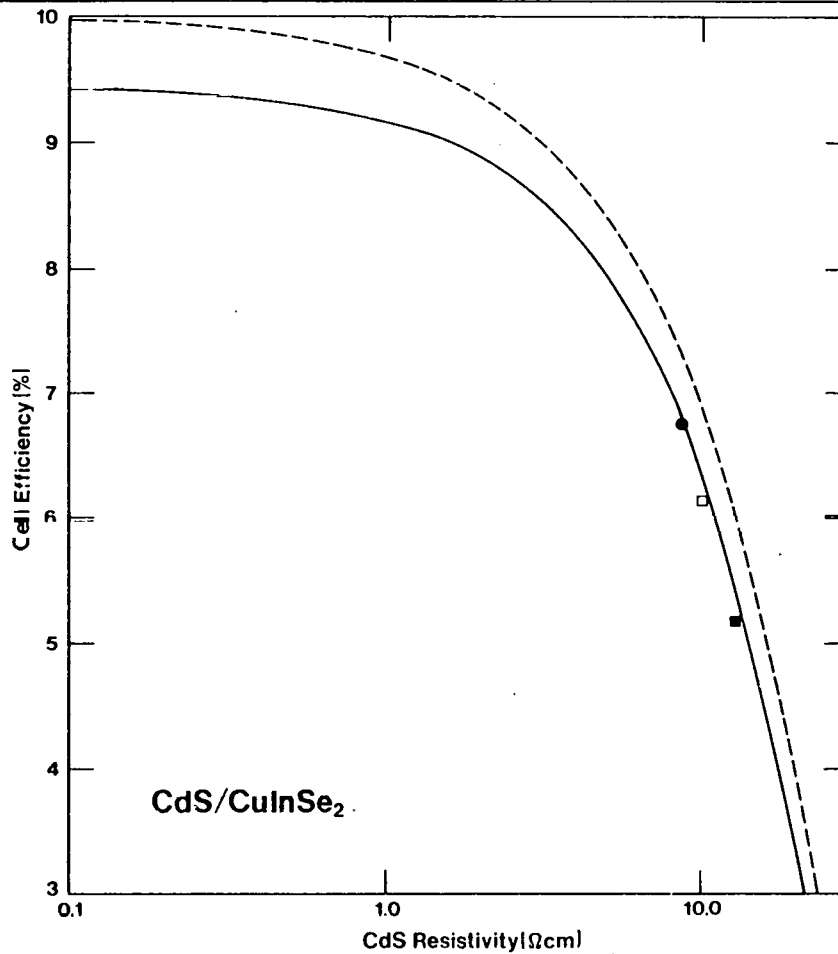


Fig. 5. Cell Efficiency as a Function of CdS Resistivity. Solid Line Indicates Calculated Data, Dashed Line is for Model with 0.25 Ω/cm<sup>2</sup> Back Contact. Symbols are Device Data, Explained in Fig. 4.

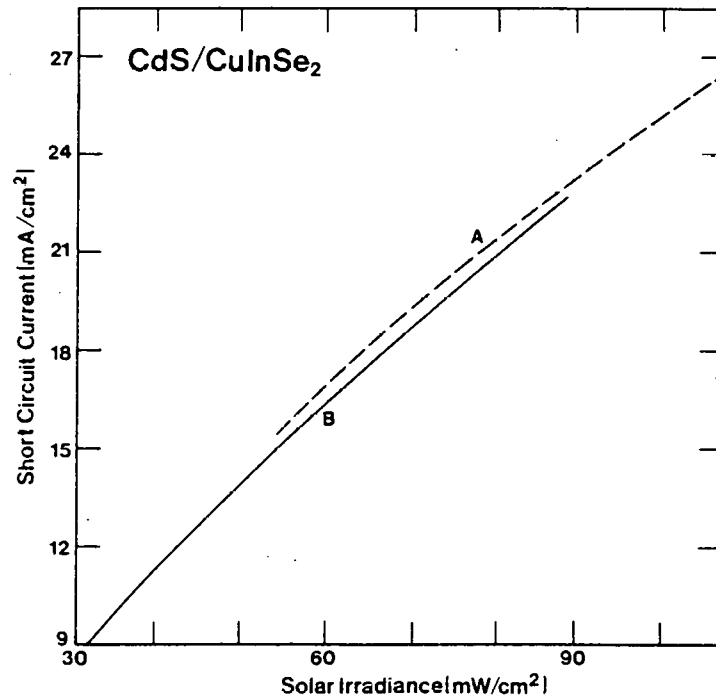


Fig. 6. J<sub>sc</sub> Dependence Upon Solar Irradiance. Curve A is for Denver, B is for Boston.

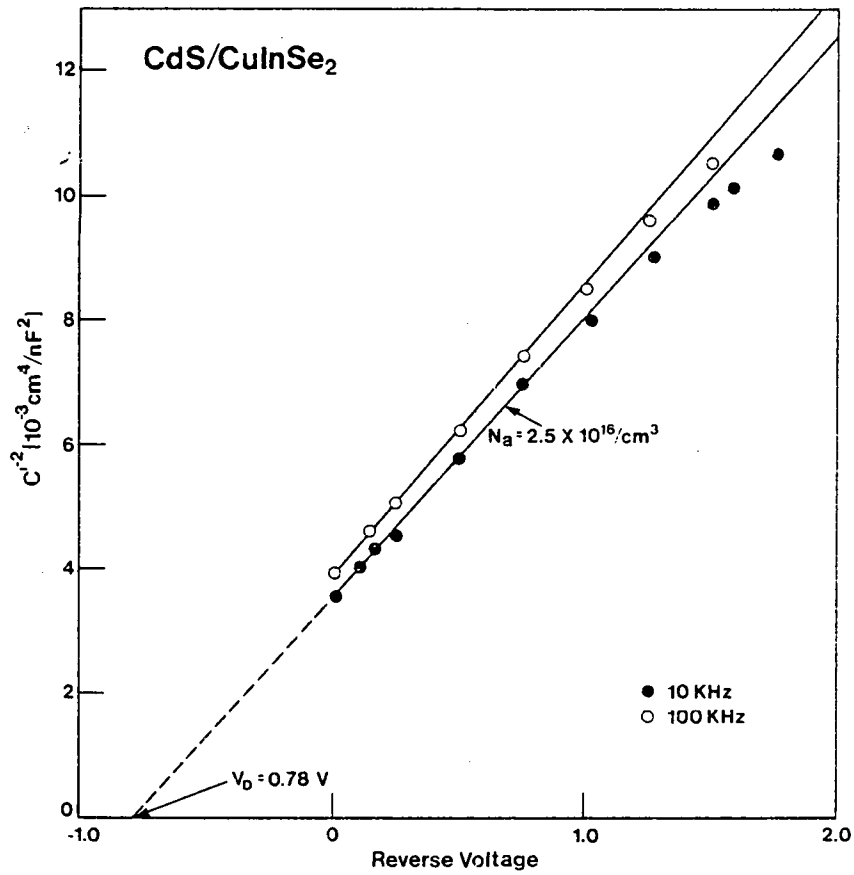


Fig. 7. Dependence of Capacitance/Unit Area,  $C^1$ , Upon Reverse Voltage. Slope Indicates  $N_a = 2.5 \times 10^{16}/\text{cm}^3$ .

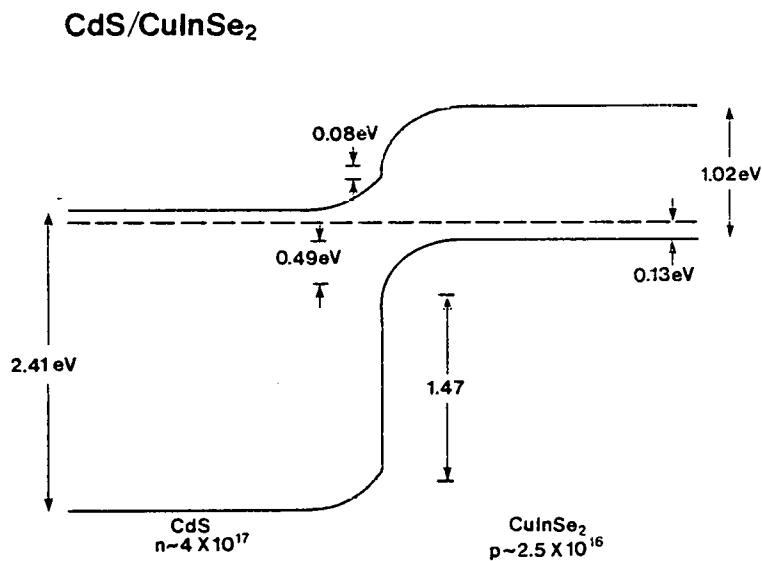


Fig. 8. Heterojunction Band Diagram for Present CdS/CuInSe<sub>2</sub> Thin Film Device.  $\Delta\chi = 0.08 \text{ eV}$ ;  $V_D = 0.78 \text{ eV}$ .

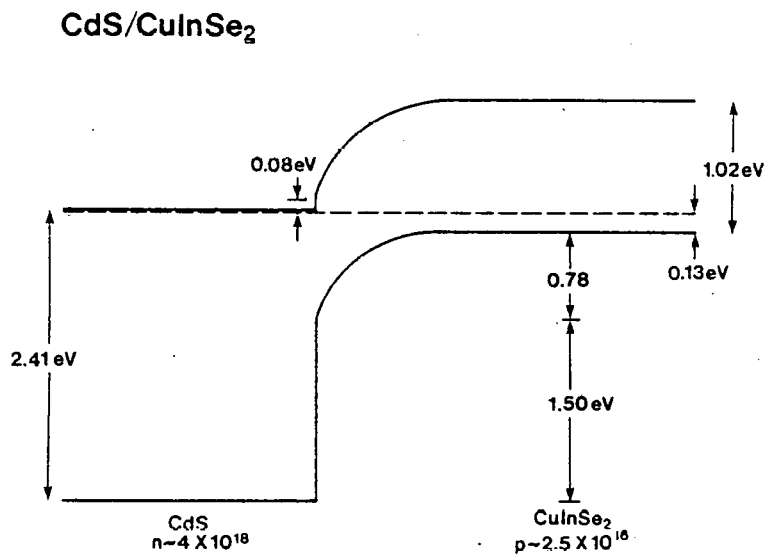


Fig. 9. Projected Heterojunction Band Diagram for CdS/CuInSe<sub>2</sub> Device.

### 3.5 FABRICATION AND CHARACTERIZATION OF ITO/CuInSe<sub>2</sub> PHOTOVOLTAIC HETEROJUNCTIONS

SERI AUTHORS: L. L. Kazmerski, and P. Sheldon

PROCEEDINGS: Proceedings of the 13th IEEE Photovoltaics Specialists Conference (IEEE New York) pp. 541-544

CONFERENCE: 13th IEEE Photovoltaics Specialists Conference  
Washington, D.C.  
June 5-8, 1978

#### ABSTRACT

The photovoltaic effect in indium-tin-oxide (ITO)/CuInSe<sub>2</sub> heterostructures has been demonstrated. An AM1 efficiency of 8.5% has been measured for a single crystal device. The thin-film analogue had a conversion efficiency of 2.08%. Although the photovoltaic effect was observed in devices with ITO deposited at room temperature, improved performance resulted at  $T_{\text{sub}} \sim 180^{\circ}\text{C}$ . Degradation in short-circuit current was noted after operation at  $200^{\circ}\text{C}$  for 10 hours in air ambient.

### 3.5.1 Introduction

Photovoltaic heterojunctions have been fabricated using Si (1), GaAs (2) and InP (2,3) in conjunction with a thin, transparent indium-tin-oxide (ITO) layer. In this application, the ITO provides a wide-bandgap window (3.7eV) which can be used effectively with a smaller bandgap (1.0-1.5eV) semiconductor. The advantage of this type of device is that the ITO heterostructure can be produced at relatively low processing temperatures, avoiding the energy intensive manufacturing steps associated with normal pn junction formation. Recent photovoltaic heterojunction calculations have indicated that the optimum bandgap of an absorbing material should lie in the range 1.0-1.2eV for utilization with a 3.7eV bandgap window (4). In this paper, the utilization of  $\text{CuInSe}_2$  ( $E_g = 1.02\text{eV}$ ) with ITO is investigated. Both ITO/ $\text{CuInSe}_2$  single crystal and thin-film devices are reported.

### 3.5.2 Experimental Techniques

The ITO films were grown by electron beam deposition, using pressed vaporization bars of 99.99% purity  $\text{In}_2\text{O}_3/9\text{M}\% \text{SnO}_2$  in the 10 KV e-beam source. The deposition procedure was performed in an ultrahigh vacuum system which had a base pressure of  $10^{-10}$  torr. The pressure in the deposition chamber was kept below  $6 \times 10^{-6}$  torr during ITO growth, with film deposition rates approximately 20-40 Å/s. The source-substrate separation was 10 cm. A conduction-type heater with a thermocouple mounted on the substrate surface was used to control substrate temperature. Although problems were encountered on glass substrates, good quality ITO was produced on  $\text{CuInSe}_2$  substrates over the temperature range 25°C-180°C. The quality of the ITO was determined using Auger electron spectroscopy (AES) compositional analysis, optical data ( $E_g = 3.7\text{eV}$ ) and, less conclusively, resistivity ( $\rho \sim 10^{-3} - 10^{-4} \Omega\text{-cm}$  at room temperature).

The substrates used in these device studies were p-type, with  $p \sim 2-8 \times 10^{16}/\text{cm}^3$ . For the polycrystalline devices, the thin-film  $\text{CuInSe}_2$  was deposited by the two-source method (5), with grain sizes in the range 1.5-2.0  $\mu\text{m}$ . The single crystal  $\text{CuInSe}_2$  substrates were grown using the Bridgman method.

The AES studies were performed with a Physical Electronics 545 Scanning Auger Microprobe operating at 3 KV, with  $I_p = 6.4 \mu\text{A}$ . Photovoltaic device performance was evaluated using a tungsten-halogen lamp, with  $100 \text{mW}/\text{cm}^2$  illumination calibrated by a  $\text{Cu}_2\text{S}/\text{CdS}$  standard (DOE/NASA Z66). A gold back contact was made to the  $\text{CuInSe}_2$ .

### 3.5.3 Results and Discussion

The initial strategy in these studies was to deposit the ITO onto the CuInSe<sub>2</sub> substrates held at room temperature. Quantitative analysis of the films showed them to be compositionally correct with sheet resistances of 100 Ω/cm<sup>2</sup>. Fig. 1 shows the dark and light I-V characteristics for an as-deposited ITO/single-crystal CuInSe<sub>2</sub> device. This device had a measured efficiency of 4.4%, with V<sub>oc</sub> = 0.31 V and I<sub>sc</sub> = 3.9 mA for the 0.125 cm<sup>2</sup> active area. Initial measurements on these small area devices led to erroneous results due to enhanced current at the edges of the ITO. (Current densities in excess of 50 mA/cm<sup>2</sup> were measured.) In order to avoid this effect, a silicon monoxide layer was deposited, leaving a 0.125 cm<sup>2</sup> aperture to the ITO.

The performance of the device in Fig. 1 was severely limited by the series resistance and low V<sub>oc</sub> of the cell. In an attempt to improve these, the device was annealed in vacuo at 200°C for 2 hours. The benefit of this treatment is shown in the I-V characteristic of Fig. 2. For this annealed device, V<sub>oc</sub> is improved to 0.41 V and FF to 0.49, with no loss in I<sub>sc</sub>. It was found, however, that no significant change was observed for annealing temperatures less than 180°C. Annealing at temperatures greater than 200°C was not attempted.

For the better transparent-layer photovoltaic devices produced to date, the ITO was grown on substrates at elevated temperatures. This apparently results in a higher quality ITO layer (lower resistivity) and an improved interface region. In this study, it was found that the ITO resistivity decreased by an order of magnitude to 5 x 10<sup>-4</sup> Ω-cm for T<sub>sub</sub> > 150°C. Fig. 3 presents the light I-V characteristic for an ITO/single-crystal CuInSe<sub>2</sub> device in which the ITO was deposited at 180°C. A further improvement in V<sub>oc</sub> (= 0.50 V) and FF (0.55), with resulting 8.5% efficiency, results. For the device in Fig. 3, the surface was ion-etched in situ before depositing the ITO. If this procedure was not followed, lower V<sub>oc</sub> and FF resulted, primarily due to the surface contamination and possibly the native oxides which occur in the normal processing routine.

The composition of the device layers and the structure of the interface region is illustrated in the AES depth-compositional profile of Fig. 4. The entire ITO layer is not shown in Fig. 4 in order to display the orderly transition from the n-type ITO to the p-type CuInSe<sub>2</sub>. Quantitative analysis of the two layers has shown them to be compositionally correct.

The large-scale deployment feasibility of devices of this type rests largely on the capability to produce intermediate efficiency versions in thin-film form (6). Fig. 5 shows the light I-V characteristics for the all thin-film version of the ITO/CuInSe<sub>2</sub> heterojunction. As experienced in most thin-film analogues, the open-circuit voltage is lower than that demonstrated in the

single crystal case. A lowering of  $J_{sc}$  also occurs. The efficiency of this  $0.125 \text{ cm}^2$  device is 2.08% with a fill factor of 0.39. It should be added that the photovoltaic effect was observed in only two of the twenty-four specimens produced. As in the case of the other thin-film ternary devices, control of the ternary layer properties is difficult and uncertain (7).

Of primary importance to the utilization of any photovoltaic device is stability. In general, the ITO devices have not experienced significant degradation when exposed to reasonable operating conditions. Fig. 6 presents the results of a stability experiment performed on one ITO/single crystal  $\text{CuInSe}_2$  device. The device was held at  $200^\circ\text{C}$  (in air) and the short-circuit current was monitored periodically.  $J_{sc}$  falls off rapidly after 10 hours of observation. No physical or elemental examination of the degraded devices was made, but this degradation mechanism may be associated with the field-aided formation of an oxide layer (perhaps  $\text{SeO}_x$  or  $\text{Cu}_x\text{O}$ ) at the interface. This effect needs further investigation, but the observed degradation is potentially a serious limitation for this device.

Anderson (8) has reported the electron affinity of ITO to be 4.5 eV. The electron affinity of  $\text{CuInSe}_2$  has been determined to be about 0.22 eV higher than this value. A schematic representation of the heterojunction band diagram of the ITO/ $\text{CuInSe}_2$  device is presented in Fig. 7.

Since  $\Delta X = -0.22\text{eV}$  (i.e., X is larger for the absorbing semiconductor), a spike occurs in the conduction band. This limits minority carrier injection (allowing recombination at the interface to dominate current flow) and lowers the potential barrier height.

#### 3.5.4 Summary

The photovoltaic effect has been demonstrated in ITO/ $\text{CuInSe}_2$  single crystal and polycrystalline (thin film) devices. An alternative method of depositing ITO thin films using electron beam techniques has been utilized. Better device performance has been observed for devices with ITO deposited at elevated substrate temperatures ( $\sim 180^\circ\text{C}$ ). A potential major problem in device degradation has been observed for devices operated at  $200^\circ\text{C}$ . The degradation mechanism has not been identified, but field-aided oxide formation at the interface is proposed.

#### 3.5.5 Acknowledgements

The authors wish to acknowledge the National Science Foundation which partially supported Mr. Sheldon through the NSF/URP Program. The assistance of Bell Telephone Laboratories in providing several single crystal substrates is also gratefully acknowledged.



### 3.5.6 References

\*This author's work partially performed at the University of Maine at Orono, ME 04473.

1. J. B. DuBow, D. E. Burk and J. R. Sites, *Appl. Phys. Lett.* 29, (1976).
2. K. J. Bachmann, W. R. Sinclair, F. A. Thiel, J. Schreiber, P. H. Schmidt, E. Spencer, E. Buehler and K. Sreeharsha, *Proc. 13th Photovoltaics Spec. Conf.* (this volume).
3. K. S. Sreeharsha, K. J. Bachmann, P. H. Schmidt, E. G. Spencer and F. A. Thiel, *Appl. Phys. Lett.* 30, 645 (1977).
4. P. J. Ireland, L. L. Kazmerski and S. Wagner (to be published).
5. L. L. Kazmerski, in Ternary Compounds 1977, Institute of Phys. Conf. Series, 35, 217 (1977).
6. E. A. DeMeo, Assessment of Cadmium Sulfide Photovoltaic Arrays for Large Scale Electric Utility Applications (EPRI Rep. ER-188, Palo Alto, CA; 1976).
7. L. L. Kazmerski, P. J. Ireland, F. R. White and R. B. Cooper, *Proc. 13th IEE Photovoltaic Spec. Conf.* (this volume).
8. R. L. Anderson, *Proc. Photovoltaics Program Semiannual Review, Advanced Materials R&D Branch, Golden, CO. DOE Publication CONF-771051* (1978), pp. 243-262.

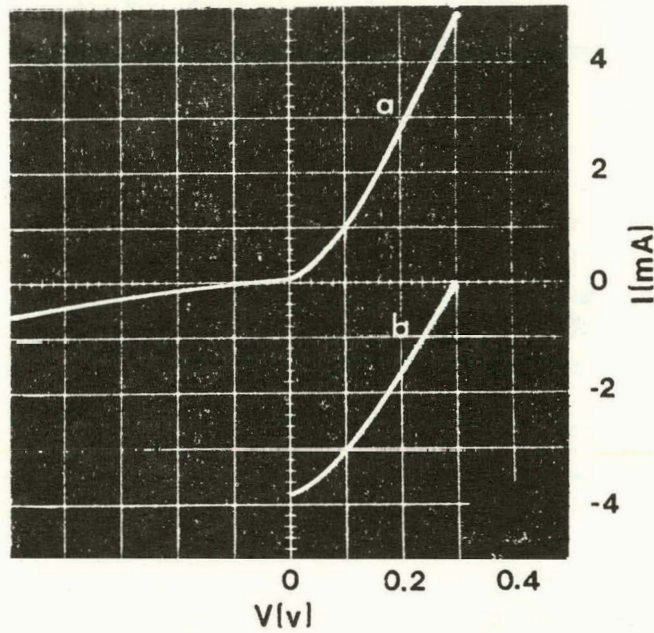


Fig. 1. ITO/CuInSe<sub>2</sub> (Single Crystal), As-Deposited Device. (a) Dark Characteristics; (b) Light Characteristics.

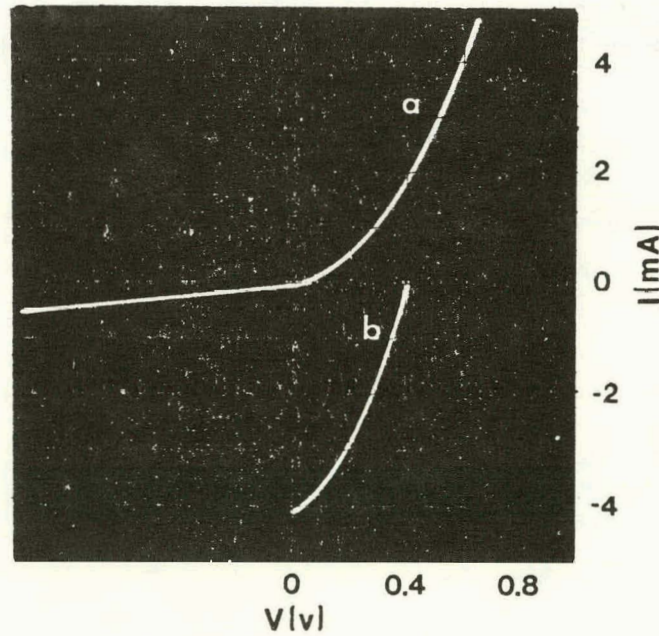


Fig. 2. ITO/CuInSe<sub>2</sub> (Single Crystal) Device, Annealed In-Vacuo, 200°C, 2 Hrs. (a) Dark Characteristics; (b) Light Characteristics.

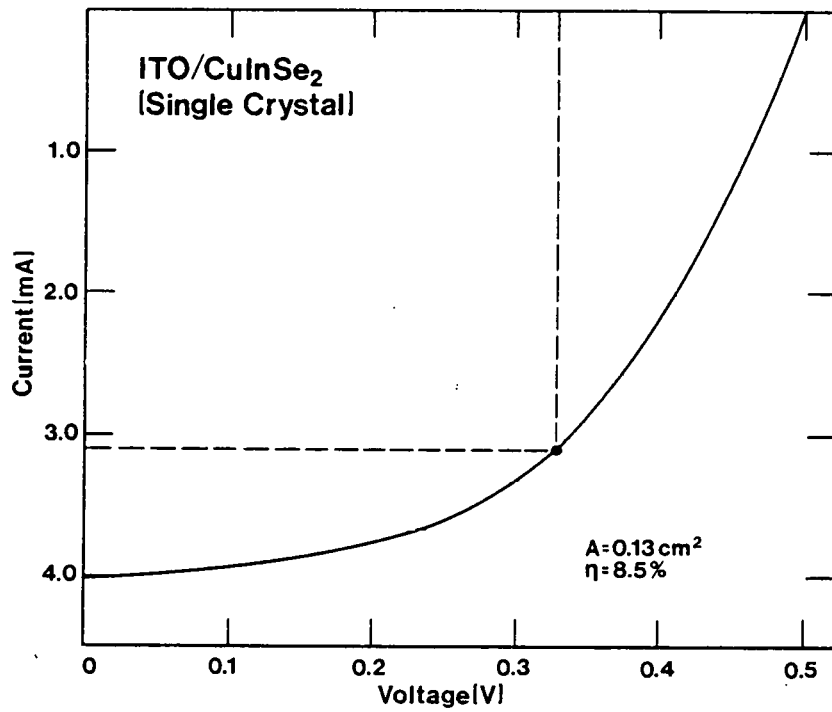


Fig. 3. Light I-V Characteristics of ITO/CuInSe<sub>2</sub> (Single Crystal) Device.

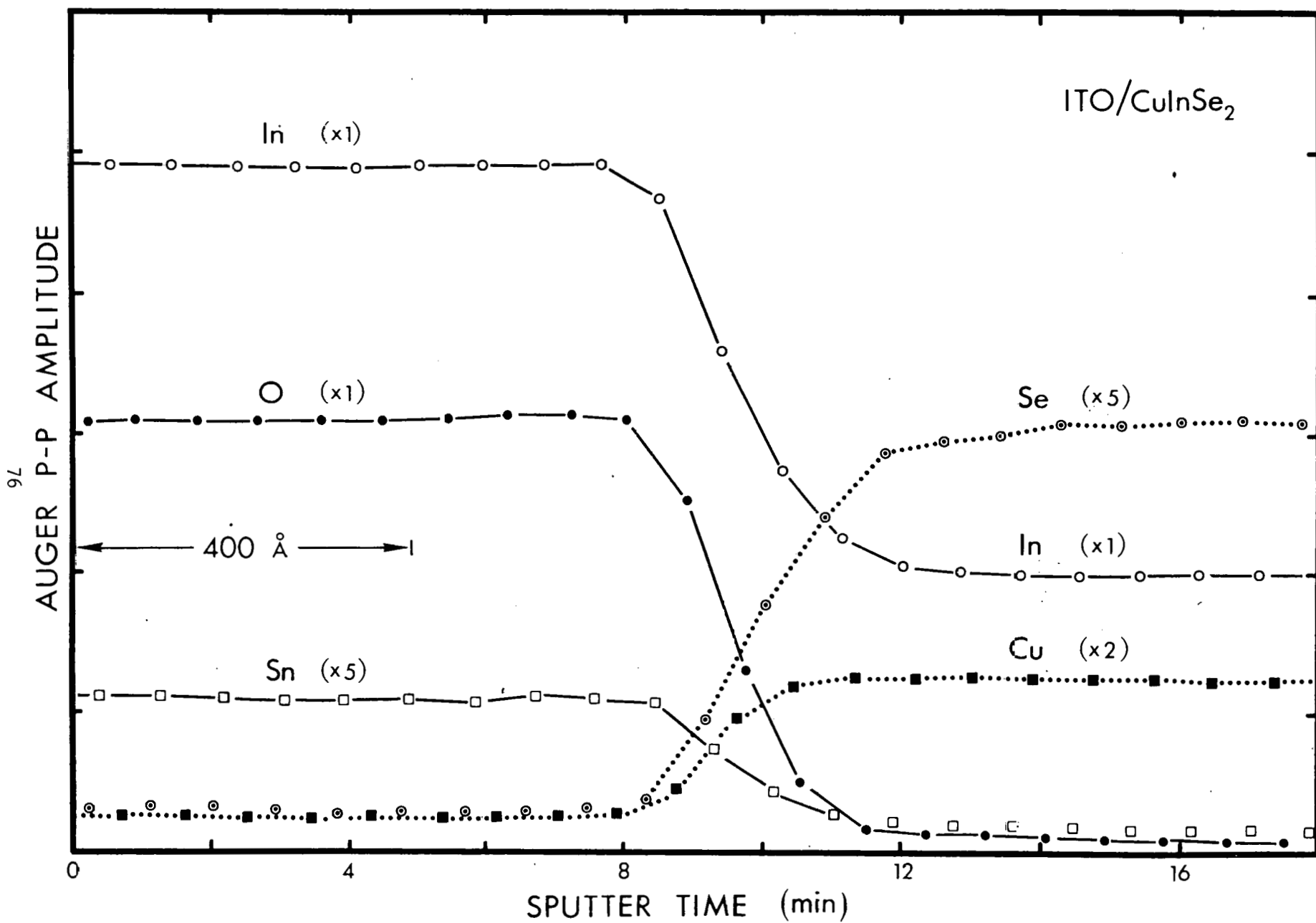


Fig. 4. AES Depth Compositional Profile of ITO/CuInSe<sub>2</sub> Photovoltaic Device.

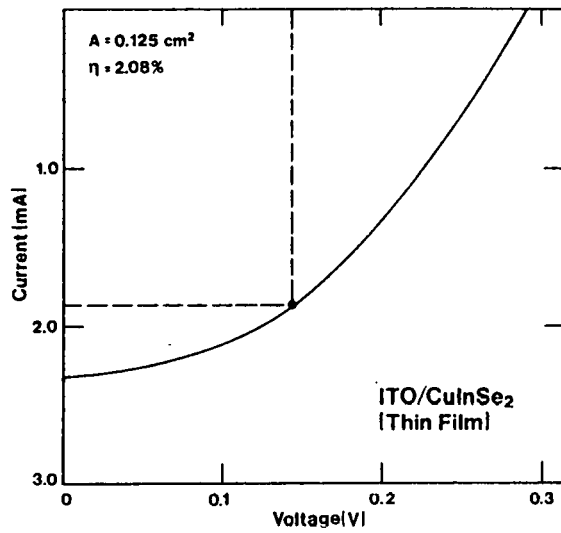


Fig. 5. Light I-V Characteristic of ITO/CuInSe<sub>2</sub> (Thin Film) Device.

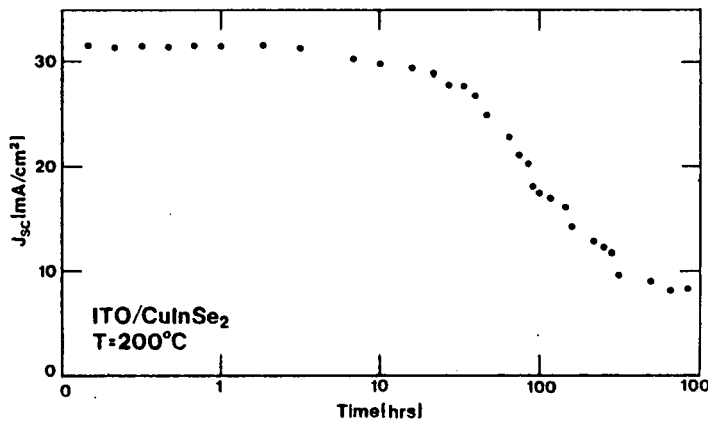


Fig. 6. Short-Circuit Current Dependence on Elevated Temperature Testing Time. ITO/CuInSe<sub>2</sub> (Single Crystal) Device Held at 200°C, in Air Ambient.

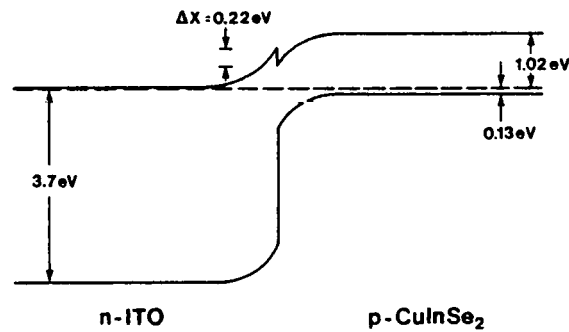


Fig. 7. Band Diagram for ITO/CuInSe<sub>2</sub> Heterostructure.

THIS PAGE INTENTIONALLY LEFT BLANK

### 3.6 EFFECTS OF GRAIN BOUNDARIES ON THE PERFORMANCE OF THIN-FILM PHOTOVOLTAIC DEVICES

SERI AUTHORS: L. L. Kazmerski, P. Sheldon, and P. J. Ireland

JOURNAL: Thin Solid Films (to appear)

CONFERENCE: 4th International Thin-Film Congress  
Loughborough, U.K.  
September 11-15, 1978

#### ABSTRACT

The effects of grain boundaries on the performance of thin-film, polycrystalline solar cells are evaluated. The dependence of the minority carrier lifetime upon grain diameter is investigated. These data are used, in turn, to determine the dependence of the collection efficiency upon grain size for various grain boundary conditions (low, medium and high-angle grain boundaries) in heterojunction solar cells. This model is compared to a geometrically derived one to account for the dependence of short-circuit current upon grain size for the CdS/CuInSe<sub>2</sub> thin-film heterostructure.

### 3.6.1 Introduction

In order to become an economical and viable entity, the thin-film, polycrystalline solar cell must demonstrate both an intermediate conversion efficiency (>10%) and adequate reliability. A major identifiable factor, among those which limit the performance and stability of this device, is the grain boundary. The relationships between grain boundary defects and the electrical and optical properties as well as the structural integrity of semiconductor thin films have been considered in several previous investigations.<sup>1-4</sup> For photovoltaic performance, Card and Yang<sup>5</sup> discussed the effects of grain boundary recombination on the open circuit voltages and short circuit currents of Si Schottky barrier and p<sup>+</sup>-n junction solar cells. Recently, Fraas<sup>6</sup> has presented a qualitative description of grain boundary effects in polycrystalline heterojunction solar cells, treating the grain boundary as a surface in accumulated, depleted or inverted conditions. The net effect of grain boundaries is to increase the dark current, reduce the short circuit (light) current, decrease the shunt resistance and series conductance and lower the open circuit voltage of the solar cells. A quantitative examination of grain boundary mechanisms in compound semiconductor thin-film photovoltaic devices has also been presented.<sup>7</sup> In this, the interrelationships between minority carrier recombination, grain size and open circuit voltage are derived. The present paper extends upon this treatment by relating the collection efficiency,  $\eta_{coll}$ , of the heterostructure to the grain boundary recombination and carrier lifetime. In turn, the AM1 short circuit currents are derived and the dependences of these currents on grain diameter and grain boundary configuration are evaluated. Finally, the validity of the results are examined for the CdS/CuInSe<sub>2</sub> heterojunction solar cell.

### 3.6.2 Discussion of Results

#### 3.6.2.1 The Grain Boundary and Carrier Lifetime

A representation of the band diagram of the region surrounding a grain boundary in a p-type semiconductor is shown in Fig. 1 for both the (a) dark and (b) illuminated cases. This model has been utilized to calculate the diffusion potential profile surrounding this defect region.<sup>7</sup> The potential is a function of the grain boundary interface state density,  $N_i$ , which corresponds approximately to the following grain boundary types:

(i) High-angle grain boundaries ( $25^\circ < \theta < 90^\circ$ ):  $N_i > 10^{13}/\text{cm}^2\text{-eV}$

(ii) Medium-angle grain boundaries ( $1^\circ < \theta < 25^\circ$ ):  $10^{13} > N_i > 10^{11}/\text{cm}^2\text{-eV}$

and,

(iii) Low-angle grain boundaries ( $\theta < 5^\circ$ ):  $N_i < 10^{11}/\text{cm}^2\text{-eV}$



where  $\theta$  is the misfit angle between the adjacent grains. The recombination current and recombination velocity can be related to the diffusion potential and, in turn, the relationship between the grain boundary minority carrier lifetime,  $\tau$ , and the grain size can be determined.<sup>7</sup> This dependence is presented in Fig. 2 for CuInSe<sub>2</sub>. The bulk (single crystal) lifetime is indicated by the dashed line. For the high angle grain boundary case, with a typical  $10^{-4}$  cm grain size, the minority carrier lifetime is in the range  $10^{-9}$  -  $10^{-10}$  s, or about an order of magnitude lower than the reported single crystal case.<sup>7</sup>

### 3.6.2.2 Grain Boundary-Solar Cell Effects

The short circuit current density for a heterojunction solar cell can be expressed:<sup>8</sup>

$$J_{sc} = \mu F(\phi') / (S_I + \mu F(\phi')) \int_{\lambda} \phi_o(\lambda) T_g R'(\lambda) A'(\lambda) \eta_{coll}(\lambda, \tau) d\lambda \quad (1)$$

where  $\mu$  is the carrier mobility;  $F$ , the electric field at the junction;  $\phi'$ , the photon flux at the junction;  $\phi_o$ , the incident photon flux;  $T_g$ , the optical transmission of the top electrode;  $R'(\lambda)$  and  $A'(\lambda)$ , functions of the reflection and absorption parameters; and,  $\eta_{coll}$ , the collection efficiency.<sup>9</sup> Rothwarf used a geometrical argument to account for carrier recombination.<sup>9</sup> In this, all carriers generated closer to the grain boundary than the junction are lost. Using a cylindrical grain model, the calculated collection efficiency is<sup>9</sup>

$$\eta_{coll} = 1 + (4/\alpha \delta) (2/\alpha \delta - 1) + \exp(-\alpha d) / (1 - \exp(-\alpha d)) \cdot (4d/\delta) (1 - d/\delta - 2/\alpha \delta) \quad (2)$$

where  $\alpha$  is the absorption coefficient;  $\delta$ , the grain diameter;  $d$ , the film thickness. Eq. 2 is for the case of a cell illuminated through the higher bandgap (window) semiconductor, with  $\delta/2 > d$ . A complementary expression was reported for  $\delta/2 < d$ .<sup>9</sup> This geometrical model qualitatively accounts for the decrease in  $J_{sc}$ , and has been used effectively in a lost minimization formalism for the terms of the minority carrier lifetime.<sup>7,10</sup>

$$\eta_{coll} = \frac{[\exp(-d/\sqrt{D_1 \tau_1}) - \exp(-\alpha d)] [\alpha - 1/\sqrt{D_2 \tau_2}]}{[\exp(-d/\sqrt{D_2 \tau_2}) - \exp(-\alpha d)] [\alpha - 1/\sqrt{D_1 \tau_1}]} \quad (3)$$

where the subscript "1" refers to the polycrystalline case and "2" to the single crystal case.  $D$  is the carrier diffusion coefficient. The dependence of  $\eta_{coll}$  (Eq. 3) upon  $\tau$  for a CdS/CuInSe<sub>2</sub> (1 $\mu$ m) device is shown in Fig. 3.

Combining Eq. 3 with the dependence of  $\tau$  on  $\delta$  (Fig. 2),  $\eta_{\text{coll}}$  can be determined as a function of grain size. This is presented in Fig. 4 for various interface state densities. Also shown by the dashed line in Fig. 4 is the corresponding data for the geometrical model (Eq. 2 and its complement). These data correspond roughly to a thin-film device with a high density of high-angle grain boundaries.

In the case of the thin-film CdS/CuInSe<sub>2</sub>, the recombination and collection efficiency geometrical model represented in Eq. 2 consistently predicts short circuit currents lower than those measured. Diffraction data taken on the ternary thin films indicate a relatively significant density of medium angle grain boundaries.<sup>7</sup> Fig. 5 shows  $J_{\text{sc}}$  as a function of grain diameter for several CdS/CuInSe<sub>2</sub> devices<sup>11</sup> with a 1  $\mu\text{m}$  thick ternary layer. The solid line indicates the model of Fig. 4 with  $N_i = 5 \times 10^{12}/\text{cm}^2\text{-eV}$ . A relatively good fit to the data, especially for higher  $\delta$  values is observed. The dashed line indicates the corresponding dependence for the geometrical model.

### 3.6.3 Observations and Conclusions

The dependence of the minority carrier lifetime on grain diameter for thin, polycrystalline solar cells has been reported. Those data have been combined with the expression for collection efficiency to evaluate  $\eta_{\text{coll}}(\delta)$  for various grain boundary conditions. These data indicate that the geometrical model for grain boundary recombination proposed by Rothwarf<sup>9</sup> roughly corresponds to a high angle grain boundary condition. An improvement over this model is observed in the case of the CsS/CuInSe<sub>2</sub> heterostructure, using the lifetime model (Eq. 3) with a mix of high and medium angle grain boundaries.

The results of this paper can be combined with previous calculations of  $V_{\text{oc}} - \delta$  dependences,<sup>7</sup> interface contributions<sup>7</sup> and fill-factor determinations<sup>8</sup> to effectively account for the performance of photovoltaic heterostructures. These evaluations can also be utilized to predict attainable efficiencies for thin-film polycrystalline solar cells.

### 3.6.4 References

1. See, for example, H. F. Matare, Defect Electronics in Semiconductors, Wiley Interscience, New York, 1971, pp. 222-234.
2. R. L. Petritz, Phys. Rev. 104 (1956) 1508.
3. T. H. DiStefano and J. J. Cuomo, Appl. Phys. Lett. 30 (1977) 351.
4. L. L. Kazmerski (Proc. of this conference).

5. H. C Card and E. S. Yang, IEEE Trans. Electron Dev. ED-24 (1977) 397.
6. L. M. Fraas, J. Appl. Phys. 49 (1978) 871.
7. L. L. Kazmerski, Proc. Int. Conf. on Recomb. in Semiconductors, Southampton (1978) (In press).
8. A. Rothwarf and A. M. Barnett, Proc. IEEE Trans. Electron Dev. ED-24, (1977) 381.
9. A. Rothwarf, Proc. 12th IEEE Photovoltaic Spec. Conf., Baton Rouge, IEEE, New York, 1977, 488.
10. S. M. Sze, Physics of Semiconductor Devices, Wiley Interscience, New York, 1969, pp. 640-647.
11. L. L. Kazmerski, in G.D. Holah (ed.) Ternary Compounds 1977, Vol. 35, Instit. of Phys. Conf. Series, London, 1977, p. 217.

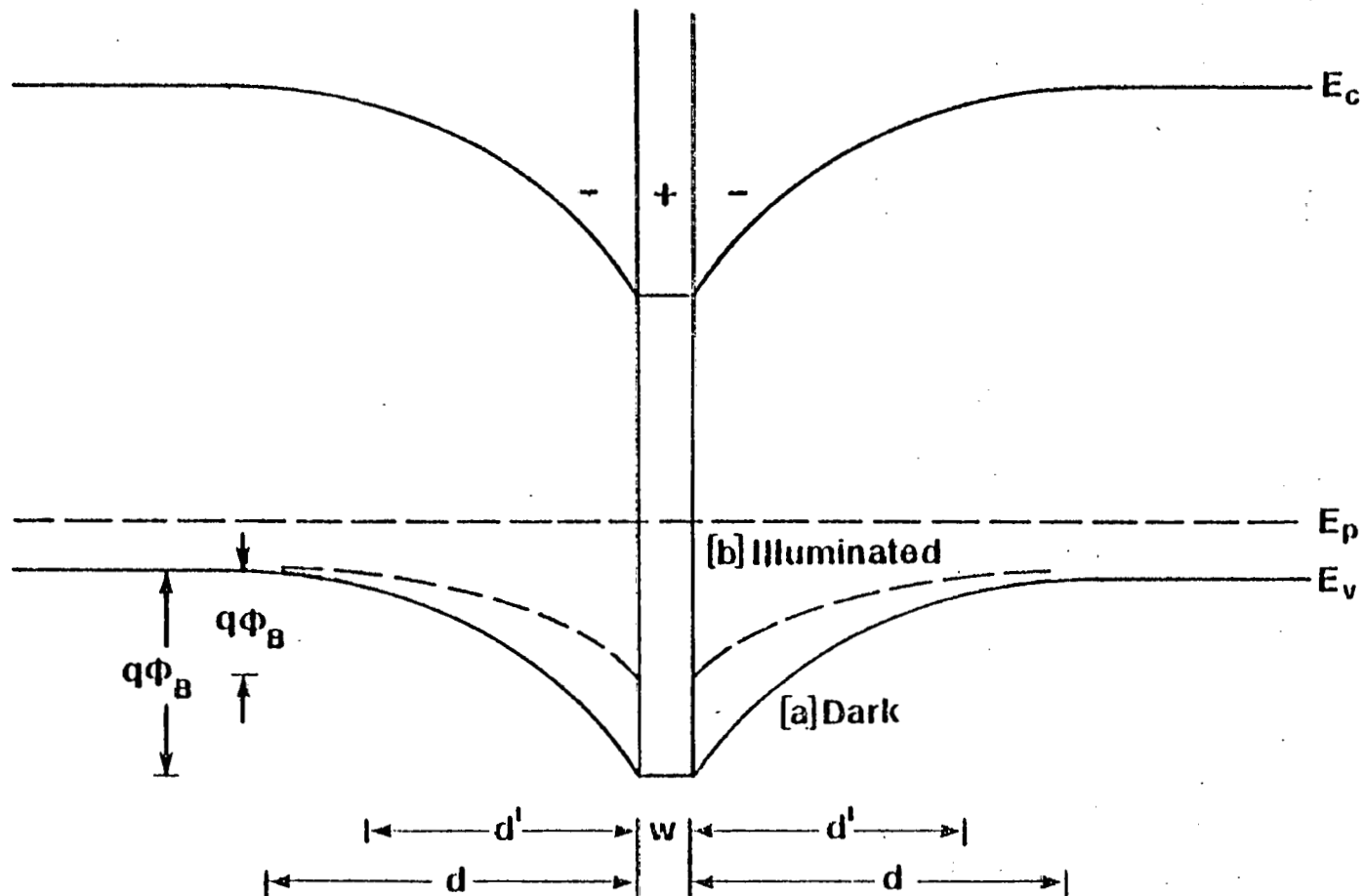


Fig. 1 Energy band diagram for the grain boundary region of p-type semiconductor: (a) Dark case with diffusion potential  $q\phi_b$ ; (b) Illuminated case, with diffusion potential  $q\phi_b'$ .

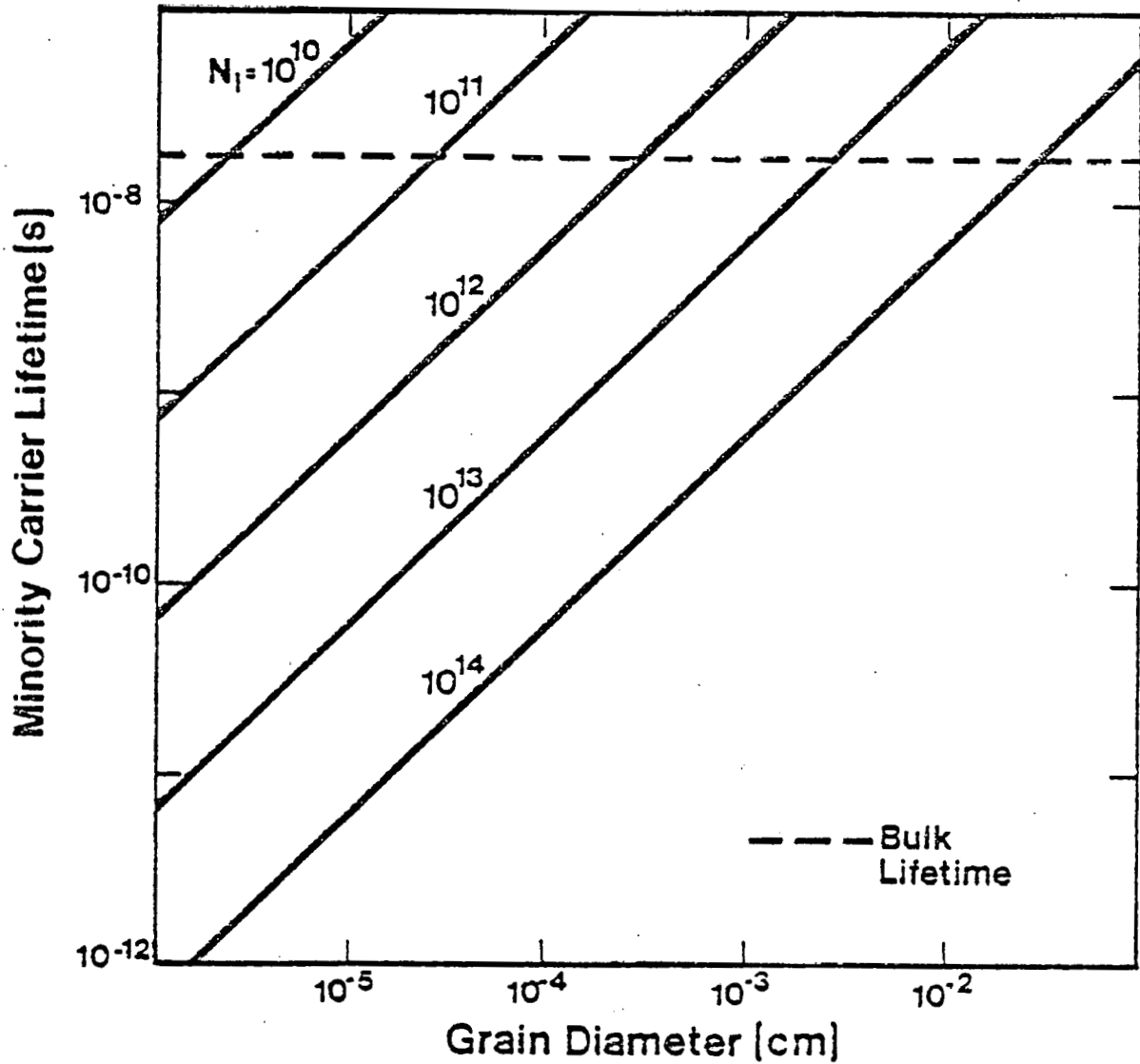


Fig. 2 Dependence of minority carrier lifetime on grain diameter for various interface state densities in p-CuInSe<sub>2</sub>. Dashed line indicates single crystal minority carrier lifetime.

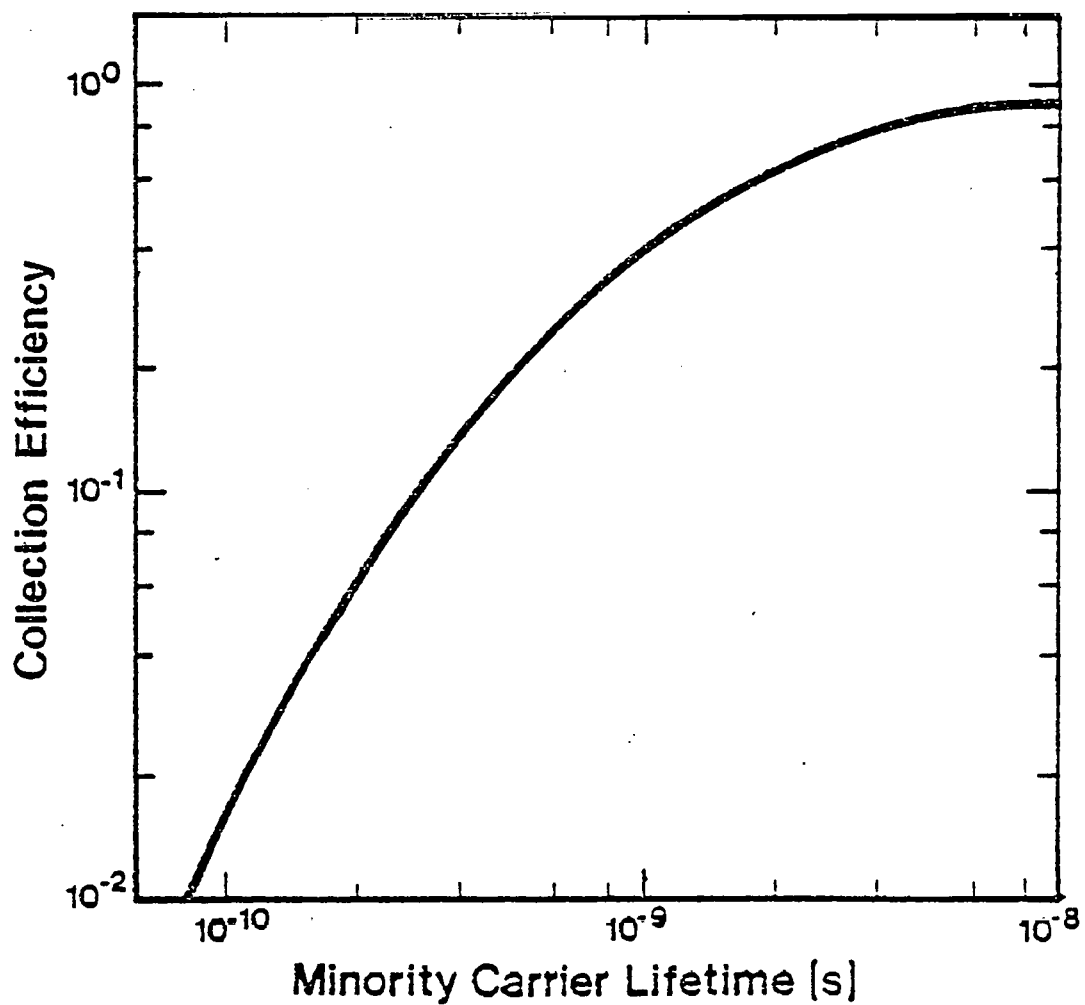


Fig. 3 Collection efficiency as a function of minority carrier lifetime for CdS/CuInSe<sub>2</sub> heterojunction. CuInSe<sub>2</sub> thickness is 1  $\mu$ m.

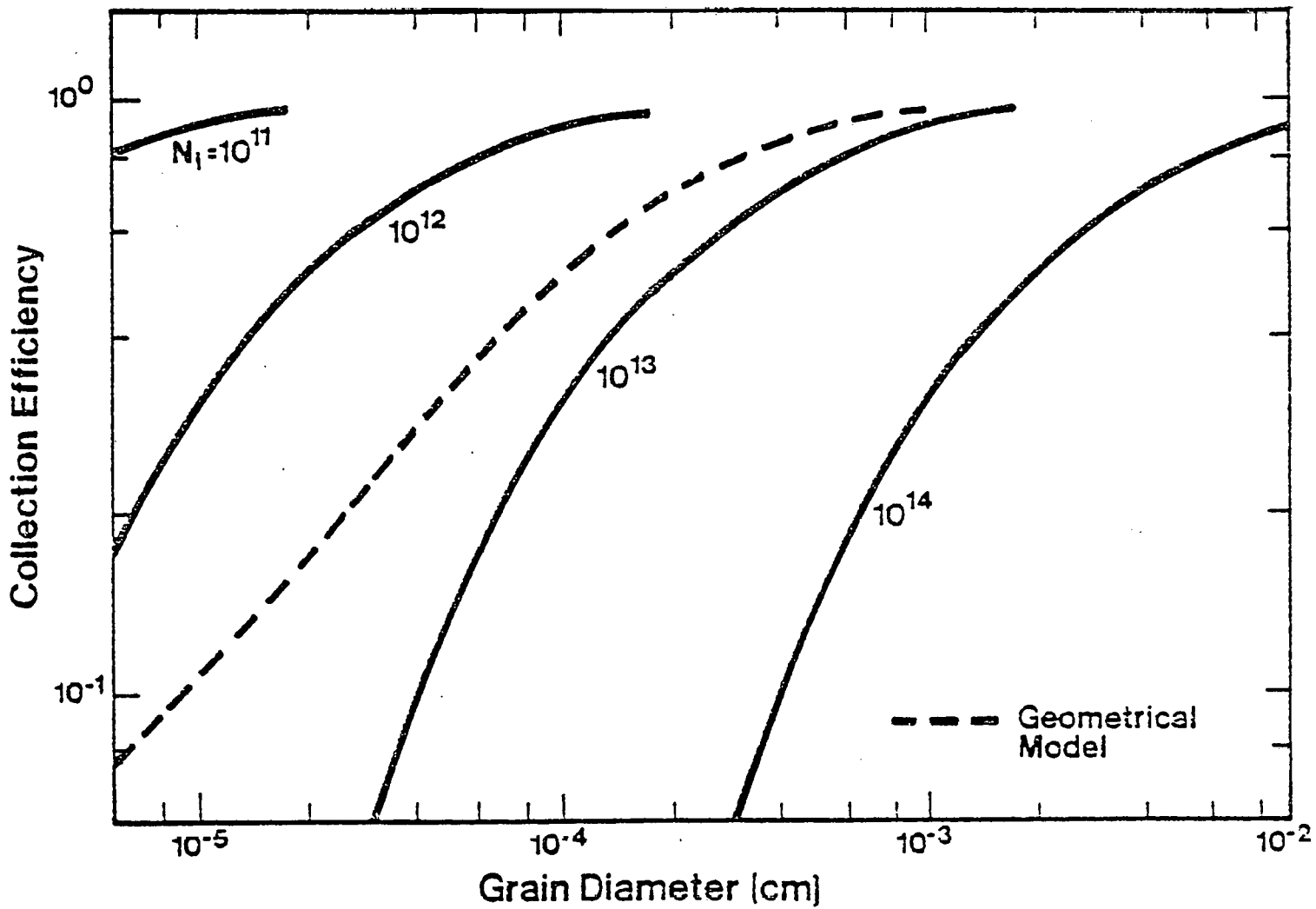


Fig. 4 Dependence of collection efficiency upon grain size for various interface state densities (CdS/CuInSe<sub>2</sub> heterostructure). Dashed line indicates geometrical model.<sup>9</sup>

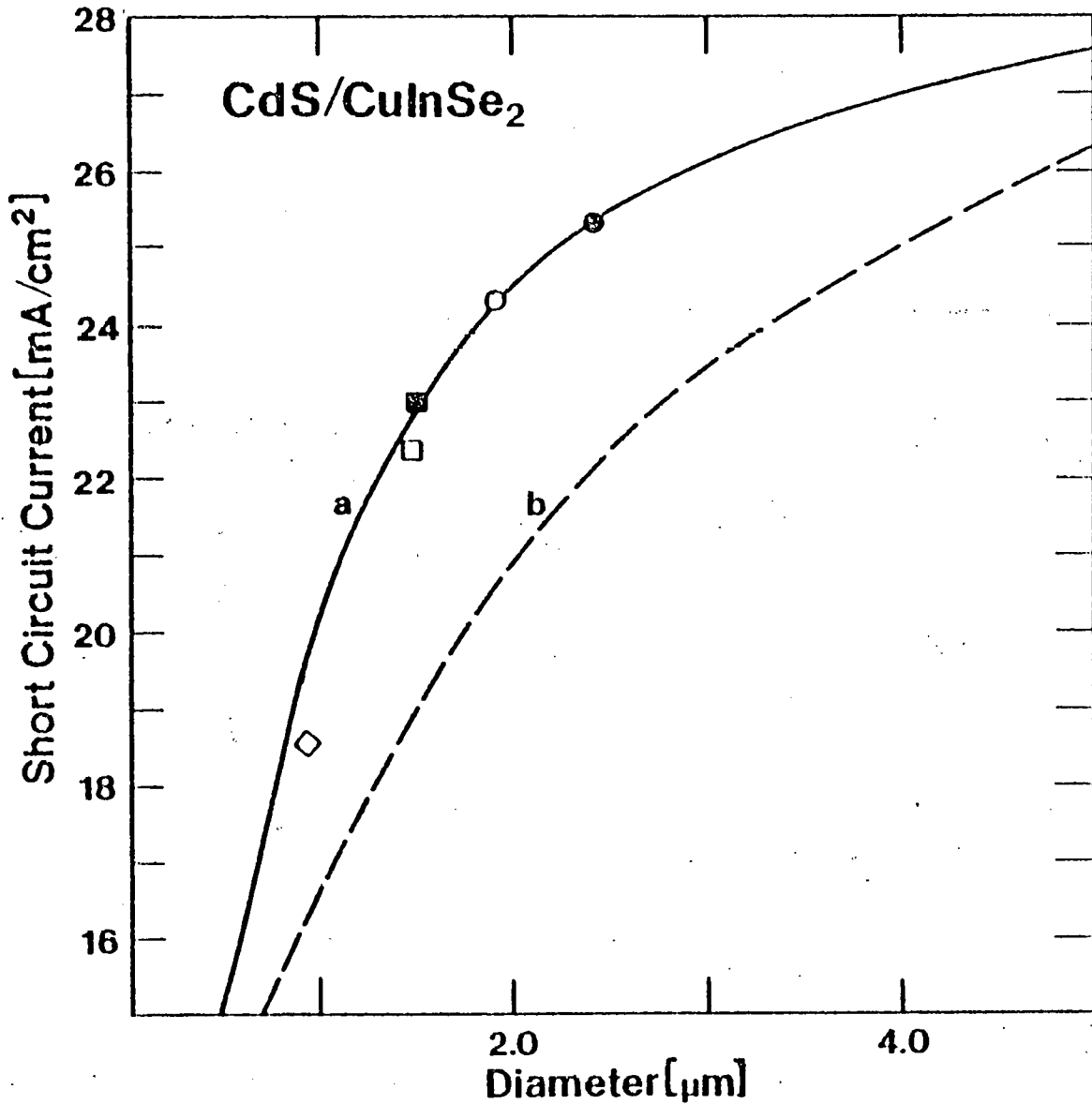


Fig. 5  $J_{sc}$  as a function of grain size. Solid line represents model of Eq. 3; dashed line, geometrical model of Eq. 2. Data are for CuInSe<sub>2</sub> thin-film devices: ● - 6.6% efficient device; ○ - 6.1% efficient device; ■ - 5.4% efficient device; □ - 5.2% efficient device; and, ◆ - 4.0% efficient device.



### 3.7 ATTAINABLE EFFICIENCIES WITH THIN-FILM HETEROJUNCTION SOLAR CELLS (Abstract Only)

SERI AUTHOR: L. L. Kazmerski, and P. J. Ireland

ABSTRACT: Bulletin of the American Physical Society

CONFERENCE: APS March Meeting  
Washington, D.C.  
March 27-30, 1978

#### ABSTRACT

The expected performances of several thin-film heterojunction solar cells are predicted based upon reliable materials' properties. The short-circuit currents, open-circuit voltages and fill-factors are calculated based primarily on the approach of Rothwarf and Barnett. These calculations consider film electrical properties (resistivity, carrier concentrations, mobility, energy bandgaps, electron affinities, grain sizes, lattice matches, interface and grain boundary recombinations). The performance status of several heterojunction (InP/CdS, CuInSe<sub>2</sub>/CdS, CuInS<sub>2</sub>/CdS) is compared with the predicted attainable values. Therefore, critical areas for device improvement are indicated and the expected device efficiencies are predicted.

THIS PAGE INTENTIONALLY LEFT BLANK

### 3.8 STABILITY AND TERNARY CHALCOPYRITE PHOTOVOLTAIC DEVICES

SERI AUTHORS: L. L. Kazmerski

PROCEEDINGS: Proceedings of the NBS Workshop of Stability of Thin Film Solar Cells and Materials

CONFERENCE: NBS Workshop on the Stability of Thin-film Solar Cells and Materials  
Gaithersburg, MD  
May 1-3, 1978

#### ABSTRACT

The photovoltaic effect in several thin-film homo- and heterodiodes using I-III-VI<sub>2</sub> semiconductors has been demonstrated. The majority of this work has centered on the Cu-ternaries (i.e, CuInS<sub>2</sub>, CuInSe<sub>2</sub>, and CuInTe<sub>2</sub>), and the success--both in demonstration and stability--has varied. CuInS<sub>2</sub> and CuInSe<sub>2</sub> thin-film homojunctions, and heterojunctions of these ternaries and CuInTe<sub>2</sub> with CdS, have been reported. Light J-V characteristics (under 100 mW/cm<sup>2</sup> illumination) of the best of these devices produced to date are presented in Fig. 1.<sup>3</sup> It should be stressed that work on the Cu-ternaries--especially the thin-film photovoltaic devices--is still in its infancy. Relatively little is yet known about the device compatibility of these materials, and much good semiconductor research remains to be accomplished for them. This paper attempts to discuss the problems and stability of the Cu-ternary devices and materials based upon the experience with some laboratory research devices.

### 3.8.1 Structure and Growth

The Cu-ternaries used in photovoltaic devices crystallize into the chalcopyrite structure. This relatively complex arrangement is shown in the 110-projection of Fig. 2. The unit cell, indicated by the dashed lines in Fig. 2, is represented more clearly for  $\text{CuInS}_2$  in Fig. 3. The chalcopyrite structure is a fairly stable arrangement for the Cu-ternaries. As an example,  $\text{CuInSe}_2$  possesses this structure to  $810^\circ\text{C}$ , above which critical temperature a pseudocubic lattice structure results.<sup>4</sup> Actually in the growth of this material, crystallization into this pseudocubic modification takes place at  $986^\circ\text{C}$  and then transforms to the tetragonal phase of  $810^\circ\text{C}$  due to the ordering of the metal atoms. As might be expected for the evaporation process used to produce these ternary compounds in thin-film form, the control of the structural, electrical and optical properties is a sensitive and complex problem which depends critically on the ensemble of deposition conditions, handling and post deposition treatments. If two layers are required (e.g. for devices), the problems multiply. To this time, a two-source deposition scheme has been necessary to control the chalcogen content, the Cu-vacancy level, and the resulting film majority carrier type. This method has produced the best device-quality layers, but better control and reproducibility are needed.

X-ray and electron diffraction data relating structural properties to deposition conditions have been reported.<sup>5</sup> Films have varied from multiphased (detecting such compounds as  $\text{Cu}_2\text{X}$  and  $\text{In}_2\text{X}_3$ , where  $\text{X} = \text{S}, \text{Se},$  or  $\text{Te}$  depending on the evaporant) to good single phase material. Recently, the presence of a semiconducting spinel ( $\text{CuIn}_5\text{S}_8$ ) has been detected in In-rich grown " $\text{CuInS}_2$ ."<sup>6</sup> This spinel has properties similar to the chalcopyrite ternary, and only a slightly smaller bandgap. The potential for existence of this spinel exists for the other ternaries as well.

### 3.8.2 Impurity Diffusion and Interdiffusion

The investigations on doping the chalcopyrite-type compounds have indicated rapid changes in the electrical conductivity upon annealing and the rapid diffusion of electrically active defects.<sup>7</sup> Examples include the increase in resistance during the preparation of CdS heterojunctions, and the net drop in acceptor concentration at the CdS/ $\text{CuInSe}_2$  interface.

Most diffusion investigations have centered on impurities in  $\text{CuInSe}_2$ . In single crystals the diffusion coefficient has been found to be essentially independent of the diffusing species, whether it be Cu, Zn, Se, Cd or Ag. The rate controlling process seems to be the in- or outdiffusion of Se. Tell et al., have reported the diffusion coefficients at  $300^\circ\text{C}$  for Cu, Zn and Cd (from an elemental film source) to be  $1.4 \times 10^{-8} \text{cm}^2/\text{s}$  into  $\text{CuInSe}_2$ .

The diffusion problem in the thin polycrystalline film is enhanced with a more rapid process at the grain boundary. The relatively high room temperature diffusion coefficients reported for Cd (and other diffusants) were perceived to be potential degradation problems in the CdS/Cu-ternary heterostructures.

Fig. 4 shows a depth-compositional profile of one of the better CdS/CuInSe<sub>2</sub> devices (efficiency = 5.2%). It was fabricated completely in situ and exhibits a relatively orderly change from the n-CdS to the p-ternary side. Neither the entire CdS layer, which was 4 μm thick, nor the entire CuInSe<sub>2</sub> (0.46 μm) is represented in Fig. 4 so that the junction region can be better examined. In addition to the five elements involved in the two thin films, the oxygen level was also monitored. In the in situ fabricated devices, no oxygen was detected either in the films or in the junction region.

A related problem which plagues the cases in which the device undergoes an external annealing (in Ar-H<sub>2</sub>Se) after ternary deposition is shown in Fig. 5. Although relatively constant CdS and CuInSe<sub>2</sub> layers are produced and good transition of the elements from one side of the junction to the other is apparent, and oxide layer results at the interface. The source of the oxide is presumed from the inevitable exposure to atmosphere during transfer and to some oxygen in the annealing environment itself. The extent of the resulting oxide region can be limited by etching the ternary prior to the CdS deposition but it has not been eliminated completely.

The device characteristics have shown significant improvement by annealing the solar cell for short periods (10-20 min) in 10<sup>-1</sup> Pa vacuum. The indication that elemental Cd has a high diffusion coefficient in CuInSe<sub>2</sub> crystals provided some concern. Since some enhancement of the diffusion process is expected along the grain boundaries of the polycrystalline thin films and since some of these devices had shown degradation in output upon heat treatments, a study of the diffusion of the Cd from the CdS layer into the ternary thin film was initiated.

Fig. 6 shows the junction region of a device which had been annealed at 600 K for two hours. This device was fabricated under the same in situ conditions as the one shown in Fig. 4 and had similar performance characteristics. The most apparent effect of the annealing treatment is the diffusion of the Cd into the ternary film. The S, Cu, In and Se profiles are not drastically changed. Using the Hall-Morabito formalism<sup>10</sup> for determining the grain boundary diffusion coefficient (using the detectability limits of AES)  $D$  can be obtained. Fig. 7 shows  $D$  as a function of inverse annealing temperature for diffusion of Cd from CdS into a CuInSe<sub>2</sub> thin film. The data are taken for devices which had been fabricated under the identical in situ conditions, and only the post-deposition annealing temperature was changed. The grain boundary diffusion coefficient follows the relationship:

$$D' = D_0 \exp(-E_a/kT) \quad (1)$$

where  $D_0 = 10.6 \text{ cm}^2/\text{s}$  and  $E_a = 1.5 \text{ eV}$  for this case.

The diffusion of Cu into the CdS is minimal as discernible in Auger data only at annealing temperature exceeding 575 K. The degradation of the Cu<sub>2</sub>S-CdS cell is partially attributed to this mechanism. It has been proposed that the Cu-grain boundary migration problem would not be as serious in the CdS/CuInSe<sub>2</sub> cell owing to the fact that Cu is more tightly bound in the chalcopyrite lattice. These diffusion studies seem to verify this proposition.

Studies similar to those of Tell et al.,<sup>8</sup> have been performed using AES and an elemental Cd film diffusion source for both single crystal and thin-film CuInSe<sub>2</sub>. Fig. 7 shows the results for:

(a) Thin film, bulk diffusion within grain, elemental Cd-source:

$$D = 154 \exp(-1.25 \text{ eV}/kT)$$

(a') Thin film grain boundary diffusion, elemental Cd-source:

$$D = 8.4 \times 10^3 \exp(-1.15 \text{ eV}/kT)$$

(b) Single crystal, bulk diffusion, elemental Cd-source:

$$D = 160 \exp(-1.22 \text{ eV}/kT)$$

(c) Single crystal, bulk diffusion, elemental Cd-source (Tell et al.)

$$D = 164 \exp(-1.19 \text{ eV}/kT)$$

For comparison:

(e) Thin-film  $\text{CuInSe}_2$ , grain boundary diffusion, CdS source:

$$D' = 13.8 \exp(-1.5 \text{ eV/kT})$$

Similar data taken for  $\text{CuInS}_2$  and  $\text{CuInTe}_2$  reveal:

(i) Thin-film  $\text{CuInS}_2$ , grain boundary diffusion, CdS source:

$$D' = 13.8 \exp(-1.7 \text{ eV/kT})$$

(ii) Thin-film  $\text{CuInTe}_2$ , grain boundary diffusion, CdS source:

$$D' = 5.05 \exp(-1.38 \text{ eV/kT})$$

The differences between the CdS and the Cd diffusant sources are attributed to (1) the differences in concentrations and concentration gradients, (2) the stress differences at the interface, and (3) the difference in activation from each source. The agreement of the Cd-source data with that of Tell *et al.*<sup>8</sup> is remarkable considering the difference in analysis techniques. It seems to support the proposition that the ternaries have high vacancy populations which dominate the diffusion process.

Recent absorption coefficient measurements on  $\text{CuInS}_2$  thin films have detected the presence and effects of the Cu-vacancies.<sup>9</sup> The shoulder in the  $\alpha$  vs photon energy characteristics (see Fig. 8) corresponds to a strong Cu-vacancy band as represented in Fig. 9.

### 3.8.3 Summary

More work on the production and demonstration of ternary devices is necessary before a useful, systematic study can be made. The initial investigations reveal, however:

- The growth techniques and deposition parameters used in ternary film production critically affect structural and electrical properties and related device stability.
- Diffusion of many elements into crystalline regions is independent of diffusion species and the diffusion coefficient is relatively high due to vacancy population in the ternary.
- Interdiffusion along grain boundaries in the CdS/Cu-ternary devices can result in device degradation and failure especially for temperatures exceeding 500 K.

- Due to the fast diffusion of metals into the ternaries, the reliability of contacts may prove to be a problem.

### 3.8.3 References

1. L. L. Kazmerski, F. R. White and G. K. Morgan, Appl. Phys. Lett. 29, 268 (1976).
2. L. L. Kazmerski, F. R. White, M. S. Ayyagari, Y. J. Juang and R. P. Patterson, J. Vac. Sci. Technol. 14, 65 (1977).
3. L. L. Kazmerski, Instit. of Phys. Conf. Series 35, 217 (1977).
4. L. S. Palatnik and E. J. Rogacheva, Sov. Phys.-Dokl. 12, 503 (1976).
5. L. L. Kazmerski, M. S. Ayyagari, G. A. Sanborn, F. R. White and A. J. Merrill, Thin Solid Films 37, 323 (1976).
6. L. J. Giling, A. W. Verheijen and J. Bloem, Instit. of Phys. Conf. Series 35, 3 (1977).
7. S. Wagner, Instit. of Phys. Conf. Series 35, 205 (1977).
8. B. Tell, S. Wagner and P. M. Bridenbaugh, Appl. Phys. Lett. 28, 454 (1976).
9. L. Y. Sun, L.L. Kazmerski, A. H. Clark, P. J. Ireland and D. W. Morton, To appear in March-April issue of J. Vac. Sci. Technol. (1978).
10. P. M. Hall and J. M. Morabito, Surface Sci. 59, 624 (1976).



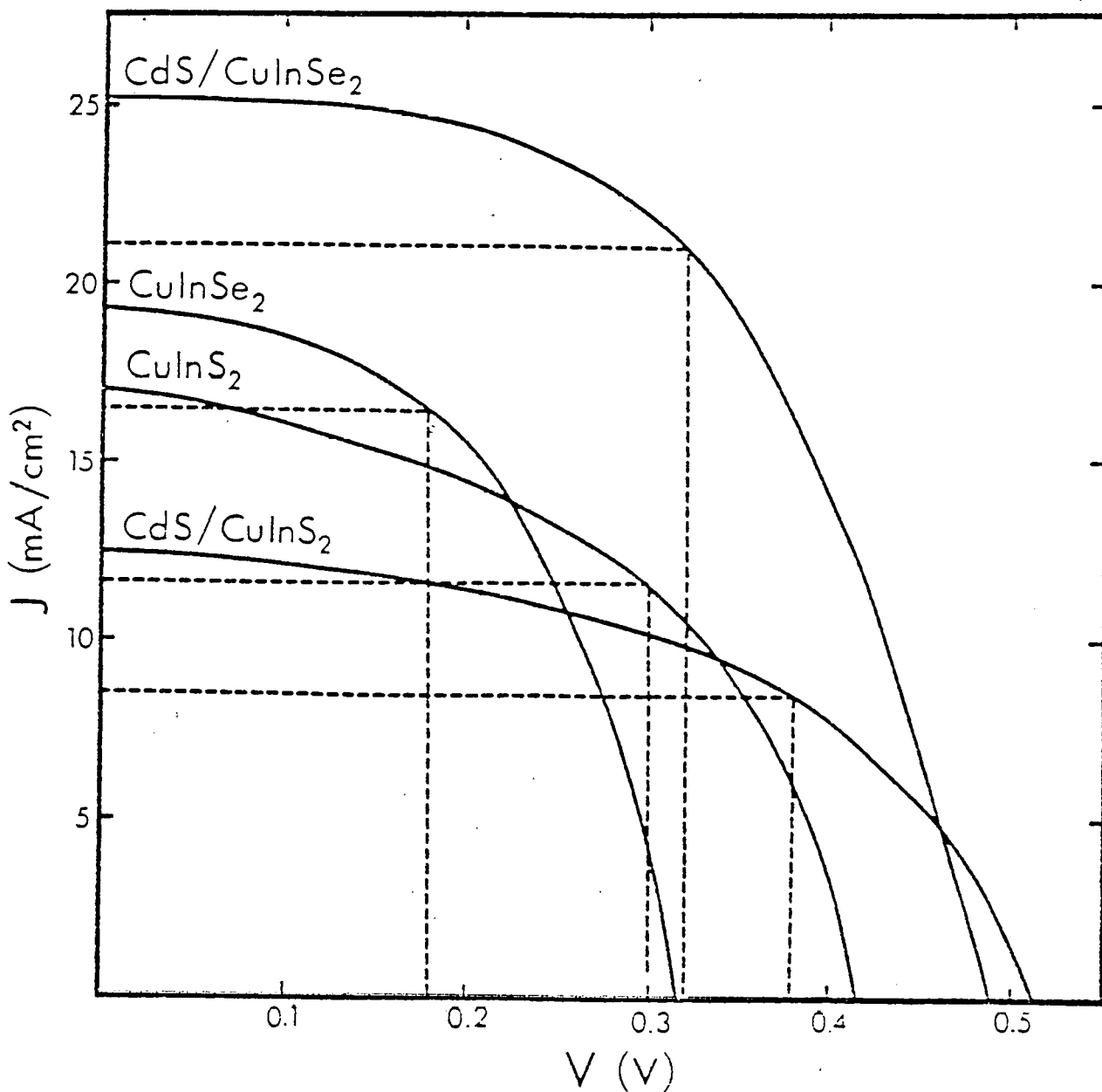


Fig. 1. Summary of J-V characteristics of Cu-ternary devices. (Illumination is 100 mW/cm<sup>2</sup>).

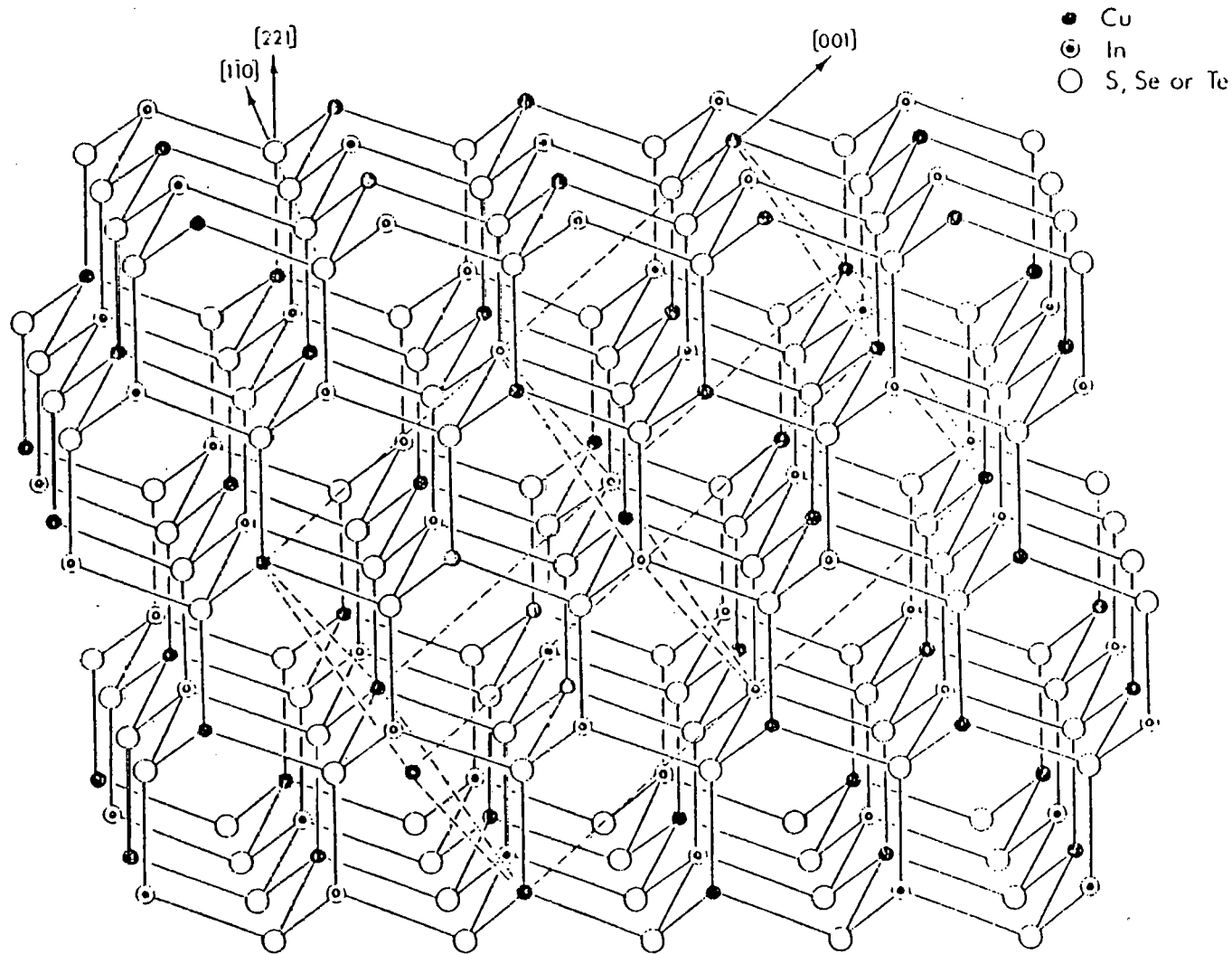


Fig. 2. 100-projection of chalcopyrite lattice. Unit cell is indicated by dashed lines.

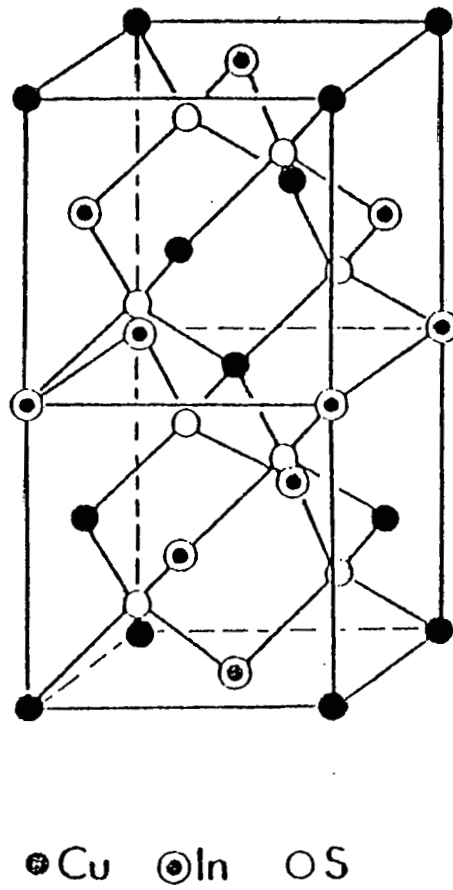


Fig. 3. Chalcopyrite Unit Cell ( $\text{CuInS}_2$ ).

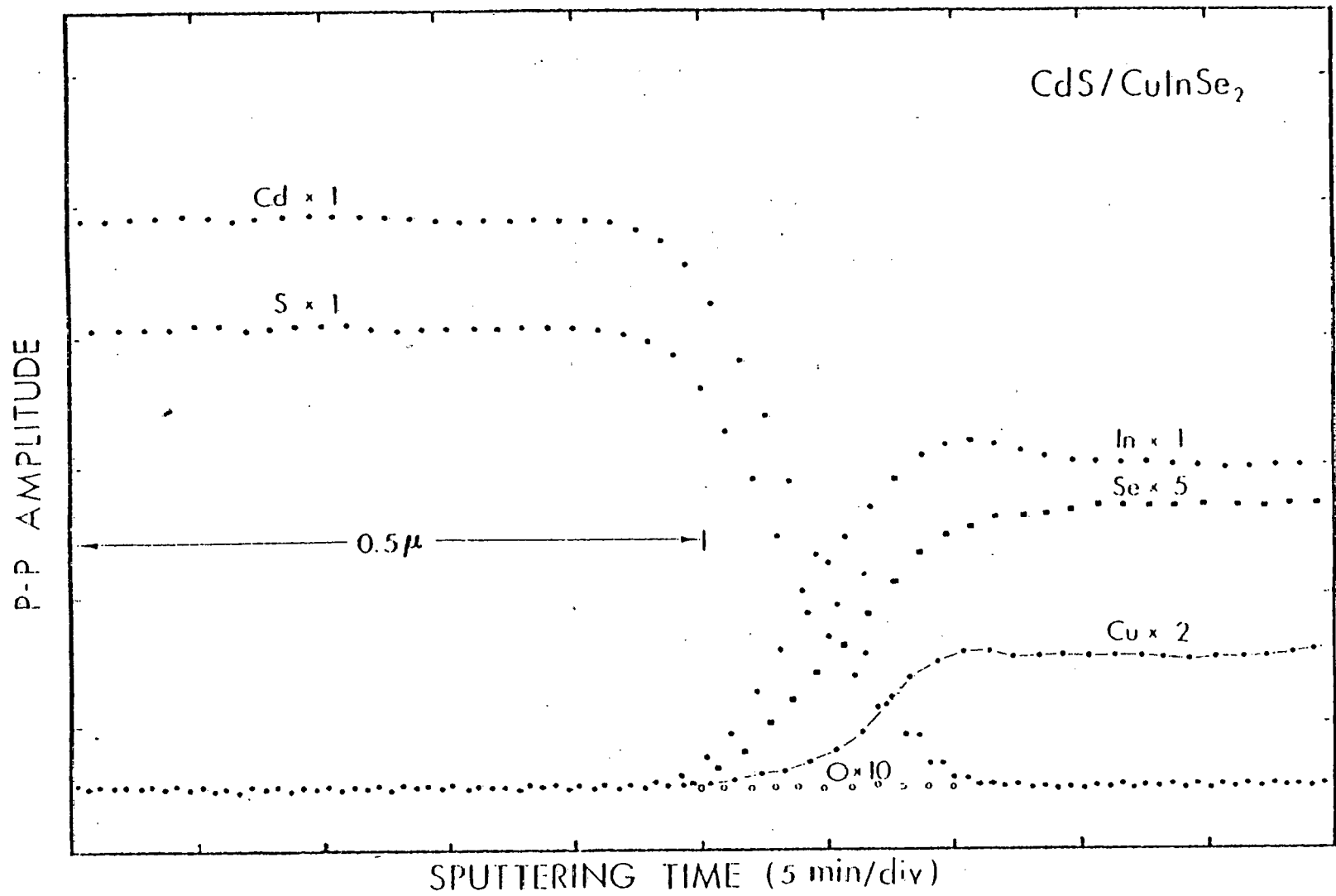


Fig. 4. Depth-compositional profile of in-situ produced thin-film device.

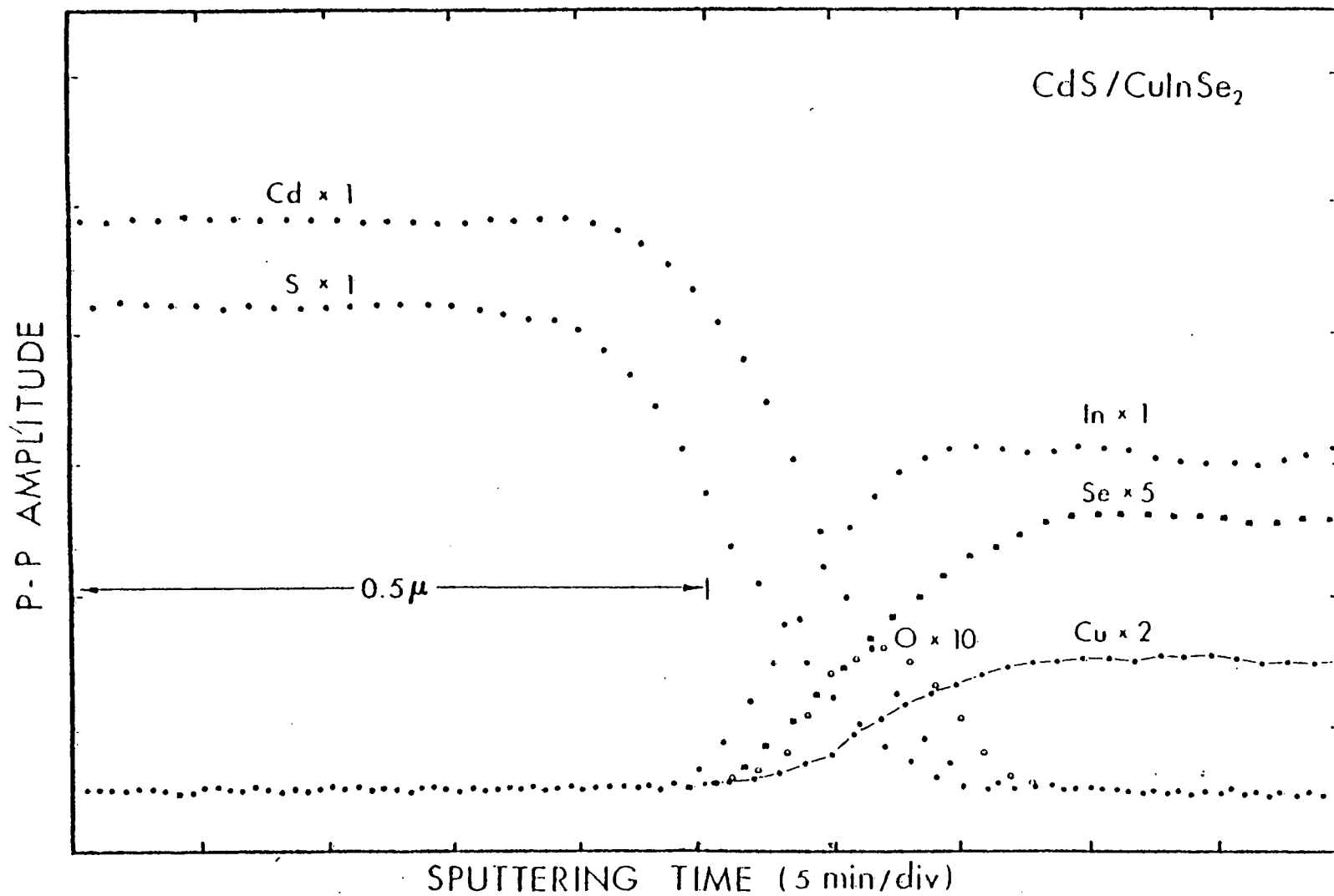


Fig. 5. AES profile of etched junction. The processing involves an external  $\text{H}_2\text{Se}$  anneal and a mild HCl etch prior to CdS deposition.

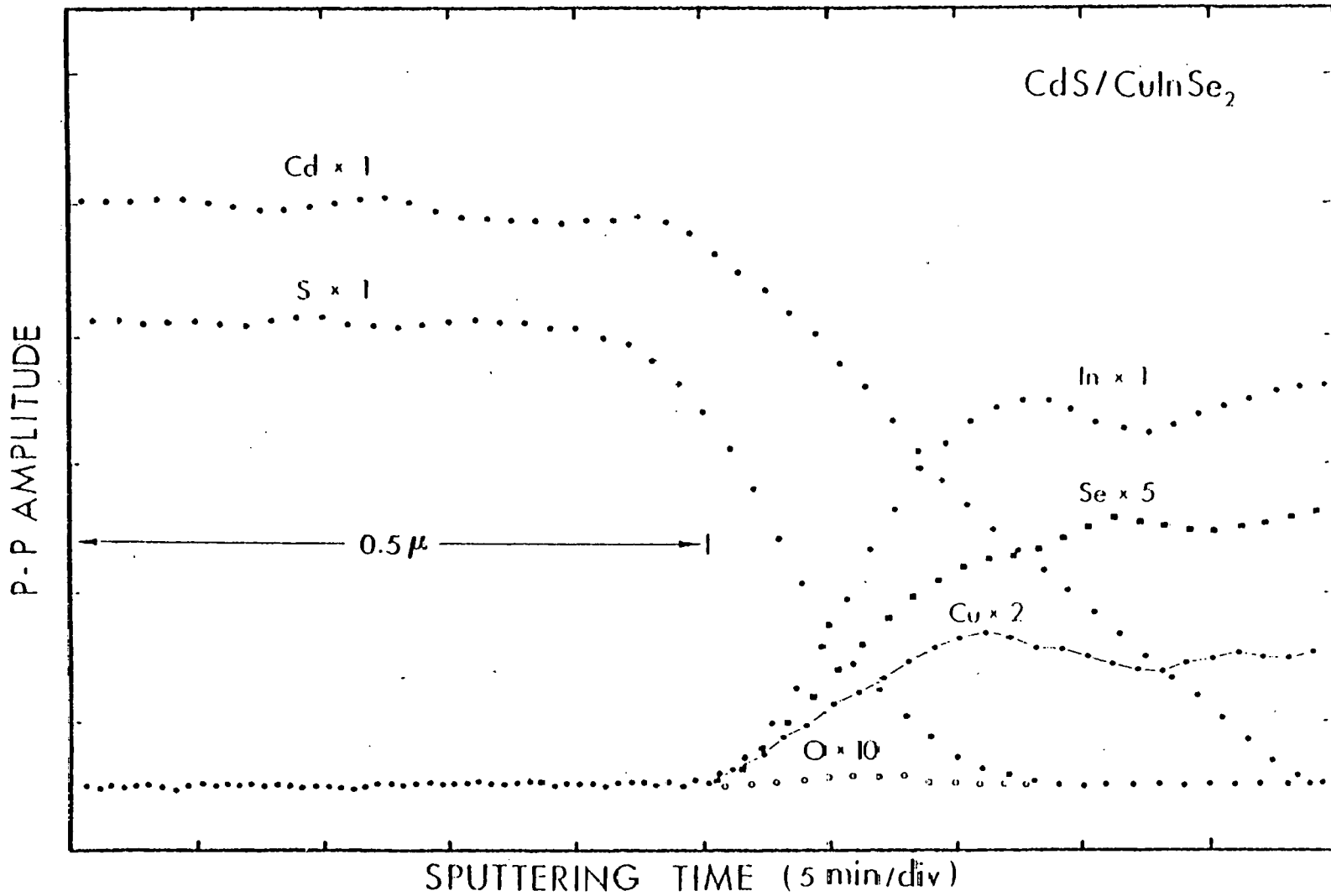


Fig. 6. Depth-compositional profile of degraded device, after annealing at 600 K, 2 hrs.

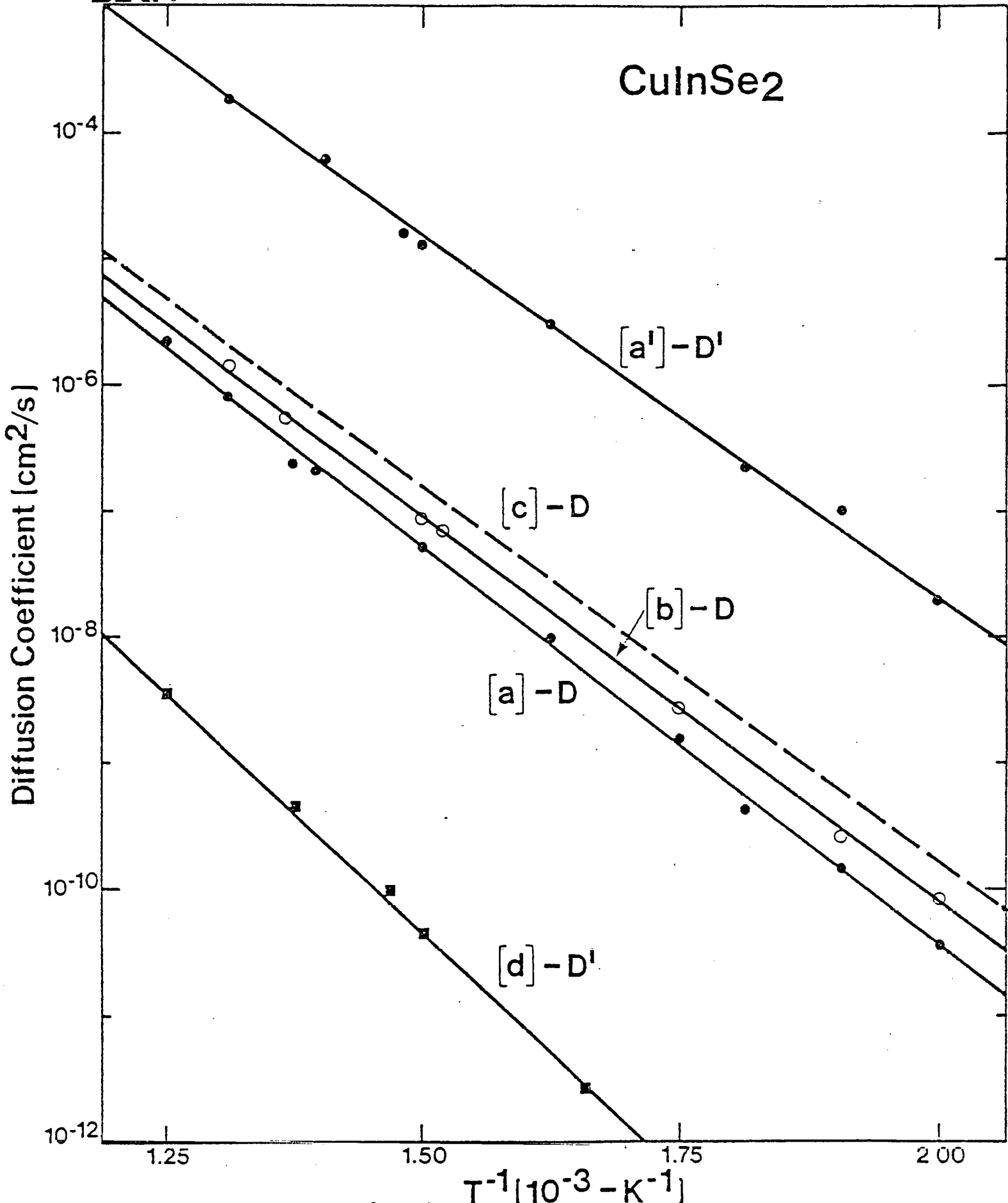


Fig. 7. See text for explanation. 103

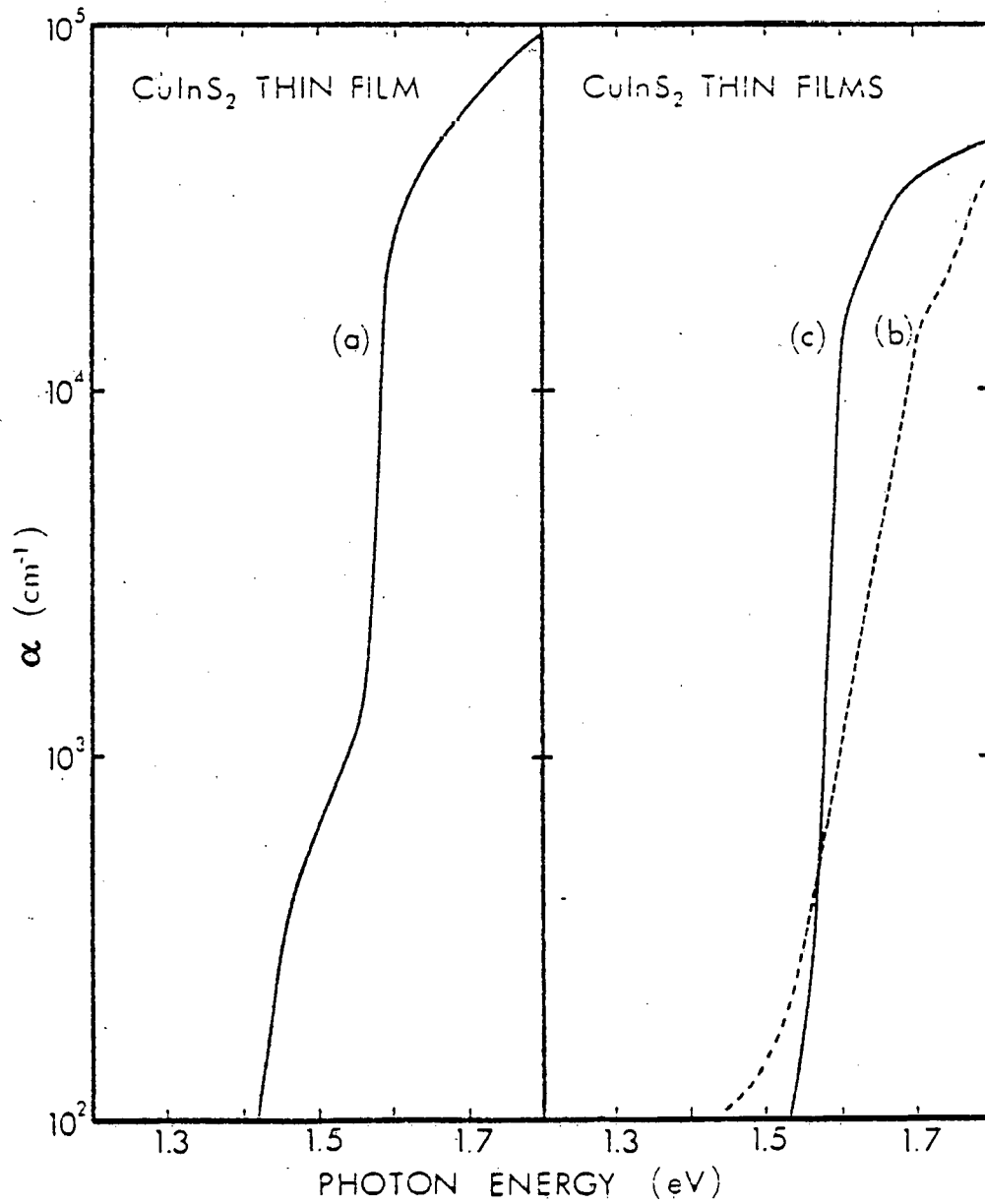


Fig. 8. Absorption coefficient dependences of photon energy.



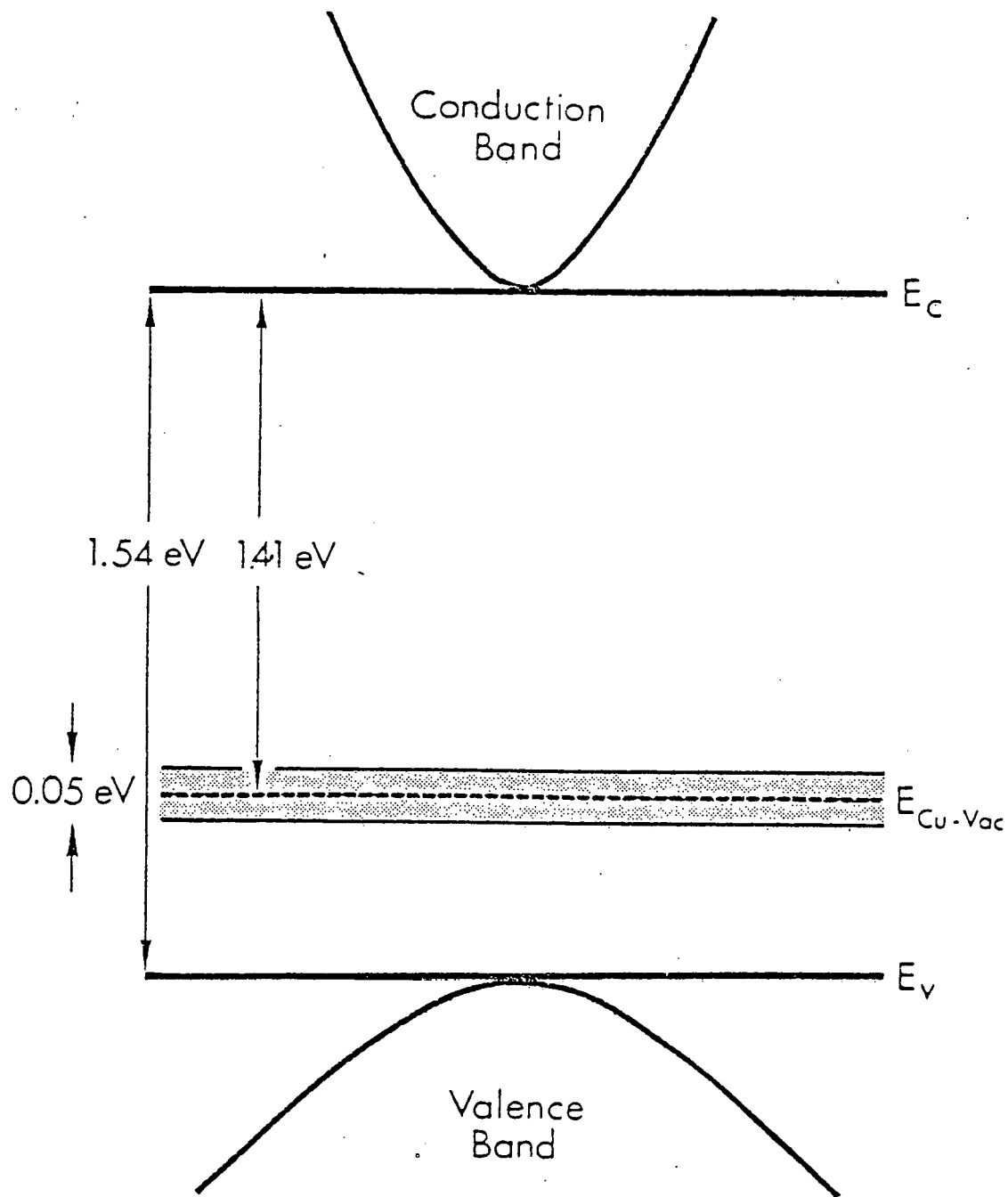


Fig. 9. Band structure representation for CuInS<sub>2</sub> thin films.

THIS PAGE INTENTIONALLY LEFT BLANK

### 3.9 INTERDIFFUSION AND INTERFACE PROBLEMS RELATING TO THIN-FILM PHOTOVOLTAIC DEVICES

SERI AUTHOR: L. L. Kazmerski

PROCEEDINGS: Proceedings of the NBS Workshop on Stability of Thin-Film Solar Cells and Materials

CONFERENCE: NBS Workshop on the Stability of Thin-film Solar Cells and Materials  
Gaithersburg, MD  
May 1-3, 1978

#### ABSTRACT

Even a cursory examination of the cross-section and microstructure of a thin-film polycrystalline solar cell can produce some skepticism in the mind of the most ardent thin-film photovoltaics advocate. How can this device, with its maze of grain boundaries, interfaces, defects, surfaces, and metallurgical junctions, be expected to remain reliable or stable even if it is allowed to remain unmolested let alone exposed to severe fields, illumination, changing loads, temperature gradients and cycling, and its entire processing sequence. In fact, the challenge of stability assurance over 10-20 year time periods is equally if not more important to the photovoltaic effort than the 10% efficient thin-film device or the \$0.50/peak watt program goals. This paper focuses on potential and real problems relating to the interaction of the materials making up the solid state devices and compounded by the special considerations of thin layers of polycrystallinity.

### 3.9.1 The Problems -- In General

A simplified but illustrative representation of a thin-film device is shown in Fig. 1. For the purposes of this paper, the major problem areas indicated are primarily considered. They are: (A) The grid or finger contact/semiconductor interface; (B) The semiconductor/semiconductor (or junction) interface; and (C) The semiconductor/back-contact region. A', B', C' represent the special cases of A, B, and C at grain boundaries where enhanced interactions can occur.

The movement of atomic species, or the diffusion mechanism, is prevalent to some extent in all solids and materials systems. Basically, diffusion can be defined in two identifiable regimes: (1) Diffusion in a material at chemical equilibrium. That is, there exists a uniform chemical and native defect composition. For the solvent species, the process is called SELF-DIFFUSION, and for the solute species, ISOCONCENTRATION DIFFUSION; (2) Diffusion entailing a net chemical flux. In this case, the system is not in equilibrium, and the resulting chemical potential gradients establish chemical fluxes. This chemical diffusion or INTERDIFFUSION results in the net flow of matter which generally leads to an expansion (but sometimes a contraction) of the diffusion region. This is illustrated in Fig. 2. At  $t = 0$ , the materials are brought into contact, some atomic interarrangement occurs for  $t > 0$ , and equal distribution is reached at infinite time. The term "interdiffusion" is usually applied to any case when atomic interpenetration is experienced after metallurgically coupling two materials. This penetration can be significantly enhanced along defects, such as grain boundaries. The interdiffusion problem and its effects on device stability form the major considerations of this paper. In addition, some other interface problems which limit device performance and result from device processing are discussed. Representative examples are cited from a variety of device types including  $\text{SnO}_x/\text{Si}$ ,  $\text{CdS}/\text{CuInSe}_2$ ,  $\text{CdS}/\text{CuInS}_2$ ,  $\text{CdS}/\text{CuInTe}_2$ ,  $\text{Cu}_2\text{S}/\text{CdS}$ ,  $\text{InP}/\text{CdS}$ ,  $\text{GaAs}$ , and amorphous  $\text{Si}$ .

### 3.9.2 The Techniques -- AES and SIMS

The diffusion process has been studied, simplified, complicated, interpreted, and misinterpreted using a variety of techniques. The relatively recent development of surface analysis techniques which can provide elemental and chemical information about fraction of monolayer thicknesses has been important to both the uncovering of diffusion-related problems and the investigation of the mechanism itself. Of the more than 60 identified surface measurement techniques which have been reported,<sup>1</sup> two which are complementary in nature have highlighted interdiffusion investigations: (1) Auger electron

spectroscopy (AES); and (2) secondary ion mass spectroscopy (SIMS). The AES technique analyzes Auger electrons generated by a radiationless process by an incident beam. SIMS, on the other hand, uses an ion probe to give rise to secondary positive and negative ions from the material under investigation. Detailed information about these techniques is available in the literature<sup>1</sup> and therefore, will not be discussed herein.

Application of the AES technique in combination with ion etching to diffusion problems and extensive interpretation of the results has been reported by Morabito and Hall for single crystal (bulk)<sup>2</sup> and grain boundary<sup>3</sup> cases. This analysis was extended and modified to account for grain boundary diffusion coefficients by observing the time for "first-appearance" at a surface using the detectability limits of AES or SIMS ( 0.1 atomic %).<sup>3</sup>

Because of the sensitivity and truly surface (e.g., Auger electrons evolve from layers 10 Å or less for AES, typically) nature of the techniques they can also be utilized to uncover process related performance-inhibiting layers (e.g., oxides at interfaces). Isotopes and oxide states can also be identified with some reasonable care.

### 3.9.3 The Problems -- Specific Cases

In this section, several interface and interdiffusion problems are cited. Some are examples from solar cell cases, and others are meant to be representative of a broad range of related problems.

**A. InP With CdS and Schottky Barriers.** InP has been demonstrated as a useful material in heterojunction and Schottky barrier devices. The single crystal, thin-film CdS/InP solar cell has been reported to be stable at temperatures to 200°C in room ambient.<sup>4</sup> A thin-film version of this device has been reported with similar stability and no detectable interdiffusion at these temperatures.

The effects of heat treatments on metal-InP Schottky barriers has been reported using SIMS.<sup>6</sup> Au, Al, Cr, Ni and Ti were used and SIMS distribution profiles of elemental species were obtained as a function of the metal and InP. Fig. 3a presents a three dimensional composite for the Al-InP case. No degradation is noted until some P outdiffusion at 500°C. In contrast, Fig. 4a shows SIMS data for a Au-InP device. The profile is well behaved to 275°C, with negligible interdiffusion. Above 350°C, In outdiffuses and at 500°C, In builds up in the Au, forming an alloy. The accompanying effect on barrier height is tabulated with the figure. The Ni/InP and Ti/InP profiles are shown in Figs. 3b and 4b respectively. A summary of the metal-InP barriers, the temperature treatment, barrier effect, and degradation mechanism is presented in Table 1. The interdiffusion and barrier degradation correlate well in each case.

**B. GaAs.** Similar interdiffusion effects have been reported for Ta-GaAs Schottky barriers, using AES.<sup>7</sup> Fig. 5a presents AES data exhibiting the interdiffusion problem for both sputtered and e-beam evaporated Ta films. The corresponding barrier height degradation is shown in Fig. 5b. For this system, the onset of interdiffusion and barrier height effects in W(Ti)/n-GaAs diodes are shown as a function of annealing in Fig. 6. AES techniques have revealed that Au has diffused through the 1000 Å W (Ti) layer to the GaAs interface, after annealing at 500-600°C for 15 hours.<sup>8</sup>

**C. Amorphous Si.** Amorphous Si films prepared by glow discharge have been shown to contain considerable amounts of bonded hydrogen (10-50 atomic %). SIMS has been used to examine the outdiffusion of hydrogen which could be disastrous to solar cells. Carlson<sup>9</sup> has measured the diffusion, and Fig. 7a shows the profiles of the control deuterated sample and a sample heated for 25 hours at 300°C. The diffusion coefficient of deuterium is found to be<sup>9</sup>

$$D = 1.17 \times 10^{-2} \exp(-1.53 \pm 0.15/kT). \quad (1)$$

**D. Cuprous Oxide.** Barrier heights in cuprous oxide Schottky barriers have been disappointingly lower than predicted. Recent AES work has shown that oxygen diffusion from the cuprous oxide to the metal interface (e.g., Mg) forms a metal oxide layer (e.g., MgO) and leaves a copper rich layer behind.<sup>10</sup> This occurs at essentially room temperature (during evaporation) and lowers the barrier height to an undesirable and unacceptable level.

**E. Cu<sub>2</sub>S/CdS.** The extent of the copper diffusion problem at the junction region of this device is not yet fully identified or understood. In some materials, an irreversible degradation results and is attributed to the electrochemical decomposition of the copper sulfide and diffusion of the copper along the boundary regions.<sup>11</sup> In other Cu<sub>2</sub>S material, similar or more devastating operating conditions have not shown this effect. The interdiffusion at the junction interface needs more attention and it is expected that interpretable information can be gained from current work on more planar heterointerfaces.

**F. Cu-Ternaries.** CdS/CuInSe<sub>2</sub> thin-film polycrystalline solar cells have been produced in both flux wall (i.e., illumination through the ternary) and backwall (i.e., illumination through the CdS) configurations. In cases where the initial ternary layer is removed from the vacuum system and etched, an oxide layer results at the junction interface.<sup>12</sup> The extent of the resulting oxide region can be limited but not eliminated by etching. A high series resistance results when such an oxide is present, limiting both J<sub>sc</sub> and the fill-factor. The detected oxide layer is shown in Fig. 8.

CdS/CuInSe<sub>2</sub>, CdS/CuInS<sub>2</sub>, and CdS/CuInTe<sub>2</sub> devices exhibit an interdiffusion degradation mode when the junctions are heated above 500 K.<sup>13</sup> Diffusion of the Cd from the CdS into the ternary has been observed using AES techniques for all devices. As an example, Fig. 9 shows a depth-compositional profile of a CdS/CuInS<sub>2</sub> thin-film device with  $\eta = 3.2\%$ ,  $V_{oc} = 0.51$  V and  $J_{sc} = 11.8$  mA/cm<sup>2</sup>. An orderly change from n-CdS to p-CuInS<sub>2</sub> is evident. Fig. 10 shows the same device junction region after a 3.5 hour, 600 K anneal. The most apparent effect of this treatment is the diffusion of Cd into the ternary film. Using the Hall-Morabito formalism,<sup>3</sup> the grain boundary diffusion coefficient has been determined, and follows the relationship<sup>13</sup>

$$D' = D_0 \exp(-E_a/kT) \quad (2)$$

for the data presented in Fig. 11. Values of the  $D_0$  have been determined:  $D_0 = 13.8$  cm<sup>2</sup>/sec (CuInS<sub>2</sub>);  $10.6$  cm<sup>2</sup>/sec (CuInSe<sub>2</sub>); and  $5.05$  cm<sup>2</sup>/sec (CuInTe<sub>2</sub>). The activation energies are 1.7, 1.5, and 1.38 eV respectively. Unlike the Cu<sub>2</sub>S/CdS device, the diffusion of Cu is not discernible over this temperature range. Device characteristics are stable for these heterostructures operating up to 423 K. Definite, irreversible degradation in performance is experienced for operating temperatures in excess of 500 K. These data may cause some concern for device lifetimes under severe operating temperatures.

**G. SnO<sub>2</sub>/Si.** A major source of degradation for the SnO<sub>2</sub>/Si heterojunction solar cell has been identified as a thin silicon oxide layer at the SnO<sub>2</sub>/Si interface.<sup>14</sup> Fig. 12 shows the major differentiated Auger spectra for Sn, O and Si at (a) the SnO<sub>2</sub> layer, just before the junction, (b) the junction interface, and (c) the silicon bulk, just after the interface. Both the energy position and shape of the oxygen peak change over the region. These data have been used to identify the interfacial layer as SiO<sub>2</sub>. A calculation of the rate of oxygen diffusion to the interface predicts a rate some 12 orders of magnitude lower than observed at the processing and operation temperatures. However, the activation energy associated with the growth of the layer is 1.1 - 1.3 eV, indicating that the oxidation results from field aided diffusion of O<sub>2</sub> - ions. Similar degradation and diffusion effects have been noted for ITO/Si cells at elevated temperatures.<sup>14</sup>

#### 3.9.4 Summary

Much work remains to be done on controlling interdiffusion mechanisms in thin polycrystalline solar cells. The minimization of such degradation processes poses a major challenge.

### 3.9.5 Acknowledgements

The author wishes to express his appreciation to Dr. S. Wagner for his suggestions and encouragement in preparing this discussion. The assistance of D. Carlson, A. Rothwarf, L. Olsen and the authors of the papers used as examples in this presentation is gratefully acknowledged and sincerely appreciated.

### 3.9.6 References

1. See, for example, D. Lichtman, in Methods of Surface Analysis, (Elsevier Scientific, New York; 1975) pp. 39-70.
2. P. M. Hall and J. M. Morabito, Surface Sci. 54, 79 (1976).
3. P. M. Hall and J. M. Morabito, Surface Sci. 59, 624 (1976).
4. S. Wagner, J. L. Shay, K. J. Bachmann and E. Buehler, Appl. Phys. Lett., 26, 229 (1975).
5. L. L. Kazmerski, F. R. White, M. S. Ayyagari and R. P. Patterson, J. Vac. Technol., 14, 65 (1977).
6. H. M. Kim, A. F. Lovas, G. G. Sweeney and T. M. S. Heng, Inst. Phys. Conf. Series 33b, 145 (1976).
7. A. Christou and K. Sleger, Inst. of Phys. Conf. Series 33b, 191 (1976).
8. A. Christou and A. C. Macpherson, J. Vac. Sci. Technol., 14, 939 (1977).
9. D. E. Carlson and C. N. Magee (to appear in Appl. Phys. Lett., 1978).
10. L. Olson (private communication).
11. H. J. Mathieu, K. K. Reinhartz and H. Rickert, Proc., IEEE Photovoltaics Spec. Conf., (IEEE, NY; 1973), pp. 93-99.
12. L. L. Kazmerski, R. B. Cooper, F. R. White and A. J. Merrill, IEEE Trans. Electron Dev., ED24, 496 (1977).
13. L. L. Kazmerski, Instit. of Phys. Conf. Series 35, 217 (1977).
14. R.L. Anderson, DOE Advanced Materials R&D Meeting, Golden, CO, Oct. 1977 (Proc. in preparation).



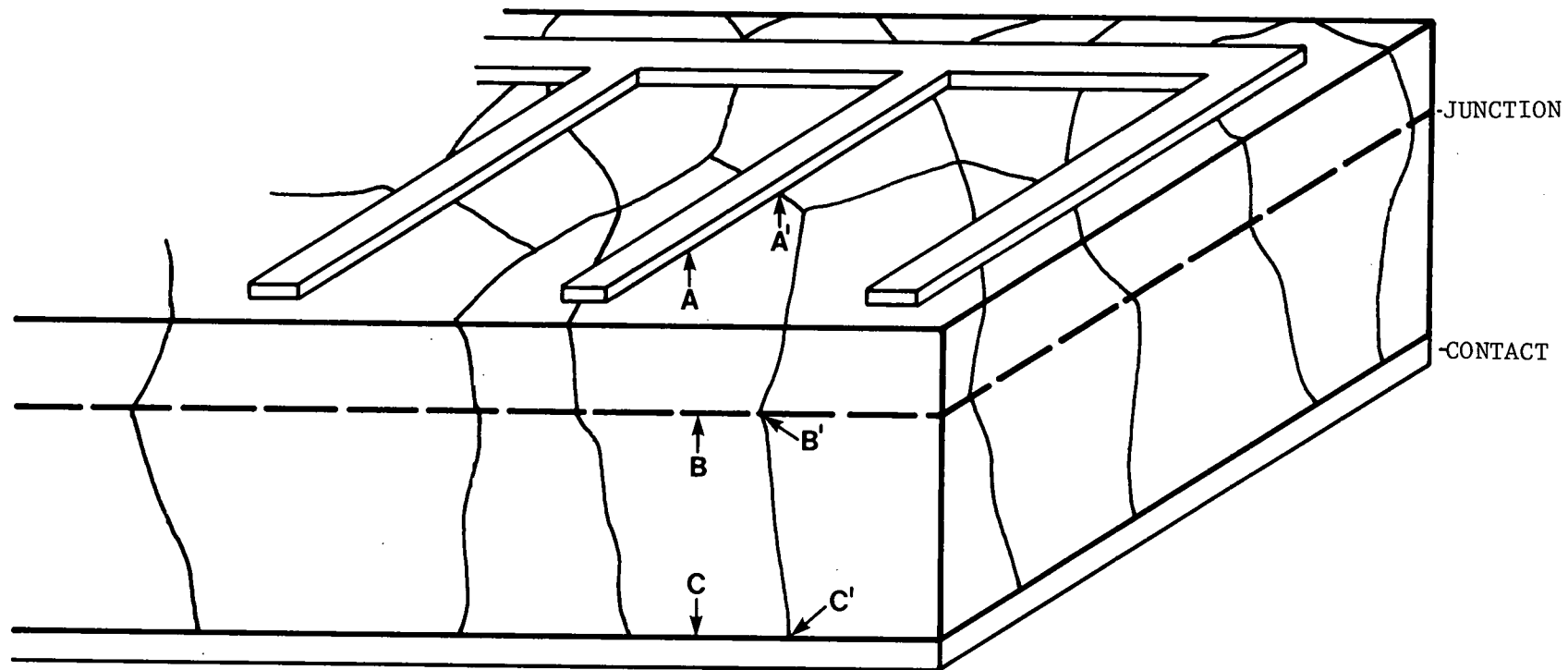


Fig. 1. Schematic representation of thin-film, polycrystalline photovoltaic device.

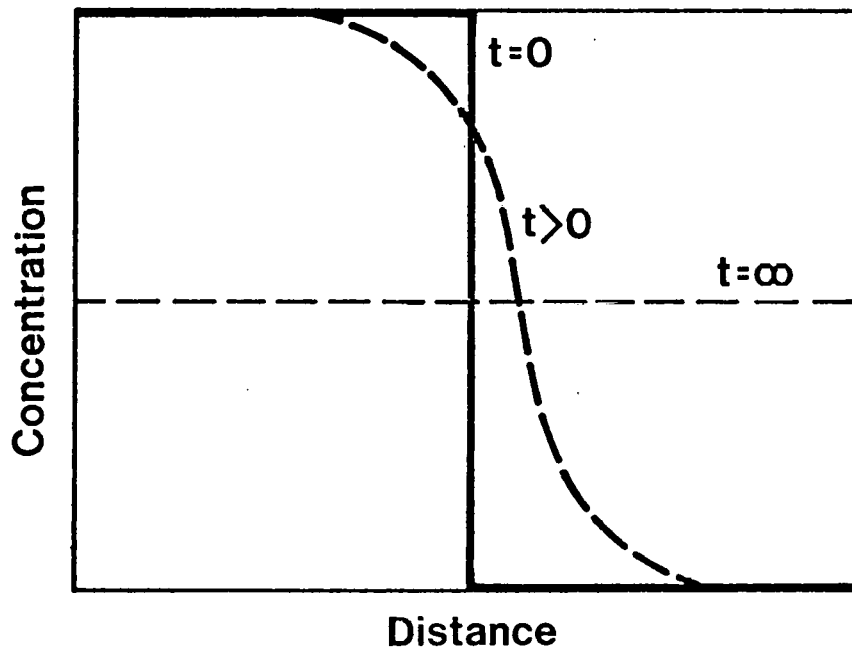
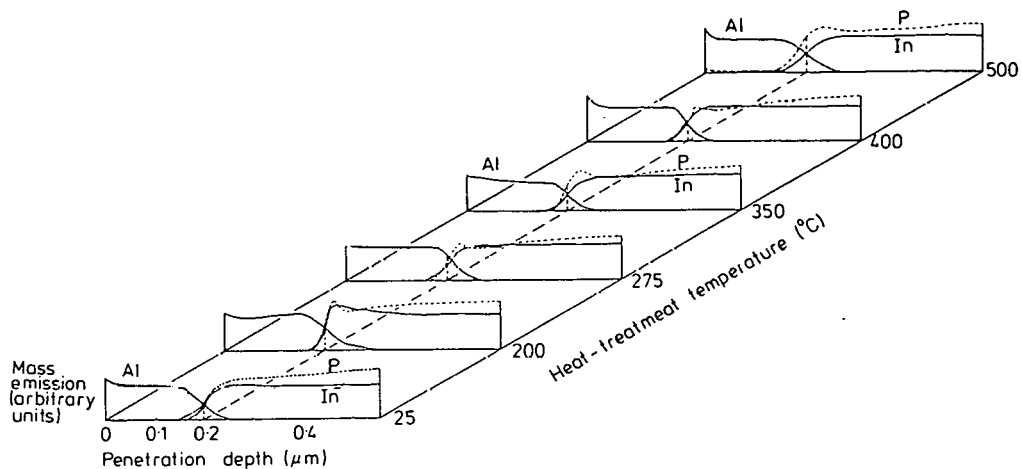
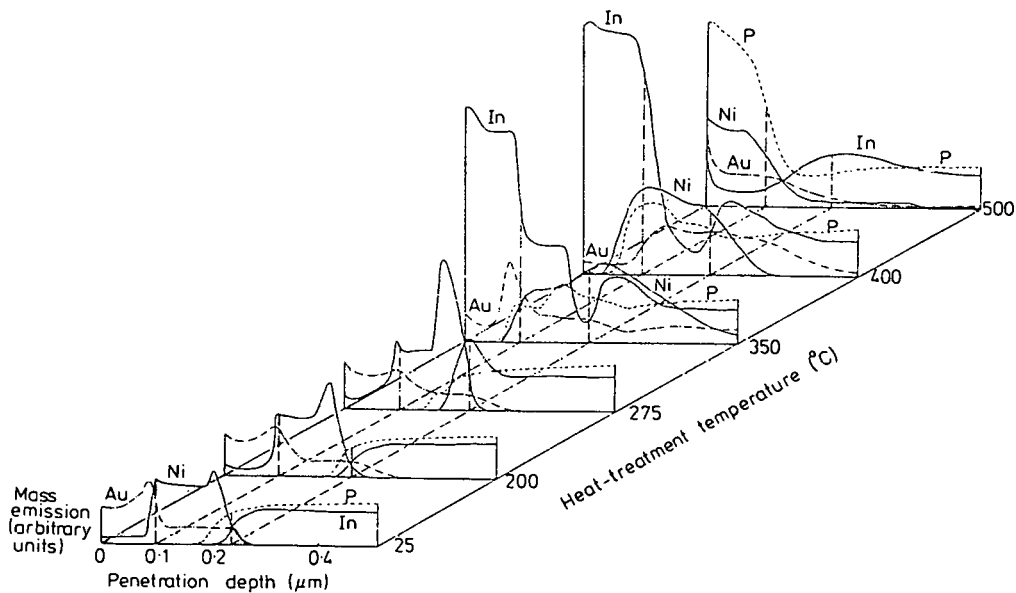


Fig. 2. Graphical representation of the interdiffusion process. "t" indicates time.



(a) Al/InP composite



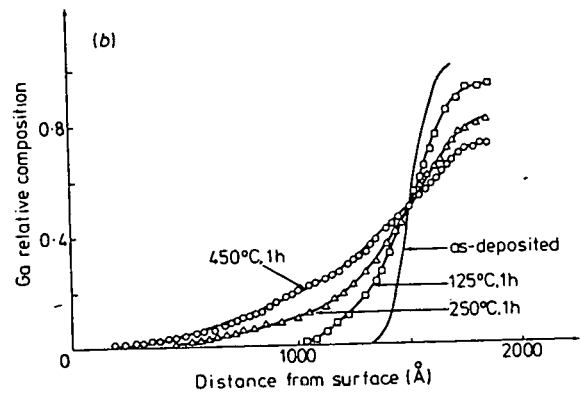
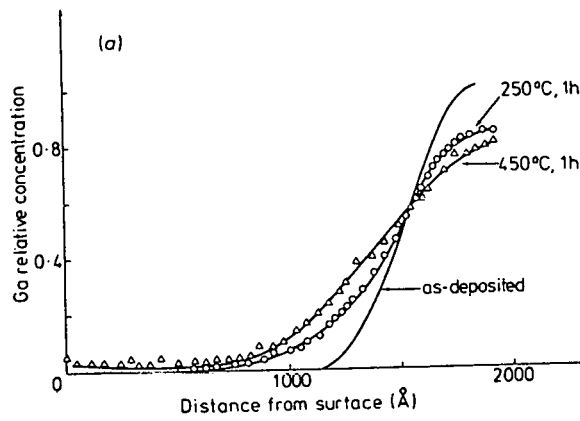
(b) (Au)-Ni/InP composite

Fig. 3. SIMS depth profiles for InP Schottky barrier devices. (After H.B. Kim et al., Instit. of Phys. Conf. Series, 33b, 145 (1976).)

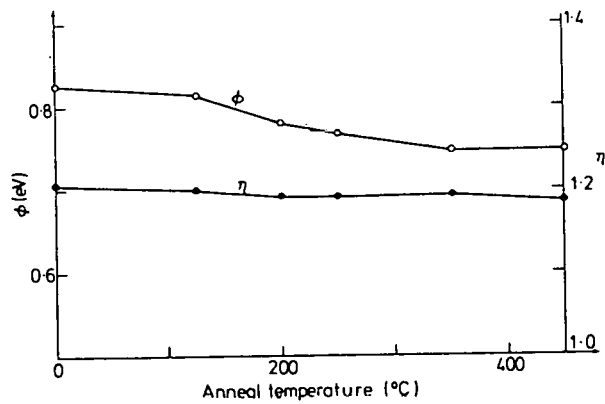
Table 1. Metal - InP Schottky Barriers

Metal		T (°C)	n	$q\phi_b$ (eV)	Degradation Mechanism	Safe T(°C)
Au	Before After	400	0.97 0.89	0.43 0.43	Au indiffusion In outdiffusion	350
Al	Before After	500	1.11 1.24	0.60 0.52	Stable	500
Cr	Before After	500	- short -		Metallurgically Stable	500
(Au)-Ni	Before After	350	- short -		Catastrophic Au, Ni indiffusion In, P outdiffusion	275
(Au)-Ti	Before After	400	0.86 0.65	0.42 0.40	Au diffusion P outdiffusion	350

H.M. Kim, et al., Proc. Sixth Int. Sym GaAs and Related Compounds, St. Louis, pp. 145-153 (1977). Inst. of Phys. Conf. Series 33b.

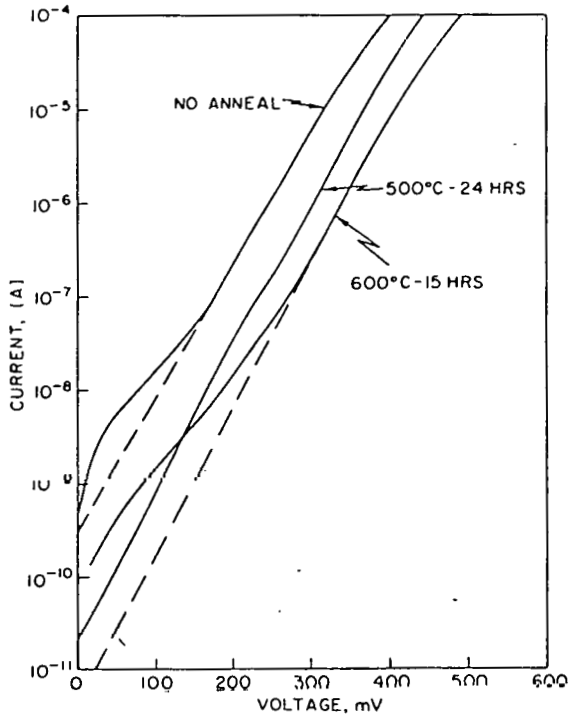


(a) AES Profiles

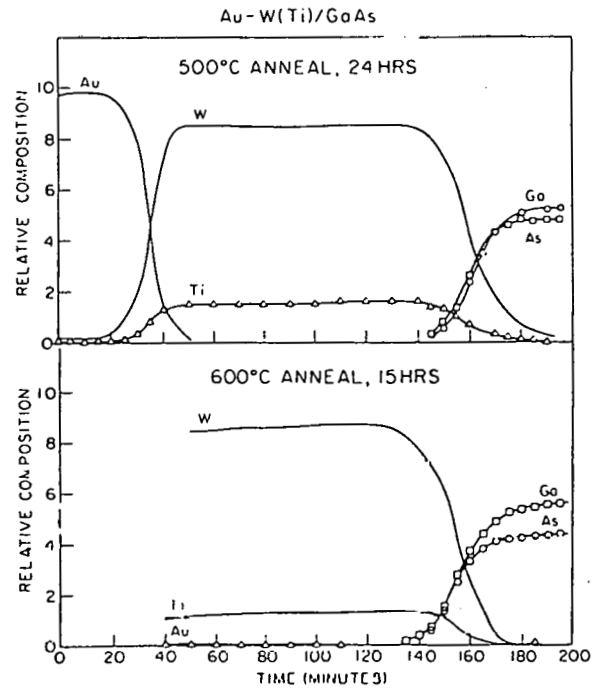


(b) Barrier heights

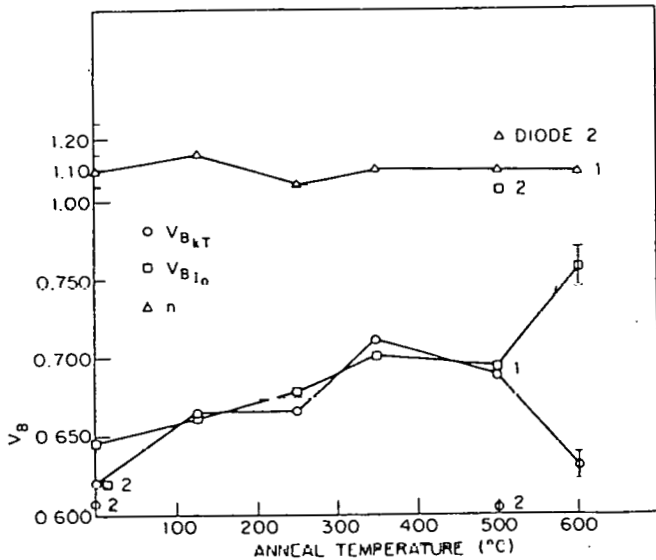
Fig. 5. AES profiles of Ta/GaAs Schottky barriers and related barrier height variations. (A. Christou and K. Sleger, *Instit. of Phys. Conf. Series #33b*, 1976.)



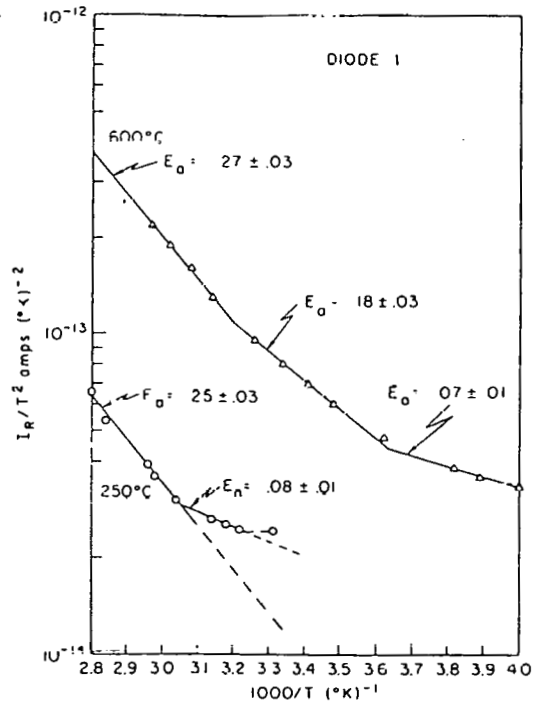
(a) I-V characteristics of Au-1000 W(Ti)/n-GaAs Schottky barriers vs anneal temperatures.



(c) AES depth profiles of Au-1000A W(Ti) metallization on GaAs.

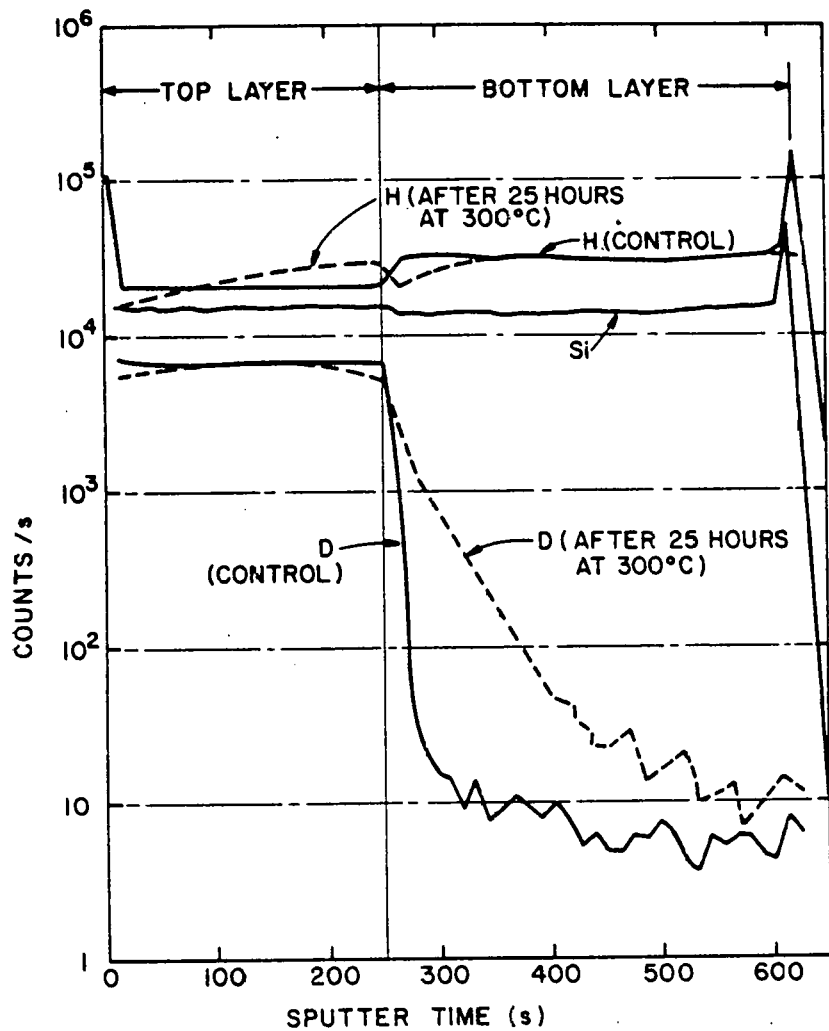


(b) Schottky barrier heights vs anneal temperature for Au-1000A W(Ti) (diode 1) and Au-100A W(Ti) (diode 2) metallizations in n-GaAs.

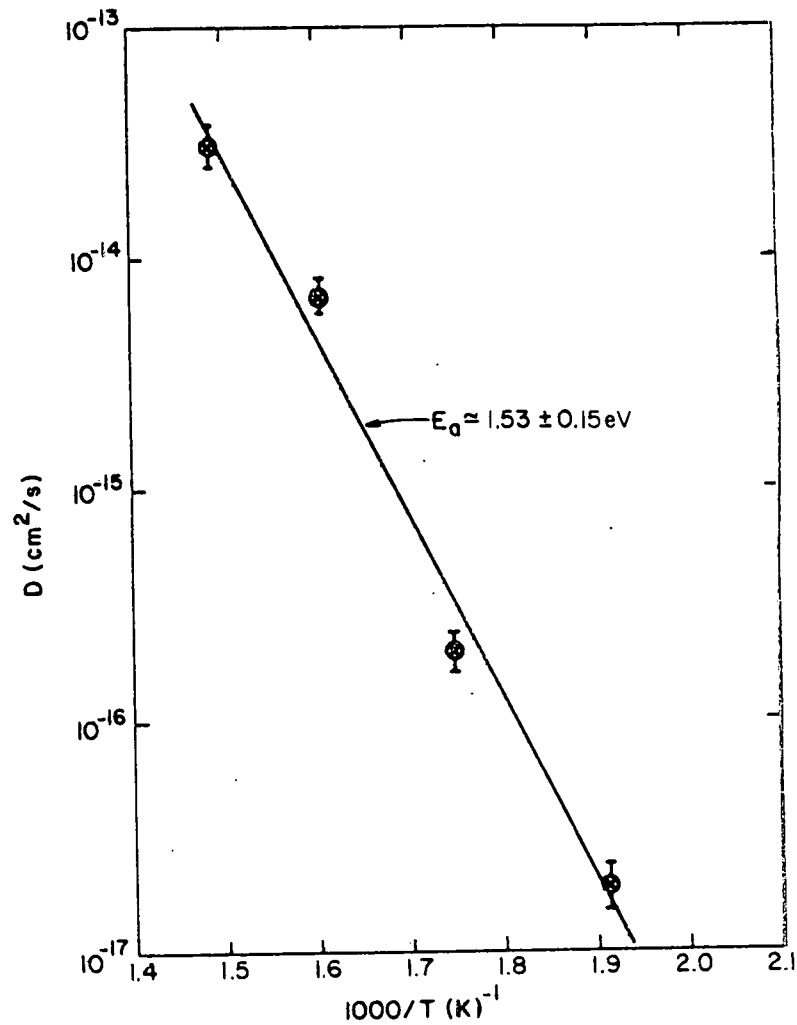


(d) Activation energy analysis of Au-1000A W(Ti)/n-GaAs diodes annealed at 250C (24 hrs) and 600C (15 hrs).

Fig. 6. Interdiffusion and Schottky-barriers in Au-W(Ti)/n-GaAs devices. (H.M.Day, A. Christou and A.C. Macpherson, J.Vac.Sci.Technol. 14, 939 (1977).



(a) SIMS profiles of a layered sample before and after 25 hrs at 300 C.



(b) Deuterium diffusion coefficient as a function of inverse temperature.

Fig. 7. Amorphous Si diffusion studies. (After Carlson, to be published in Appl. Phys. Lett.)

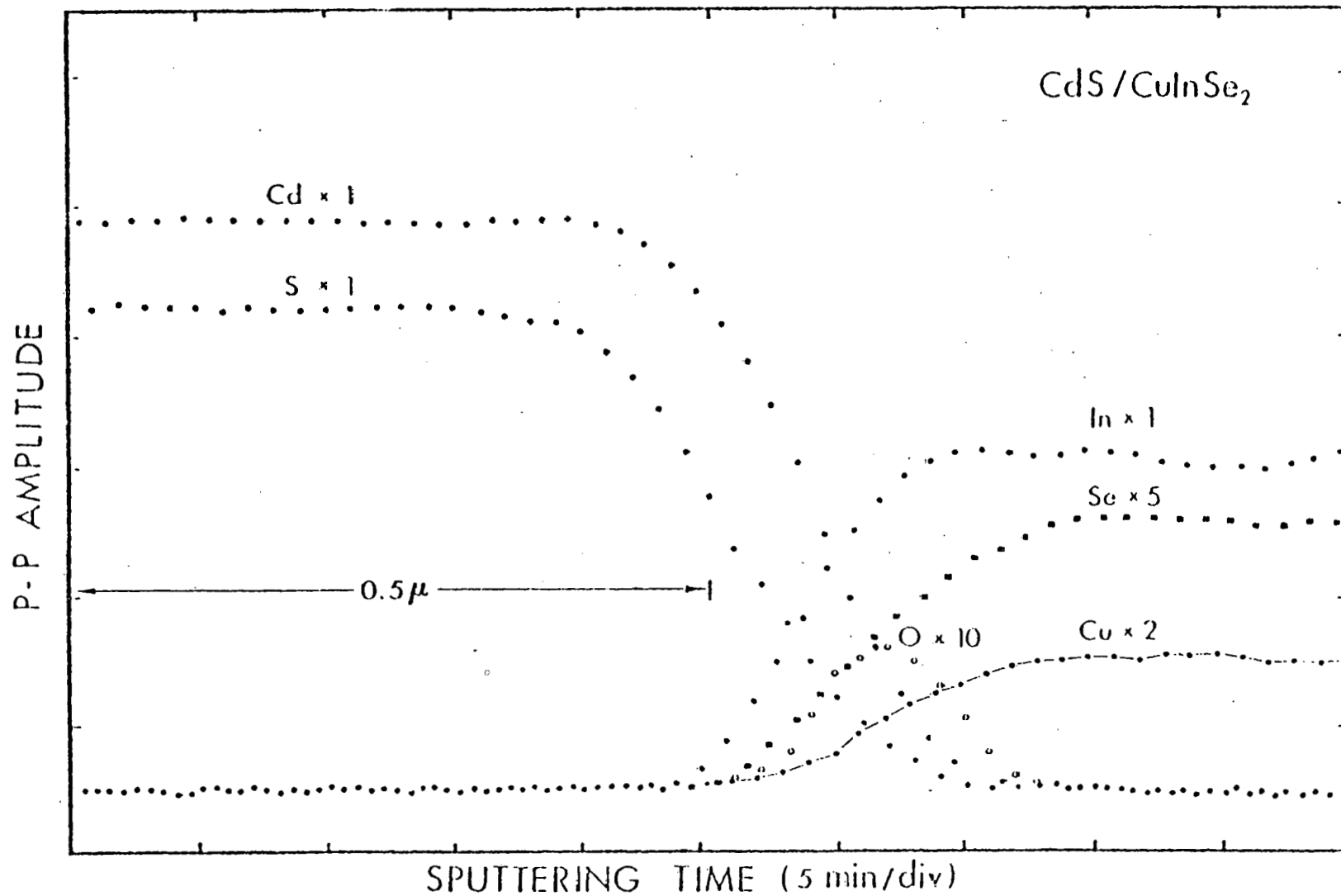


Fig. 8. AES profile of etched junction. The processing involves an external H<sub>2</sub>Se anneal and a mild HCl etch prior to CdS deposition.



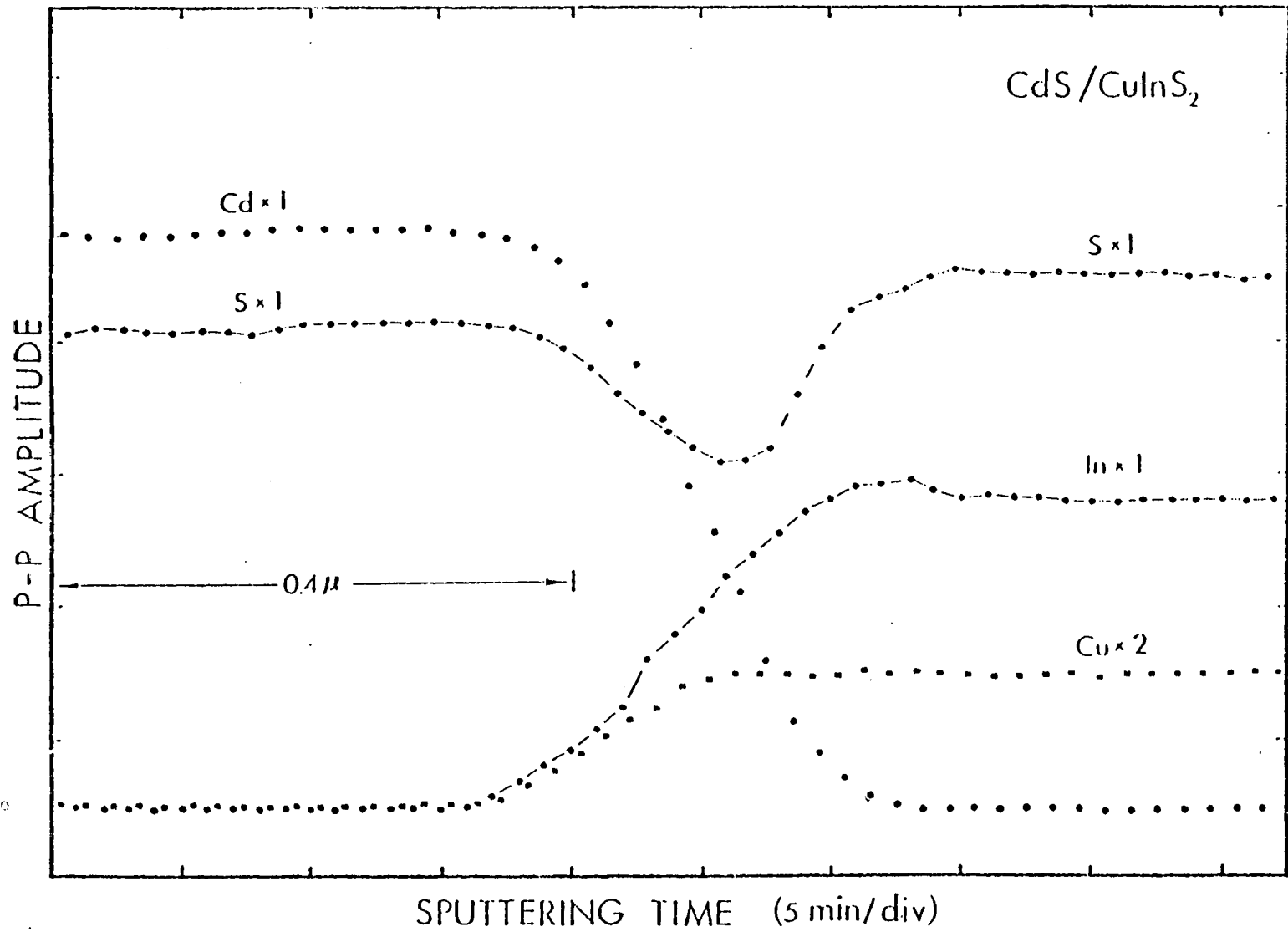


Fig. 9. AES depth compositional profile of CdS/CuInS<sub>2</sub> thin-film solar cell with 3.2% efficiency.

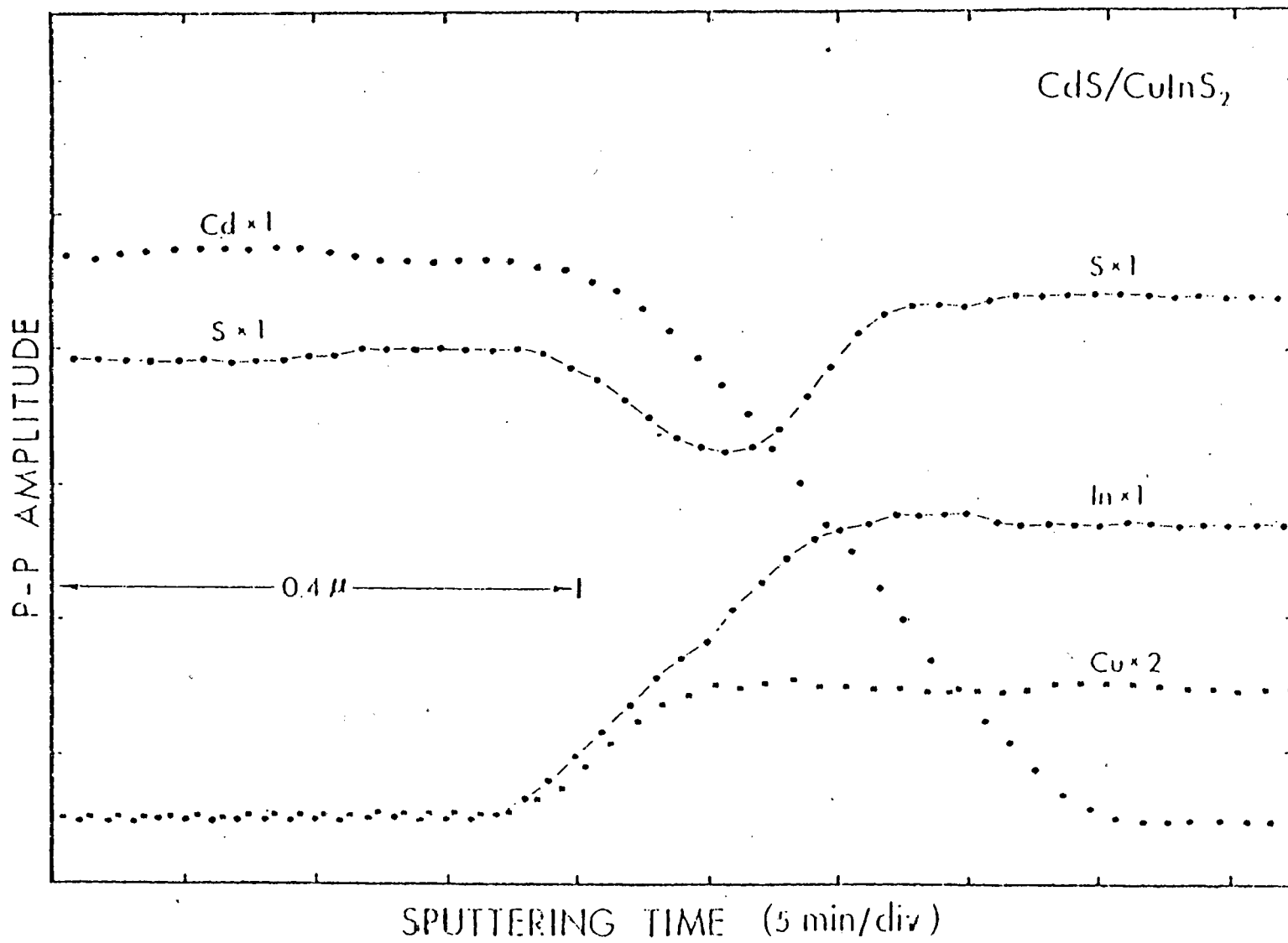


Fig. 10. AES depth compositional profile of device annealed for 3.5 hrs at 600K.

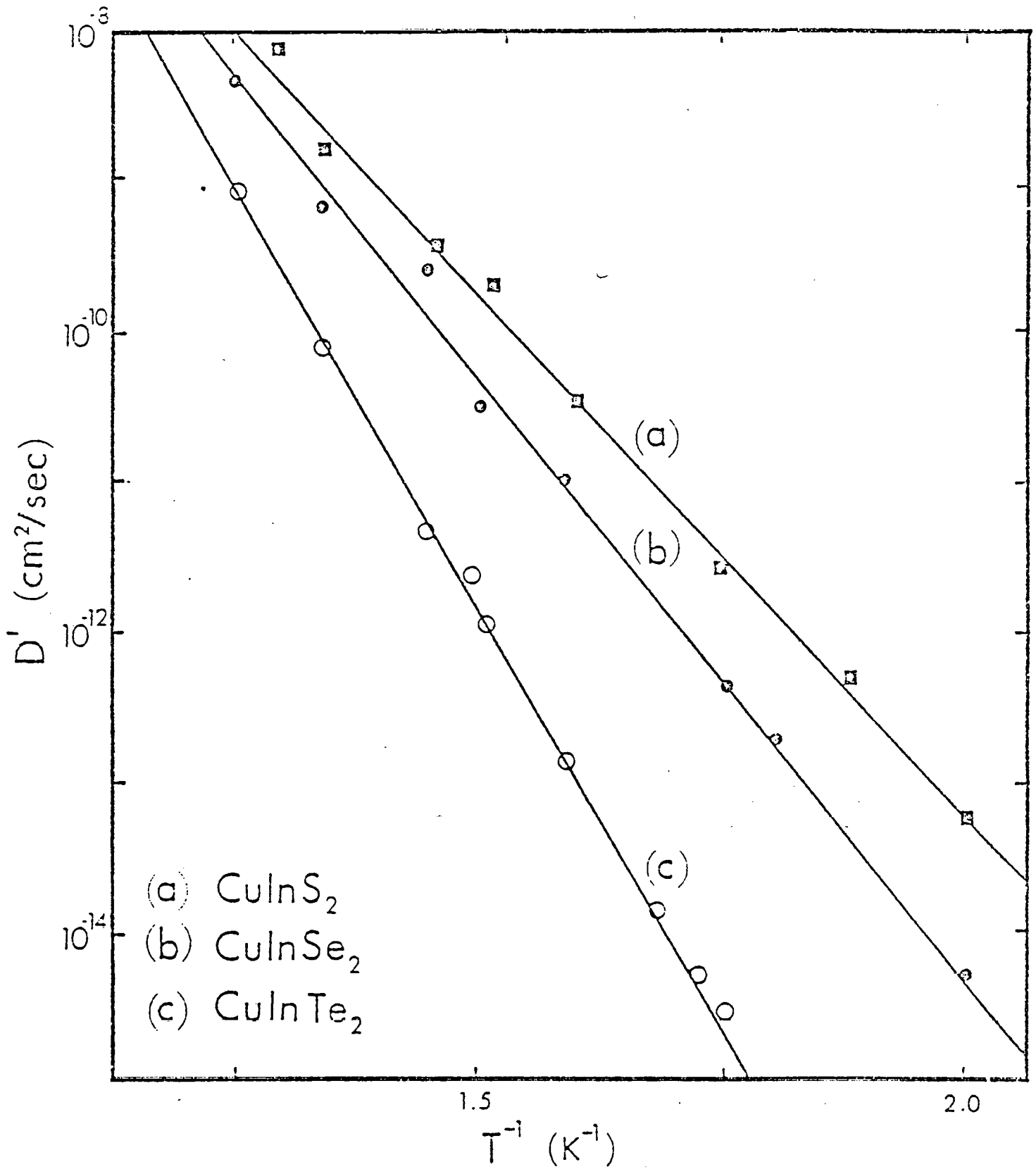


Fig. 11. Temperature dependence of grain boundary diffusion coefficient,  $D$  for Cd from the CdS thin film layer.

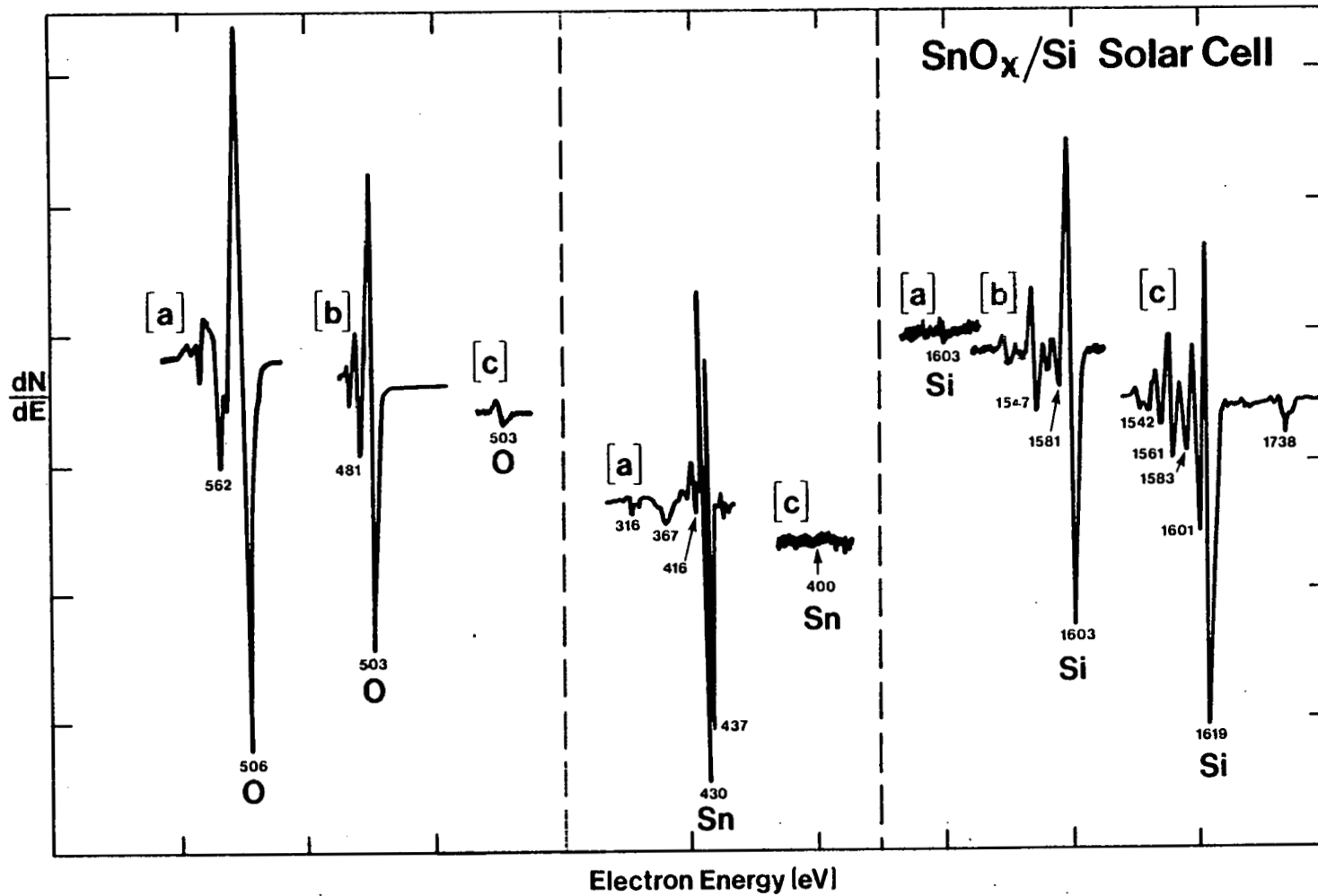


Fig. 12. Differentiated AES spectra for  $\text{SnO}_x/\text{Si}$  heterojunction solar cell. (a) is in  $\text{SnO}_2$  layer, just before interface, (b) is detected  $\text{SiO}_2$  layer at interface, and, (c) is in Si, just after junction interface.

### 3.9.7 Diffusion Definitions

#### I. Diffusion in a material at chemical equilibrium

-Uniform chemical and native defect composition

(i) SELF DIFFUSION: For solvent species

(ii) ISOCONCENTRATION DIFFUSION: For solute species

#### II. Diffusion entailing a net chemical flux

-System not in equilibrium; chemical potential gradients establish chemical fluxes.

(i) INTERDIFFUSION (or Chemical Diffusion): Results in net flow of matter which generally leads to an expansion or contraction of the diffusion region.

THIS PAGE INTENTIONALLY LEFT BLANK

**3.10 REPORT ON THE STABILITY OF CdS AND AMORPHOUS BASED THIN-FILM SOLAR CELLS**

SERI AUTHOR: L. L. Kazmerski

OTHER AUTHOR: J.D. Meakin (IEC Delaware)

PROCEEDINGS: Proceedings of the NBS Workshop of Stability of  
Thin Film

CONFERENCE: NBS Workshop on the Stability of Thin-film Solar Cells  
and Materials  
Gaithersburg, MD  
May 1-3, 1978

## REPORT FROM GROUP 1

Co-chairman - Larry Kazmerski and John D. Meakin

Group 1 covered the conventional CdS/Cu<sub>2</sub>S cell, InP/CdS and copper ternaries with CdS. Amorphous silicon was also included in the group but, unfortunately, was virtually unrepresented for much of the discussion. We will not attempt to cover things in the order in which they were considered as the discussions tended to move from topic to topic in a somewhat random manner. The makeup of the group rather obviously influenced the areas which were of concern and on which most time was spent. Probably a majority of the group are engaged in research on what were christened "infant cells." These are cells which are so young that much of the present work is concerned more with materials than complete devices. The second major component of the group were those engaged in either research or development of the traditional CdS/Cu<sub>2</sub>S cell. For obvious practical reasons, at least some of these people are now becoming directly concerned with cell lifetimes and stability. We were fortunate to have present representatives of both the commercial companies now entering the manufacturing stage. We will now deal with the specific topics that were discussed to a reasonable extent and in which a fair amount of consensus was achieved.

### Degradation Mechanisms

The first viewgraph shows a listing of five degradation mechanisms which seem to cover all the failures that one could expect in the cells under discussion. Interdiffusion implies mass transfer. This could be the motion of an atomic species from one part of the junction to another or in the case of amorphous silicon, this could be actual effusion of hydrogen out of the device. Under the chemical category would be things like oxidation, corrosion, or any other change in chemical state. Electrolytic decomposition implies the motion of charged ions under the influence of an electric field. Such an effect has been extensively reported for the Cu<sub>2</sub>S component of the CdS/Cu<sub>2</sub>S cell. Photochemical degradation would encompass any change that is directly photon induced. The final category, mechanical or structural degradation, is something of a catch-all. Typical examples would be grids lifting from the surface of the cell or delamination of various cell layers.

I think it is fair to say that much of the thinking that went into the above list was in the framework of completed devices. However, one can probably take all that was said and mutatis mutandis apply it to component materials rather than total devices. Much of the research work on infant cells will in fact involve exploring the above types of effects with regard to the component materials. In due course, the studies will have to be extended to complete devices. There are, of course, a very large number of tests and analytical



procedures that will be used in exploring or investigating these degradation mechanisms but there seems little to be gained by trying to list them.

The next subject covered was probably dealt with toward the end of the discussion rather than at the logical time which would have been right at the beginning. How does one define degradation? In the context of actual use of cells and deployment there was universal agreement that efficiency is the key parameter. Degradation is then the change of efficiency, presumably a reduction, over a time period. For research purposes, all the cell parameters are critical and the major concern here was that reporting of experimentation should be very full and complete. Even if the major point of an experiment is to monitor a single cell parameter such as short circuit current, the reporting should be as complete as possible and give information on all other critical aspects of the tests. A particular concern expressed was that the zero time data should be very fully given. In the absence of a complete description of cell structure and properties before degradation is induced, it is difficult if not impossible to assess the significance of the degradation data.

### Accelerated Testing

Much of the discussion in this area was motivated by the paper presented by Dr. Thomas of Battelle. The second viewgraph shows the goal of accelerated testing and some rules which were suggested. The goal is to project the usable deployment lifetime from short term testing. The rules are probably not all those necessary to insure meaningful and reliable accelerated testing but represent our first efforts to provide guidance. The first requirement is to establish a meaningful base population of cells. This is what we have been calling the zero time data. It is then necessary to establish that failures induced by the stressing have their equivalence in deployment failures. In order to be able to project performance, it is necessary to establish either empirically or theoretically the functional relationship between the stressing and lifetime. In this area, questions of continuous (e.g., diffusion) and discontinuous (e.g., cracking) failure modes must be addressed. Finally, although Dr. Thomas indicated that he felt from a statistical point of view five stress levels were necessary, the experimentalists were unenthusiastic about the amount of testing that this implies. In the end we went on record as recommending that at least three stress levels are necessary although acknowledging that five might well be preferable.

To try to summarize the above rules and considerations, we have put together a hypothetical stress-performance graph as shown in viewgraph No. 3. The graph shows a range of accelerated testing and the anticipated deployment range. The accelerated range should be as wide as possible and is shown with five stress levels as discussed above. The same failure mode will presumably be established on the basis of failure analysis of cells from the field and from

accelerated testing. The straight line relationship shown is to indicate the continuity of failure from the accelerated into the deployment range. The fourth point on the view-graph is the data base corresponding to the zero time cell population. Finally, lacking an obvious place to mark it on the graph, we have put a question mark referring to the possible effects of synergism or interaction between intentional and possibly unintentional stress situations.

Recalling some of my opening remarks about experiments on new materials and infant cells, there is obviously a subset of the above accelerated testing applying predominantly to materials and components. Results of investigations in this area are unlikely to be functional relations between stress situations and device lifetime. However, there will be very valuable data generated relating the effects of various stresses on new and developing materials. The remarks made above about the necessity for complete reporting and zero time data apply equally well in this area.

#### Deployment (Real-Time) Testing

Discussions in this area did not lead, or even show any promise of leading, to specified test procedures for real time or deployment testing. Substantial agreement was, however, reached in defining the manner in which such testing will be reported. The fourth viewgraph shows in summary the results of the discussions. Complete reporting of insolation conditions is well known to be extremely difficult, but a fair amount of information can be given so that other research groups can at least assess the reported results. Total insolation and peak insolation rates are reasonably easily measured and the requirement here would be to specify the measuring technique. Spectral content is an entirely different matter but as a minimum, the source of illumination should be specified. For example, AMI simulation could be achieved with ELH lamps or with water filtered quartz-iodine. In the thermal area the important measurements would be the ambient temperature giving both the extreme and the average. There was at least one vigorous proponent of requiring that actual device temperatures also be reported. Other possibly important thermal data would be measurements of both time and spatial gradients of temperature. The experience with the flat-plate silicon arrays suggest that mechanical stresses may also play a prominent role in degradation. Ideally, one would like to know the residual stresses due to the thermal history of the device or array and also those stresses imposed due to thermal cycling, wind pressure and so on. The electrical loading of a cell or array obviously strongly influence its lifetime and full information on the loading system should be given. Other ambient parameters which could influence cell life should be specified as appropriate.

This category could include information on humidity, wind, rain, dust and so on. Finally on the viewgraph, although possibly it would have been more appropriate to put this first, would be complete information on the zero time

data. This could include the sample size, its manner of selection, and a complete description of the base or undegraded properties of the cells under test.

### Other Subjects

In addition to the subject covered above, there were various amounts of discussion on a number of other matters. These occurred at various times during the discussion period and we shall make no attempt to put them in any sort of logical order or rank them in order of priority.

The question was raised as to whether a central testing facility was necessary or desirable. Those engaged in purely research activities could see no benefit to such a facility and felt that the turn around time for information would be far too long. We do not wish to misquote the manufacturers who were represented, but my memory is that they felt other more conventional market forces would establish the credibility of a given product and so again there was little benefit in a central facility. One or two people could conceive of some value of such an activity to the sponsoring agencies who may be presented with the task of assessing and comparing the stability studies of different laboratories and organizations. A possible alternative that would serve most groups was seen as the establishment of a set of testing procedures which all parties would adhere to.

In the limited time, there were many topics not dealt with adequately or even in fact mentioned. We would suggest that a vital fact which we shall not be able to ignore is the high likelihood of synergism or interaction between various stressing systems. In due course, we will obviously have to take account of such interactions. Another area that received little if any attention was the precision with which accelerated testing would have to be conducted. If short term tests are to be used to project over long time periods, there are obviously some very rigorous requirements for the precision with which measurements are taken. A number of people drew attention to the fact that special research techniques will have to be developed for degradation studies. Finally, a subject which Dr. Feucht raised in one of the small meetings was that of using time shortening studies in contrast to actual accelerated testing. If the degradation mechanism is caused by the cycling of illumination rather than the total amount of illumination, then one could simulate a year's exposure in about a month by simulating very short days. There may as well be a number of degradation modes which will fit in this category and considerable economy of testing time should be achievable.

DEGRADATION MECHANISMS

CHEMICAL	(CHEM. CHANGE)
ELECTROLYTIC	(ION MOBILITY)
PHOTOCHEMICAL	(PHOTON INDUCED)
MECHANICAL	(STRUCTURAL)

View Graph 1

## ACCELERATED TESTING

### GOAL

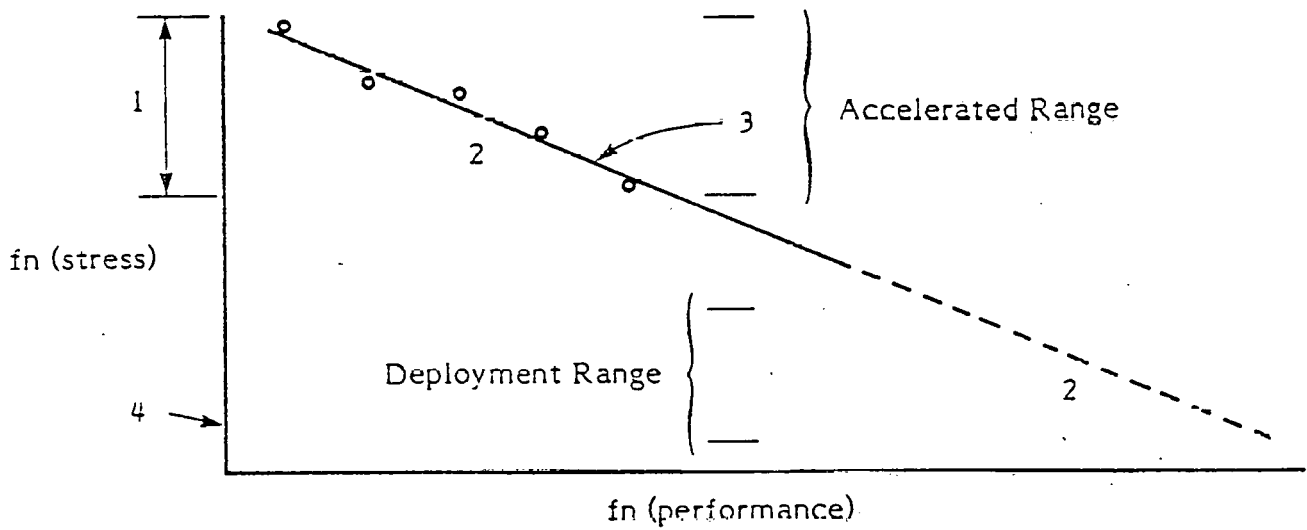
Project Deployment Lifetime

### RULES

- 1 Establish base population
- 2 Establish that accelerated failure mode matches deployment failure mode
- 3 Establish functional relation between stress and performance.  
(Note any anomalies and continuity or discontinuity of failure mechanism)
- 4 Conduct testing over at least 3 or preferably 5 stress levels.

View Graph 2

ACCELERATED TESTS



- 1 As wide as possible
- 2 Same failure mode
- 3 Continuity
- 4 Zero time cell population
- ? Synergism

View Graph 3

DEPLOYMENT-REAL TIME TESTING

INSOLATION	TOTAL PEAK SPECTRAL
THERMAL	AMBIENT DEVICE
STRESS	RESIDUAL DEPLOYMENT
ELECTRICAL LOADING	STATIC DYNAMIC
AMBIENT	HUMIDITY RAIN,DUST
ZERO TIME	SAMPLE SIZE SELECTION BASE PROPERTIES

View Graph 4

THIS PAGE INTENTIONALLY LEFT BLANK



### 3.11 GROWTH OF $\text{CuInSe}_2$ ON $\text{CdS}$ USING MOLECULAR BEAM EPITAXY

SERI AUTHOR: L. L. Kazmerski

OTHER AUTHORS: A. H. Clark, M. C. Graf, and F. R. White  
(University of Maine)

JOURNALS: Journal of Applied Physics (to appear)

#### ABSTRACT

Molecular beam epitaxy has been used to grow  $\text{CuInSe}_2$  on  $\text{CdS}(0001\text{B})$ . Epitaxial growth, as determined from in situ reflection electron diffraction, was observed at a substrate temperature of  $300^\circ\text{C}$ . This is the first report of MBE growth of a ternary compound.

The technique of molecular beam epitaxy<sup>1,2</sup> (MBE) is becoming an increasingly important method of producing high quality semiconductor films for both devices and basic studies. To our knowledge, MBE has thus far been restricted to the growth of binary (e.g., GaAs,<sup>1,2</sup> ZnTe<sup>3</sup>) or binary alloy compounds ( $\text{Al}_x\text{Ga}_{1-x}\text{As}$ ,<sup>1,2</sup>  $\text{ZnSe}_x\text{Te}_{1-x}$ <sup>3</sup>). In this letter we report epitaxial growth of the ternary chalcopyrite  $\text{CuInSe}_2$  on CdS using MBE.

$\text{CuInSe}_2$  is a material with potential optical and electro-optical applications (1.04 eV direct gap). In particular, the  $\text{CuInSe}_2$ -CdS system has nearly optimum efficiency as a heterojunction solar cell<sup>4</sup> and has already shown promising results in a completely thin-film form.<sup>5</sup> The lattice mismatch between the (0001) surface of CdS and the (221) surface of  $\text{CuInSe}_2$  is 1.16%.

The MBE apparatus in this study employs an ultra-high vacuum ion-pumped system (base pressure in the low  $10^{-10}$  Torr range). The effusion cells are mounted at  $20^\circ$  to the vertical in a source-shroud assembly (Physical Electronics, Inc.) which provides water cooling around the cells and a liquid nitrogen shroud around the entire assembly. The source-substrate distance is approximately 3 inches. A quadrupole residual gas analyzer, 5 kV sputter ion gun, and a 3 kV grazing incidence ( $\sim 3^\circ$ ) reflection electron diffraction system (RED) are incorporated into the system.

The  $\text{CuInSe}_2$  films were grown from three elemental sources at the following temperatures: copper  $1020^\circ\text{C}$  to  $1050^\circ\text{C}$ , indium  $850^\circ\text{C}$ , and selenium  $215^\circ\text{C}$  to  $230^\circ\text{C}$ . The pressure during growth was in the  $10^{-8}$  Torr range. The CdS substrates (0001B) were chemomechanically polished using an aqueous solution of HCl and KCl (pH = 1.0).<sup>6</sup> Prior to deposition the substrates were sputter cleaned and annealed at  $350^\circ\text{C}$ .

Stoichiometry control is more critical in a ternary as compared to a binary alloy compound. In these initial experiments, the effusion rates were controlled by source temperature rather than by beam fluxes directly. The composition of our best films was within 2% to 3% of stoichiometry, as determined by Auger spectroscopy. This was not sufficient to give consistent electrical properties, but an x-ray powder pattern taken on a polycrystalline film deposited onto fused silica showed only  $\text{CuInSe}_2$  lines. In addition, optical absorption coefficients were measured on several films, and all showed an absorption edge at about 1.04 eV.<sup>7</sup>

Fig. 1 shows the RED pattern of (a) the CdS substrate prior to deposition, and (b) a 3000 Å  $\text{CuInSe}_2$  layer deposited at a  $300^\circ\text{C}$  substrate temperature (deposition rate  $\sim 1\mu/\text{hour}$ ). Layers deposited at lower substrate temperatures showed no discernible diffraction patterns.

A more detailed description of structural, electrical, and optical properties of these films will be presented in a subsequent paper.

The authors wish to thank S. Mittleman, S. Wagner and W. Unertl for helpful discussions.

### References

1. A. Y. Cho and J. R. Arthur, Progress in Solid State Chemistry, edited by J. McCaldin and G. Somorjai (Pergamon, New York, 1975), pp. 157.
2. L. L. Chang, L. Esaki, W. E. Howard, R. Ludeke and G. Schul, J. Vac. Sci. Technol. 10, 655 (1973).
3. D. L. Smith and V. Y. Pickhardt, J.A.P. 46, 2366 (1975).
4. P. J. Ireland, L. L. Kazmerski and S. W. Wagner, submitted for publication.
5. L. L. Kazmerski, F. R. White, and G. K. Morgan, Appl. Phys. Lett. 29, 268 (1976).
6. A. A. Pritchard and S. Wagner, J. Electrochem. Soc. 124, 961 (1977).
7. L. Y. Sun, L. L. Kazmerski, A. H. Clark, P. J. Ireland and D. W. Morton, J. Vac. Sci. Technol. 15, 265 (1978).

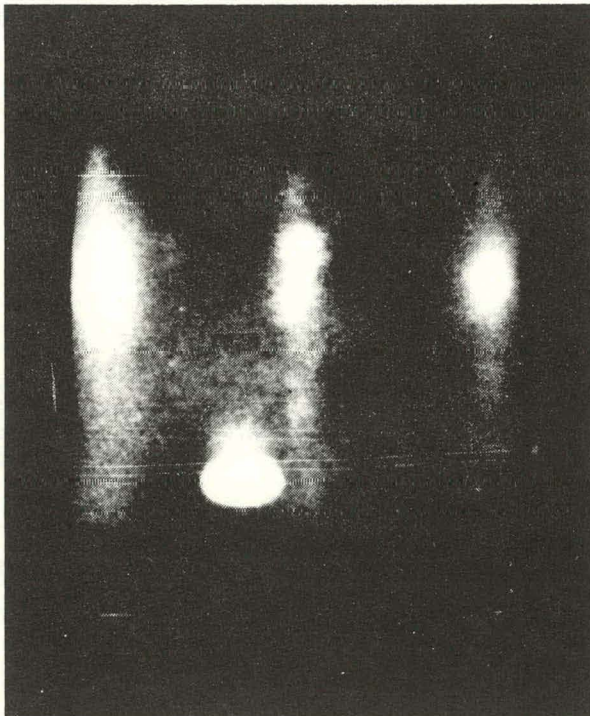


Fig. 1a. RED pattern of CdS  
Substrate prior to  
deposition.

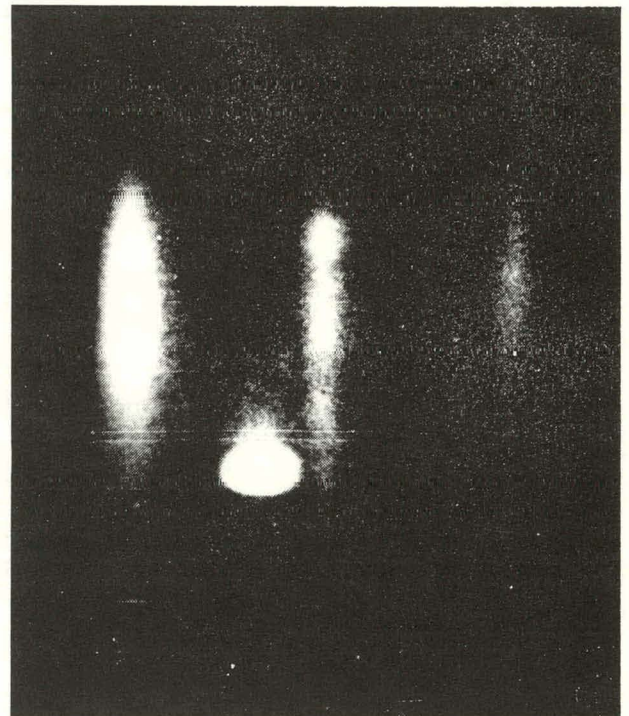


Fig. 1b. RED pattern of 300 Å<sup>o</sup>  
CuInSe<sub>2</sub> layer deposited  
at a 300°C substrate  
temperature (deposition  
rate ~ 1μ/hour).

### 3.12 ABSORPTION COEFFICIENT MEASUREMENTS FOR VACUUM DEPOSITED Cu-TERNARY THIN FILMS (Abstract Only)

SERI AUTHORS: L. L. Kazmerski and P. J. Ireland

OTHER AUTHORS: L. Y. Sun, A. H. Clark, and D. W. Morton  
(University of Maine)

CONFERENCE: 24th Annual AVS Symposium  
Boston, MA  
November 8-11, 1977

#### ABSTRACT

The absorption coefficients of polycrystalline  $\text{CuInS}_2$  and  $\text{CuInSe}_2$  thin films have been determined at room temperature using transmission measurements. For each of these semiconductors, an absorption edge corresponding to the direct band-gap transition ( $1.54 \pm 0.02$  eV for  $\text{CuInS}_2$ , and  $1.00 \pm 0.02$  eV for  $\text{CuInSe}_2$ ) is observed in the  $\alpha$  vs  $h\nu$  spectrum. In p-type  $\text{CuInS}_2$  thin films, another edge is evident at lower energies (1.41 - 1.42 eV) and is attributed to transitions from a copper vacancy band to the conduction band. The effects of annealing on the absorption coefficient spectra of these chalcopyrite materials are presented. An additional absorption region appears in the  $\text{CuInSe}_2$  spectra at higher energies ( $h\nu > 1.28$  eV), and is critically dependent on the Se concentration of the films. This effect is discussed in terms of band structure, film stoichiometry and structural characteristics of the films.

THIS PAGE INTENTIONALLY LEFT BLANK

### 3.13 A COMBINED IRRADIANCE - TRANSMITTANCE SOLAR SPECTRUM AND ITS APPLICATION TO PHOTOVOLTAIC EFFICIENCY CALCULATIONS

SERI AUTHORS: P. J. Ireland, S. Wagner, L. L. Kazmerski, and R. L. Hulstrom†

#### ABSTRACT

SOLTRAN is a flexible computer model for the direct solar beam intensity spectrum at the earth's surface. It has been derived by combining the extraterrestrial solar spectrum with the atmospheric transmittance spectrum. Application of SOLTRAN to the calculation of the potential efficiency of photovoltaic cells demonstrates the effect of atmospheric absorption bands which prevent unequivocal assignment of optimum energy gap values.

†Energy Resource Assessment Branch

### 3.13.1 Introduction

In this paper we report the development of a new solar power density spectrum and its application to the calculation of maximum potential efficiencies of photovoltaic cells.

The SOLTRAN computer model is derived by combining the extraterrestrial solar spectrum with the atmospheric spectral transmittance. Earlier solar spectra in the region between  $\lambda = 0.8$  and  $1.0 \mu\text{m}$  are discussed in some detail because of their interest to photovoltaic converters. It is shown that SOLTRAN correctly incorporates the accepted water absorption bands as do Moon's spectra (1). The terrestrial spectra reported by Gates (2) and by Thomas and Thekaekara (3) are found to be incorrect in this wavelength regime.

Solar cell short circuit currents have been derived from the SOLTRAN model and incorporated in efficiency calculations for single homodiode, for heteroface and for multijunction cells. A number of calculations has been reported on the maximum light-to-electrical power conversion efficiency attainable with photovoltaic solar cells. Early papers dealt with shallow homodiode cells, applying semi-empirical device analysis (4,5) or thermodynamic arguments (6). All photons with energies above the band gap were considered to contribute to the photocurrent. In the course of the development of heterojunction cells, efficiencies of cells incorporating "window" layers were projected (7,8). The economic prospects of multijunction converters to be used in concentrator systems have stimulated calculations for cascaded cells with individual narrow spectral responses (9-18). In this paper a simple phenomenological diode model (5) was employed together with a constant fill factor. Series optical and electrical structures were assumed for multijunction cells. These photovoltaic efficiency calculations show that the water absorption bands prevent the unequivocal identification of maxima in the efficiency vs. energy gap functions.

#### 3.13.1.1 Solar Power Density Spectrum

SOLTRAN is a combined solar irradiance-atmospheric transmittance computer model, capable of predicting the direct solar beam intensity spectrum (0.25 to  $3.0 \mu\text{m}$ ) at the earth's surface. At present, the spectral resolution is  $200 \text{ cm}^{-1}$ . The extraterrestrial solar spectrum (3) was folded into a modified atmospheric transmittance program, LOWTRAN, (20) and the solar vector geometry. SOLTRAN produces direct (i.e., excluding circumsolar radiation) solar beam intensity spectra at the earth's surface as a function of:

- (a) Six atmospheric conditions: 1962 U.S. Standard; tropical -  $15^\circ\text{N}$ ; midlatitude summer -  $45^\circ\text{N}$  July; midlatitude winter -  $45^\circ\text{N}$  January; subarctic summer -  $60^\circ\text{N}$  July; subarctic winter -  $60^\circ\text{N}$  January. Actual temperature, pressure, and water vapor data can be inputted at 1 kilometer altitude increments.



- (b) Relative air mass for 0 to 90° solar elevation, and including the influence of atmospheric refraction.
- (c) Site altitude.
- (d) Aerosols; a surface visual range densities atmospheric clarity (a measure of aerosol concentration) and its altitude profile. Actual aerosol data can also be incorporated.

Shown in Fig. 1 is the spectrum employed in this paper for Golden, Colorado, with the following parameters: midlatitude summer-45°N July; relative air masses 0, 1, and 2; 1707 meters site altitude; clear atmospheric-35 kilometers visibility. Under these conditions, the AMI power density is  $101 \text{ mW cm}^{-2}$ .

Comparison of SOLTRAN spectra with earlier data has revealed an interesting discrepancy. Shown in Fig. 2 is an AMI spectrum calculated by Thomas and Thekaekara (TT) (3), which is based on and nearly identical to the earlier work of Gates (2). Gates' work and technique have been used by numerous other investigators to produce similar solar power density spectra. Visual comparison of the AMI spectra of Fig. 1 and Fig. 2 reveals a discrepancy in the  $\lambda = 0.8$  to  $1.0 \mu\text{m}$  region. Fig. 2 shows deep absorption/attenuation between  $0.84$  and  $0.95 \mu\text{m}$  whereas the SOLTRAN spectrum (Fig. 1) shows little absorption except for the narrow band at  $0.94 \mu\text{m}$ .

The discrepancy may indicate an error in spectral measurement or evaluation procedures that calls for correction. Also, the width and intensity of the band is of interest to photovoltaic conversion, as it is used to argue in favor of GaAs ( $\lambda_{\text{gap}} = 0.868 \mu\text{m}$ ) over InP ( $\lambda_{\text{gap}} = 0.926 \mu\text{m}$ ). Therefore we carried out a preliminary investigation by directly comparing the fractional atmospheric transmittance of SOLTRAN to TT.

The major source of atmospheric attenuation in the  $\lambda = 0.8$  to  $1.0 \mu\text{m}$  region is water vapor. The available TT data are for sea level with precipitable water content of 20 millimeters. The SOLTRAN program for sea level at midlatitude includes 34 mm precipitable water. A 34 mm precipitable water content in the TT data would cause even deeper water-related absorption than shown in Fig. 2. The spectral shape however, which is the more important question to be addressed, will be comparable. In Fig. 3 relative transmittances are plotted for SOLTRAN (curve A) and for TT (curve B). As expected, a major discrepancy exists. SOLTRAN exhibits the well known  $\rho$  and  $\sigma$  water absorption bands (21), but not the  $\tau$  band due to currently insufficient resolution. Curve B is anomalous; it is not attributable to water vapor. A comparison with the data of Moon (1) shows that the structure of Moon's spectral attenuation curves at  $\lambda = 0.8$  to  $1.0 \mu\text{m}$  are similar to that of SOLTRAN. Further analysis is underway with the aim of exploring the anomalous attenuation reported by TT and by Gates.

### 3.13.1.2 Solar Cell Efficiency

The cell efficiency,  $\eta$ , was computed from the short circuit current density,  $J_{sc}$ , the open circuit voltage,  $V_{oc}$ , the curve fill factor,  $F$ , and the incident solar power flux density,  $P$ , as

$$\eta = \frac{J_{sc} V_{oc} F}{P} \quad (1)$$

$J_{sc}$  was calculated assuming a quantum efficiency,  $Q$ , of 0.90, uniform over the spectrum to which a specific diode can be sensitive according to band gap consideration:

$$J_{sc} = qQ \int_{\lambda_1}^{\lambda_2} \phi(\lambda) d\lambda \quad (2)$$

where  $q$  is the electronic charge,  $\phi(\lambda)$  the photon flux density derived from SOLTRAN,  $\lambda_1$  the short and  $\lambda_2$  the long wavelength cutoff, respectively.

$V_{oc}$  was calculated for two series of devices (5). In one, dark current-voltage characteristics are controlled by bulk injection; in the other, by recombination within the space charge. This procedure does not take into account the transition from bulk to space charge controlled current when passing from large to small band gap members of a multijunction device, nor does it consider non-ideal contributions, for example, from bulk or series resistance. However, the results clearly delineate the regime of attainable efficiencies and of optimum band gap values.

The single current type diode equation leads to the following expression for  $V_{oc}$ :

$$V_{oc} = \frac{AkT}{q} \ln\left(\frac{J_{sc}}{J_0} + 1\right) \quad (3)$$

( $A$  is the diode factor, equal to 1 for diffusion controlled current, and equal to 2 for recombination controlled current,  $k$  is the Boltzmann constant,  $T$ , the absolute temperature, and  $J_{sc}$  is the short circuit current density).

The reverse saturation current density,  $J_0$ , was expressed as a function of the energy gap  $E_g$ :

$$J_0 = B_0 \exp(-E_g/BkT) \quad (4)$$

$B_0$  was set to a value of 15, in combination with  $A = B$  (either 1 or 2) to provide realistic values of  $J_0$ . A fill factor of 0.80 was chosen for both single and multiple junction cells. No spurious optical losses (arising from reflection, lower than bandgap absorption, etc.) were taken into account.

In multiple junction cells, band gaps were adjusted to provide current continuity. Efficiencies were computed using the common short circuit current, a common fill factor of 0.80, and the sum of the open circuit voltages for the individual layers. Expressed in terms of the absorber material with the lowest gap,  $\lambda_g = hc/E_g$ ,

$$J_{sc} = \frac{qQ}{N} \int_0^{\lambda_g} \phi(\lambda) d\lambda \quad (5)$$

where  $N$  is the number of active layers. The open circuit voltage is represented by

$$V_{oc} = \sum_{i=1}^N \frac{AkT}{q} \ln \left( \frac{J_{sc}}{J_{oi}} + 1 \right) \quad (6)$$

### 3.13.1.3 Results and Discussion

Fig. 4 shows the calculated efficiency of single diode heteroface cells with  $A=B=1$  and at AM1 as a function of the energy gap ( $E_g$ ) of the absorber. Three typical "window" materials (ZnSe,  $E_g = 2.70$  eV; CdS,  $E_g = 2.42$  eV; CdSe,  $E_g = 1.70$  eV) were considered as well as the limiting case of a homodiode without an absorbing window layer. The wide range of band gaps with potentially high conversion efficiency has been noted in the earliest publications. It can be seen that detailed inclusion of the terrestrial absorption bands does result in pronounced leveling near the maxima. For instance, uncoated diodes can reach efficiencies above 29% with band gaps ranging from 0.92 to 1.37 eV. A plot of  $\eta_{max}$  vs. the  $E_g$  of the window, Fig. 5 does not reveal a significant effect of atmospheric absorption. Band gaps at maximum efficiency ( $\eta_{max}$ ) were taken to be the average of the upper and the lower band gap value at  $2\sigma$  (95.45%) of the numerical efficiency maximum. It is evident from Fig. 6 that  $E_g$  at  $\eta_{max}$  is rather insensitive to the  $E_g$  of the window. It was noticed that variation of the terrestrial air mass value has no significant effect on  $E_g$  of the absorber at  $\eta_{max}$ . For example, the AM2 curve is adequately described by the AM1 function in Fig. 6. Only when going to extraterrestrial illumination (AMO) a noticeable effect is produced.

The optimum range of absorber energy gaps depends little on the current transport mechanism. Furthermore, it is evident from Fig. 6 that the position of this optimum is rather insensitive to the band gap of the window semiconductor, taking into account the wide range of values denoted by the central points plotted in Fig. 6. In particular, the curves for AM1 and AM2 virtually superpose.

Since the key procedure of the multijunction cell calculation is the proper spectral splitting for photocurrent continuity, no passive absorbing window layers were taken into account. In Fig. 7 and 8,  $N$  denotes the number of active junctions. Identical diode current-voltage characteristics were

assumed for each diode of a given multijunction cell. The maximum efficiencies for cells with up to seven active layers as a function of the value of the lowest energy gap are as shown in Fig. 7 for  $A=B=1$  and in Fig. 8 for  $A=B=2$ . Large numbers of active layers appear unrealistic with present semiconductor technology. However, the calculations also provide a useful estimate of efficiencies attainable through other technologies with potential for photovoltaic conversion. One example could be a multilayer device produced from a series of organic semiconducting dyes, each with its characteristic narrow spectral response. Again it is evident that the atmospheric absorption bands are positioned such as to level out what would otherwise be flat but well defined efficiency maxima. The maxima efficiency as a function of  $N$ , Fig. 9, demonstrates the diminishing incremental efficiency per added layer. In fact, it is evident that optical losses somewhat larger than those implied by the assumed quantum efficiency of 0.90 could lead to a maximum in the  $\eta_{\max}$  vs.  $N$  curve, an effect that has been recognized in studies of spectral splitting (13).

### 3.13.2 References

1. P. Moon, J. of the Franklin Institute 20, 600 (1940).
2. D. M. Gates, Science 151, 523 (1966).
3. A. P. Thomas and M. P. Thekaekara in Sharing the Sun-Solar Technology in the Seventies, 1, 338, Winnipeg 1976 (The American Section of the International Solar Energy Society, Florida, 1976).
4. M. B. Prince, J. Appl. Phys. 26, 534 (1955).
5. J. J. Loferski, J. Appl. Phys. 27, 777 (1956).
6. W. Shockley and H.J. Queisser, J. Appl. Phys. 32, 510 (1961).
7. H. J. Hovel, Semiconductors and Semimetals, Vol. II (Academic Press, New York, 1975), p. 83.
8. A. de Vos, Energy Conversion 16, 67 (1976).
9. N. S. Alvi, C. E. Backus, G. W. Masden, Proceedings of 12th Photovoltaic Specialists Conference, Baton Rouge, 1976 (IEEE, New York, 1976), p. 948.
10. J. J. Loferski, Proceedings of 12th Photovoltaic Specialists Conference, Baton Rouge, 1976 (IEEE, New York, 1976), p. 957.
11. G. W. Masden and C. E. Backus, Proceedings of 13th Photovoltaic Specialists Conference, Washington, D.C. 1978 (IEEE, New York, 1978), p. 853.

12. R. L. Moon, L. W. James, H. A. Vanderplas, Y. G. Chai and G. A. Antypas, Proceedings of 13th Photovoltaics Specialists Conference, Washington, D.C., 1978 (IEEE, New York, 1978), p. 859.
13. A. Bennett and L. C. Olsen, Proceedings of 13th Photovoltaic Specialists Conference, Washington, D.C., 1978 (IEEE, New York, 1978), p. 868.
14. M. F. Lamorte and D. Abbott, Proceedings of 13th Photovoltaic Specialists Conference, Washington, D.C., 1978 (IEEE, New York, 1978), p. 874.
15. J. A. Cape, J. S. Harris and R. Sahai, Proceedings of 13th Photovoltaic Specialists Conference, Washington, D.C., 1978 (IEEE, New York, 1978), p. 881.
16. L. M. Fraas and R. C. Knechtli, Proceeding of 13th Photovoltaic Specialists Conference, Washington, D.C., 1978 (IEEE, New York, 1978), p. 886.
17. A. G. Milnes, Proceedings of 13th Photovoltaics Specialists Conference, Washington, D.C., 1978 (IEEE, New York, 1978), p. 892.
18. M. Arienzo and J. J. Loferski, Proceedings of 13th Photovoltaic Specialists Conference, Washington, D.C., 1978 (IEEE, New York, 1978), p. 898.
19. Detailed information about SOLTRAN may be obtained from R. L. Hulstrom, SERI, 1536 Cole Blvd., Golden, Colorado 80401.
20. J. E. A. Shelby and R. A. McClatchey, Technical Report AFGL-TR-75-0255, E.R.P. No. 513, AD-A017 734, 1975. The Airforce Geophysics Laboratory has expended significant effort in developing LOWTRAN. SERI has applied LOWTRAN to calculating the solar spectrum terrestrial transmittance. SERI would like to acknowledge the efforts of AFGL in improving the atmospheric transmittance calculations.
21. R.M. Goody, Atmospheric Radiation, I. Theoretical Basis (Clarendon Press, Oxford, 1964).

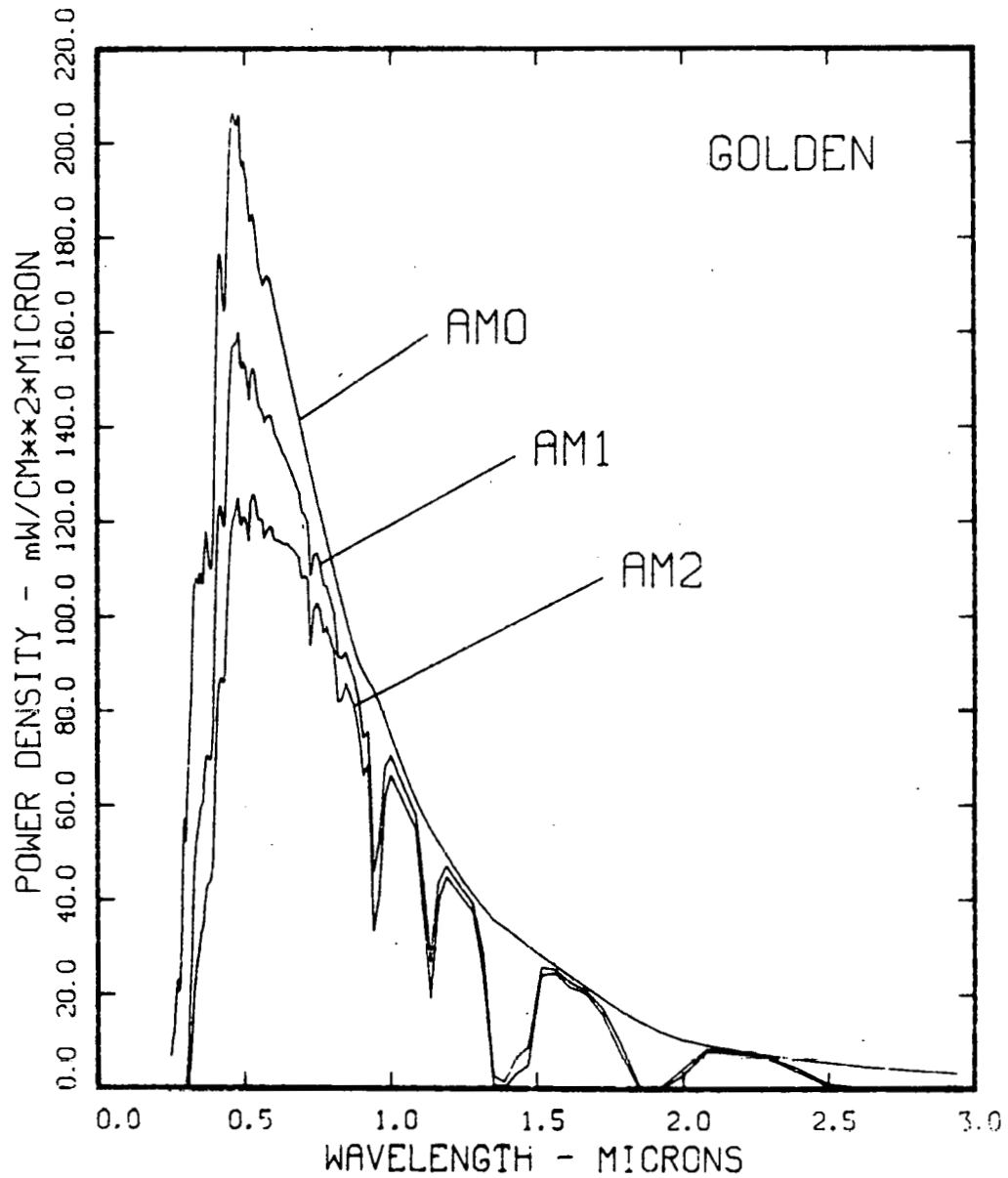


Fig. 1 Typical SOLTRAN spectra for AMO, AM1, and AM2 at mid-latitude (Golden) with a visibility of 35 km.

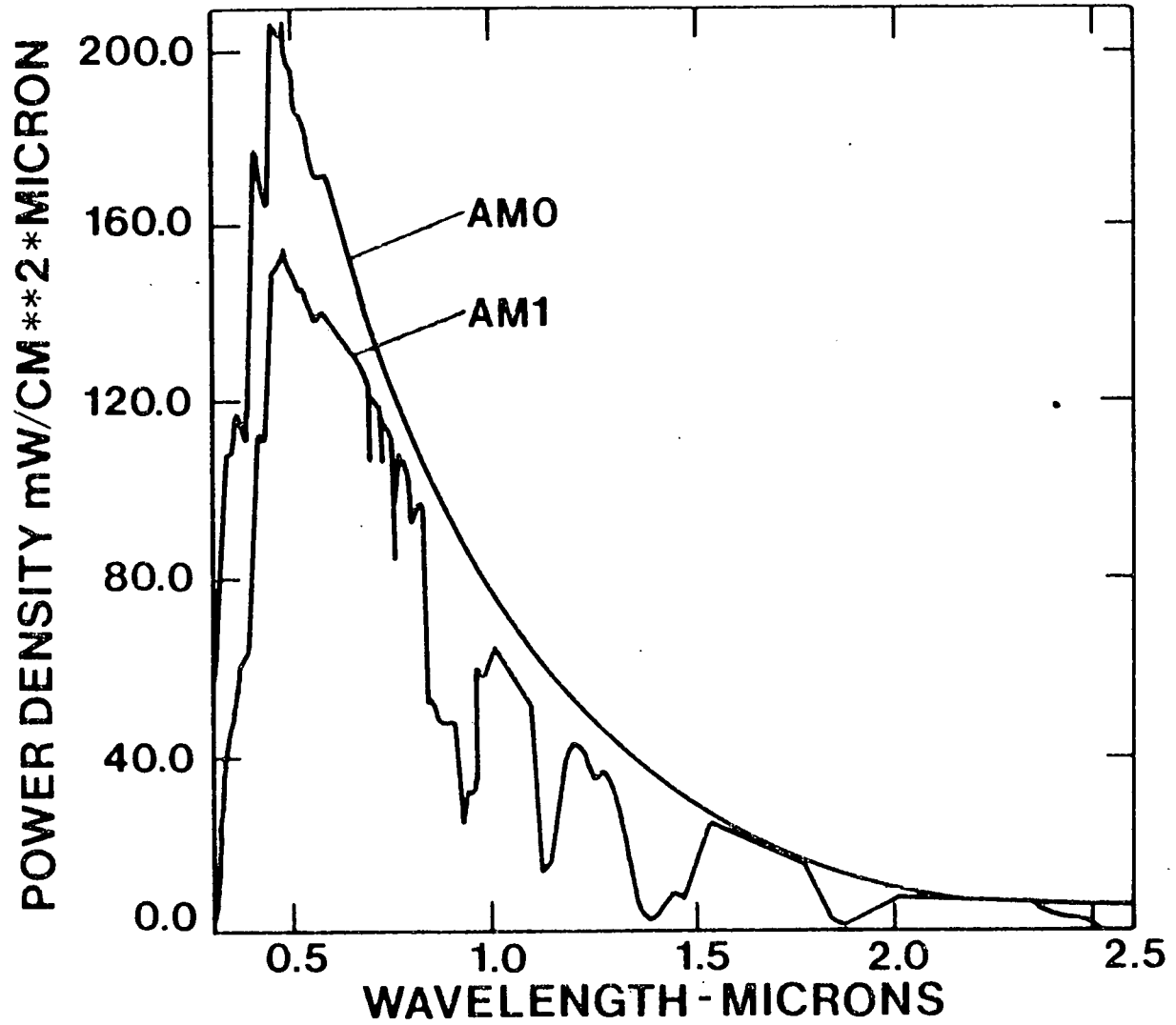


Fig. 2 Power density versus wavelength spectra of Thomas and Thekaekara (3) for mid-latitude, sea level conditions and visibility of 23 km.

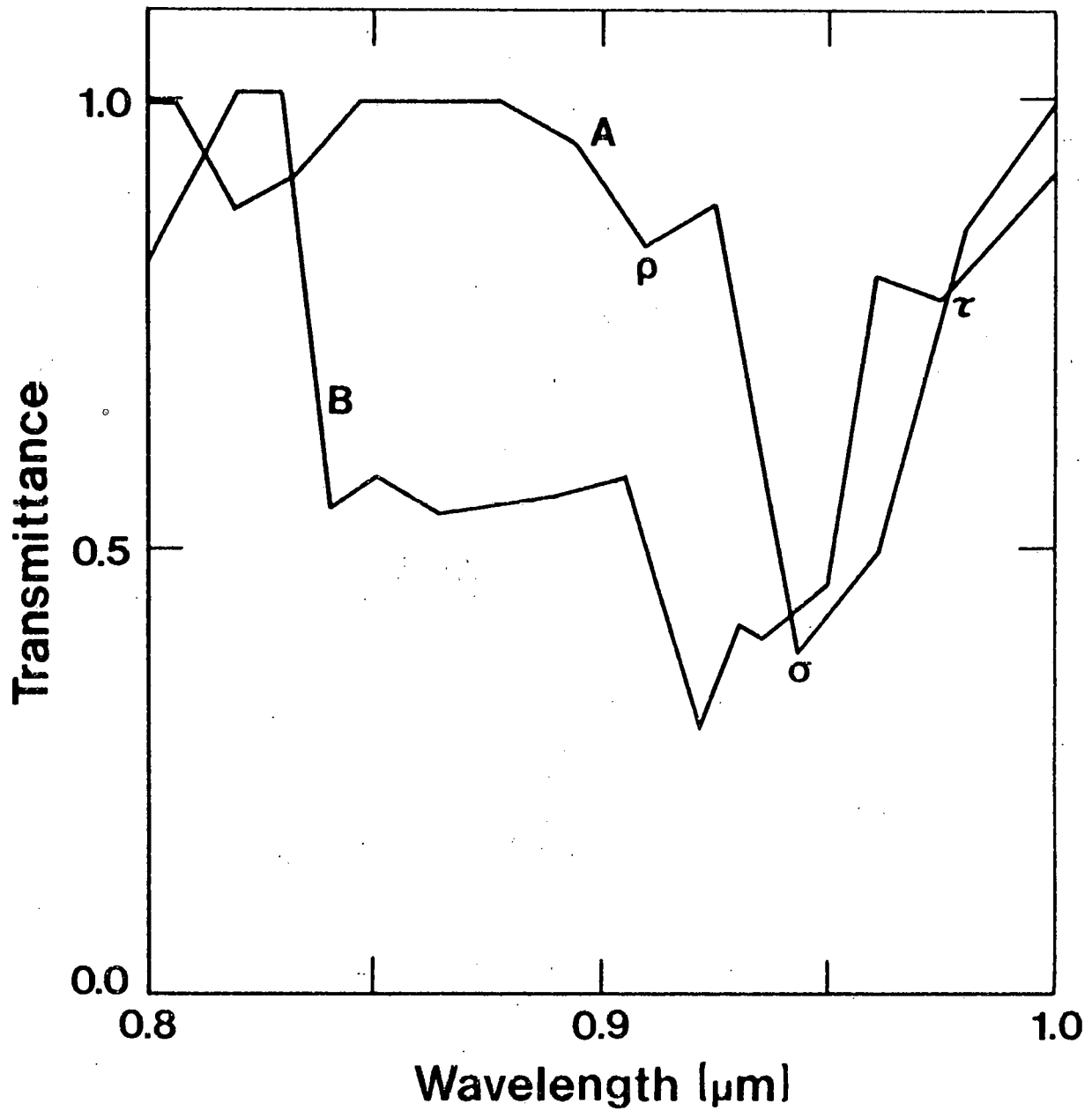


Fig. 3 Calculated water vapor transmittance curves for SOLTRAN at sea level (A) and Thomas and Thekaekara's (3) data (B) showing the water vapor bands  $\rho$ ,  $\sigma$ , and  $\tau$ .



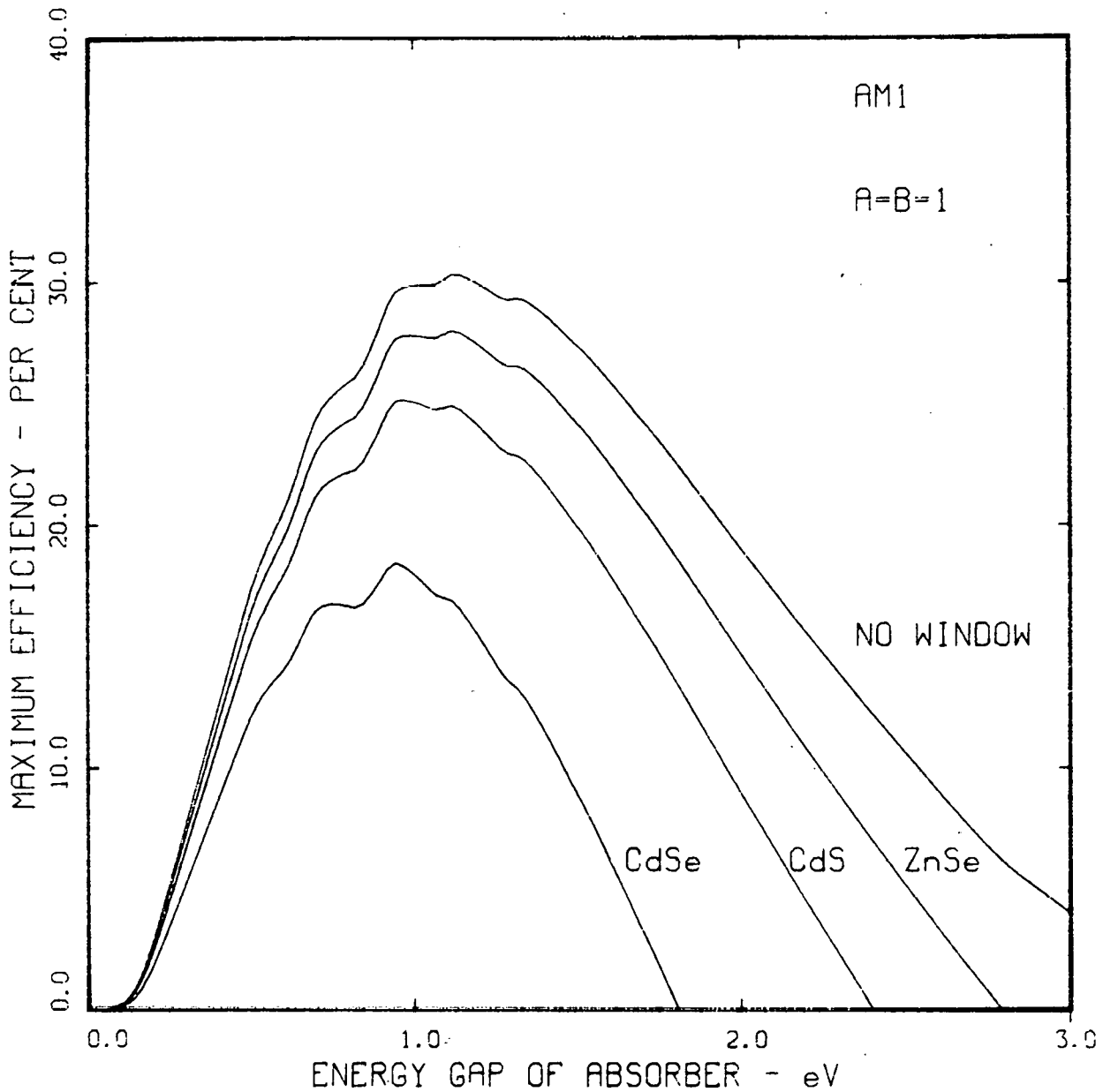


Fig. 4 Maximum efficiency calculated for heteroface diodes with  $A=B=1$  with varying absorber energy gaps and for different window energy gaps; CdSe (1.70 eV), CdS (2.42 eV), ZnSe (2.70 eV), and no window layer (5.0 eV).

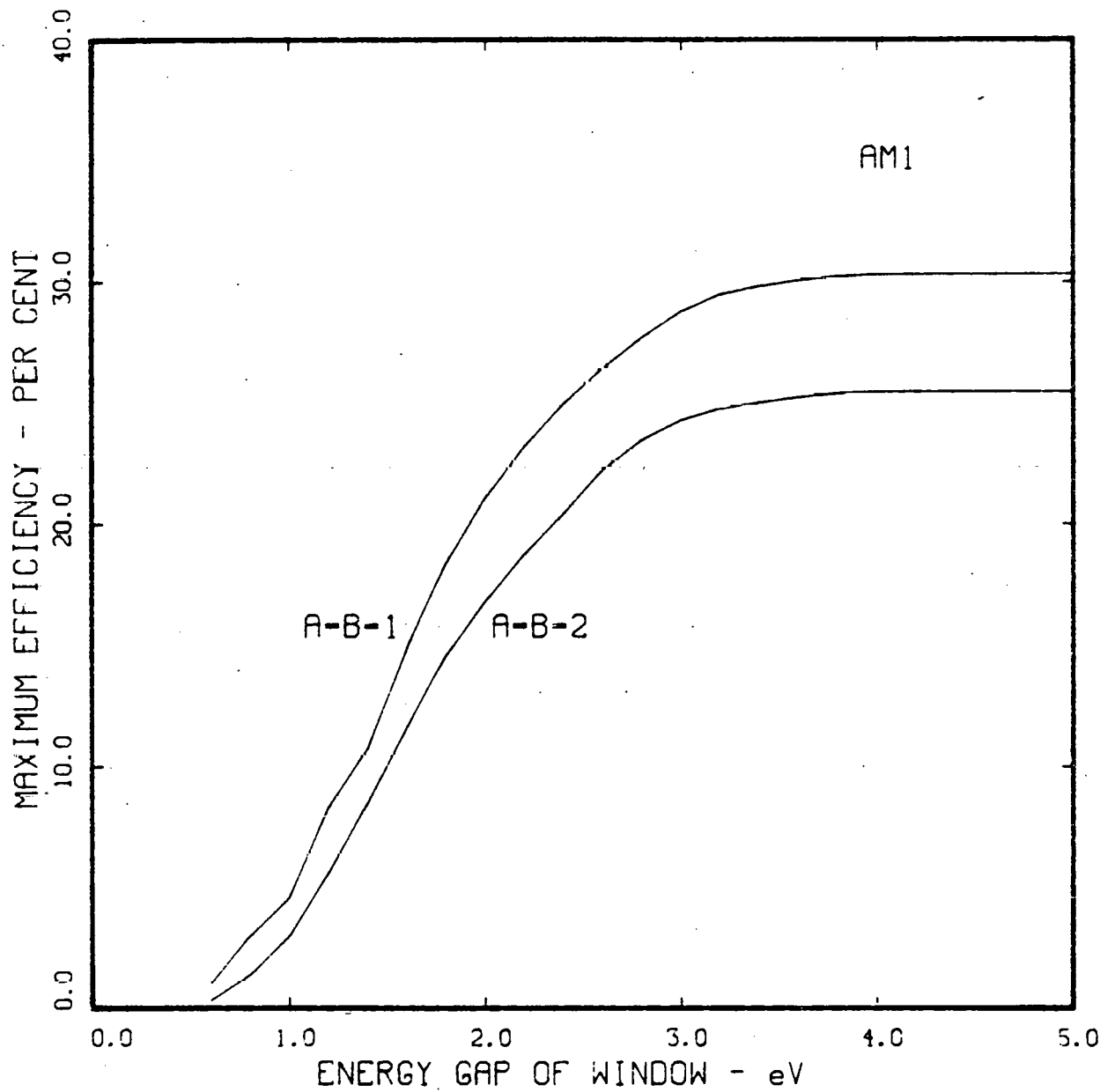


Fig. 5 Variation in maximum efficiency versus window cutoff band gap for  $A=B=1$  and  $A=B=2$ .

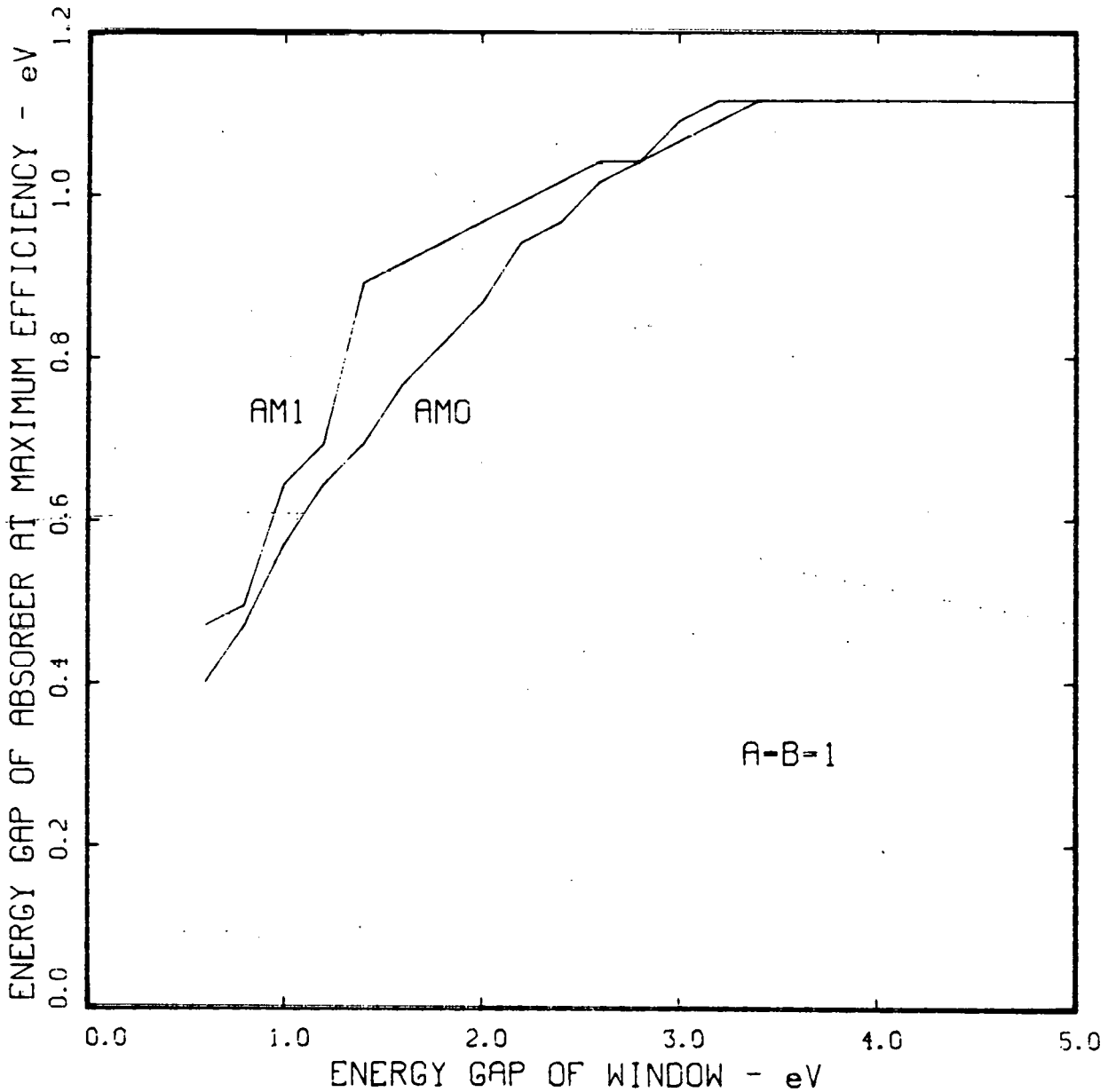


Fig. 6 Band gap at maximum efficiency as a function of the window band gap under AMO and AM1 (also AM2) conditions.

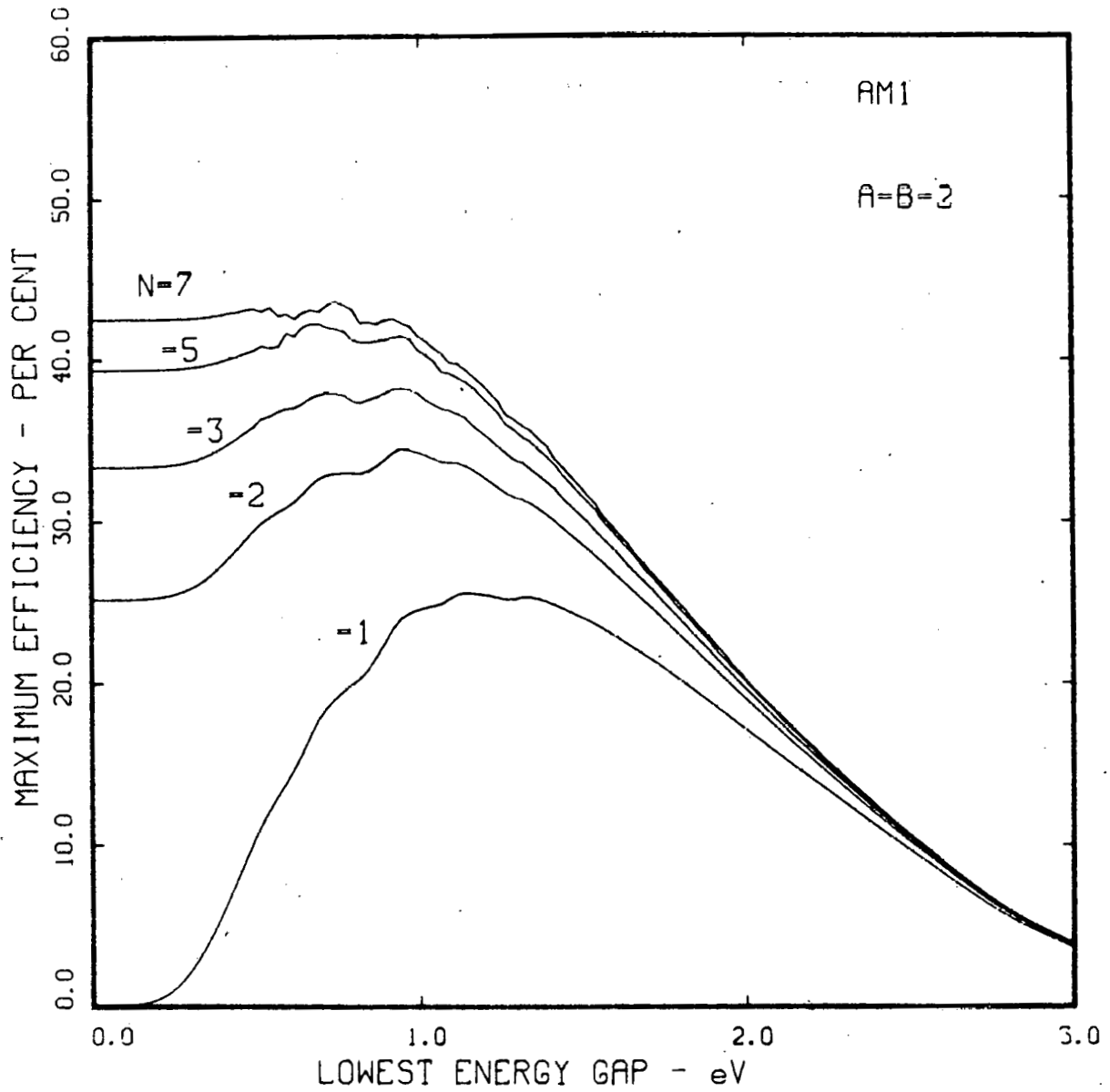


Fig. 7 Multilayer cell efficiency for 1 to 7 absorber layers A=B=1.

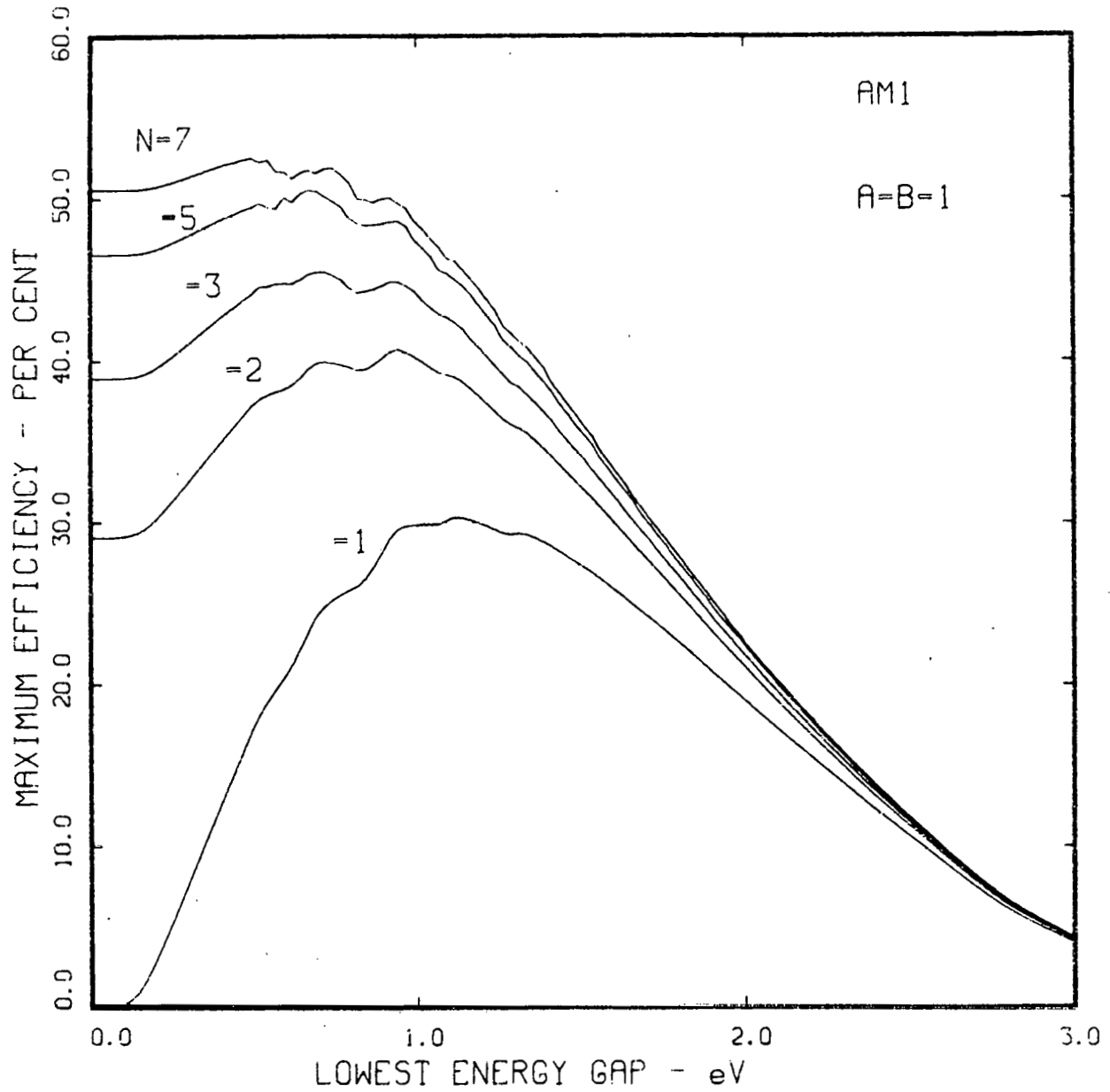


Fig. 8 Multilayer cell efficiency for 1 to 7 absorber layers with A=B=2.

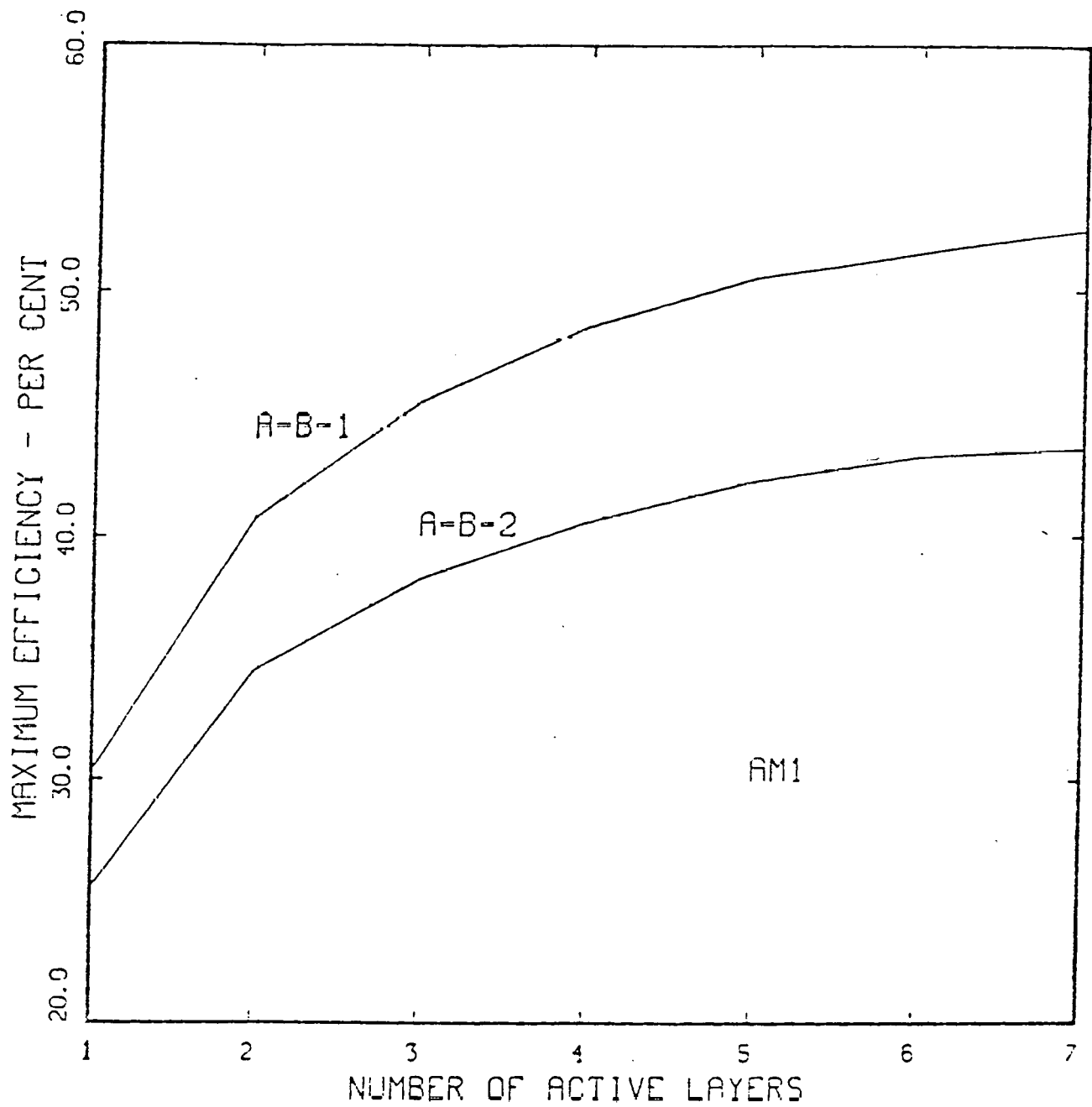


Fig. 9 Highest attainable efficiency as a function of the number of active layers under AM1 conditions.

## SECTION 4.0

## CONFERENCE PRESENTATIONS

During FY78, SERI Photovoltaics Branch members participated in technical and professional meetings relating to their areas of expertise. This provided a basis for keeping the research staff current on pertinent R&D activities and also provided the appropriate forum for dissemination of their own research results. This section summarizes the technical conference presentations of the Photovoltaics Branch staff during the FY78 period.

1. "Copper-Ternary Thin-Film Solar Cells," Presented at 152nd Electrochem. Soc. Meeting, Atlanta, GA, Oct. 9-14, 1977 (Abst. J. Electrochem. Soc. 124, 31C [1977] [L. L. Kazmerski]).
2. "Auger Electron Spectroscopy Studies of I-III-VI<sub>2</sub> Chalcopyrite Compounds," Presented at Annual American Vacuum Society Symposium, Boston, MA, Nov. 1-3, 1977 (L. L. Kazmerski).
3. "Attainable Efficiencies with Thin-Film Heterojunction Solar Cells," Presented at March Meeting of the Amer. Phys. Soc., Washington, D.C., March 27-30, 1978. Abst. Bull. APS 279, (1978), (P. J. Ireland and L. L. Kazmerski).
4. "Thin-Film Ternary Solar Cells," Presented at DOE Semiannual Review, Advanced Materials R&D Program, Reston, VA, (1978), (L. L. Kazmerski).
5. "Advanced Solar Cell Research and Development: An Overview," Presented at Mat. Sci. Conf., Argonne National Laboratory, Argonne, IL, April 1978 (invited) (L. L. Kazmerski).
6. "Fabrication and Characterization of ITO/CuInSe<sub>2</sub> Photovoltaic Heterojunctions," Presented at 13th IEEE Photovoltaic Spec. Conf., Washington, D.C., June 5-7, 1978, (P. Sheldon and L. L. Kazmerski).
7. "The Performance of Cu-Ternary Based Thin-Film Solar Cells," Presented at the 13th IEEE Photovoltaics Spec Conf., Washington, D.C., June 5-7, 1978, (P. J. Ireland and L. L. Kazmerski).
8. "Interdiffusion and Interface Problems Relating to Thin-Film Photovoltaic Devices," Presented at NBS Workshop on Stability of Thin-Film Solar Cells and Materials, Gaithersburg, MD, May 1-3, 1978, (invited) (L. L. Kazmerski).
9. "Stability of Ternary Chalcopyrite Photovoltaic Devices," Presented at NBS Workshop on Stability of Thin-Film Solar Cells and Materials, Gaithersburg, MD, May 1-3, 1978, (invited) (L. L. Kazmerski).

10. The Effects of Grain Boundary and Interface Recombination on the Performance of Thin-Film Solar Cells," Presented at International Conf. on Recombination in Semiconductors, Southampton, UK, Aug.30 to Sept. 1, 1978, (L. L. Kazmerski).
11. "Grain Boundary and Inter-Diffusion Studies in Compound Semiconductors Thin Films and Devices," Presented at 4th Int. Thin Films Congress, Loughborough, UK, Sept. 11-15, 1978, (L. L. Kazmerski).
12. "Effects of Grain Boundaries on the Performance of Thin-Film Photovoltaic Devices," Presented at 4th Int. Thin Films Congress, Loughborough, UK, Sept. 11-15, 1978, (L. L. Kazmerski, P. J. Ireland and P. Sheldon).
13. "AES and SIMS Applications to Device Interface Investigations" (Tutorial), Presented at AVS Special Surface Analysis Regional Meeting, Denver, CO, Oct. 6, 1978, (L. L. Kazmerski).
14. "Relationships Between Grain Boundary and Interface Recombination at the Performance of Thin-Film Solar Cells," Presented at Annual AVS Symposium, San Francisco, CA, Nov. 1978, (L. L. Kazmerski, P. J. Ireland and P. Sheldon).
15. "Growth of  $\text{CuInSe}_2$  Film Using Molecular Beam Epitaxy," Presented at Annual AVS Symposium, San Francisco, CA, Nov. 1978.
16. "Overview of Photovoltaic Research," Material Science Conference, Argonne National Laboratory, June 1, 1978, (invited) (L. L. Kazmerski).
17. "Directionally Solidified Solar Grade Silicon Using Carbon Crucibles," Fourth American Conf. on Crystal Growth, NBS, Gaithersburg, MD, July 17-19, 1978, (T. Ciszek).
18. "Rate Studies in Chemical Vapor Transport Crystal Growth," Fourth American Conference on Crystal Growth, Washington, D.C., July 16-19, 1978, (J. Olsen).
19. "Photovoltaics Research," Physics Department, Colorado School of Mines, Golden, April 10, 1978; Electrochemical Society Rocky Mountain Chapter, Denver, April 27, 1978, (S. Wagner).
20. "Heterodiodes Solar Cells," Electrical Engineering Department, University of Colorado, Boulder, May 2, 1978, (S. Wagner).
21. "Stable Room Temperature Light Emission from Metal-Lusulator - Metal-Junctions," Electrochemical Society Spring Meeting, Seattle, May 23, 1978, (S. Wagner).



22. "Electrochromism in Ni-Doped  $\text{SrTiO}_3$ ," Electrochemical Society Spring Meeting, Seattle, May 20, 1978, (S. Wagner).
23. "EMF Measurements on  $\text{Li}_x/\text{WO}_3$  Electrochromic Cells," Electronic Materials Conf., Santa Barbara, June 29, 1978, (S. Wagner).

THIS PAGE INTENTIONALLY LEFT BLANK

APPENDIX A  
PHOTOVOLTAIC STAFF SUMMARY -FY78

---

<u>Name/Title</u>	<u>Area</u>	<u>Starting Date</u>
1. Sigurd Wagner Branch Chief	Heterodiodes	February, 1978
2. Lawrence L. Kazmerski Senior Scientist	Surfaces and Interfaces	September, 1977
3. Ted F. Ciszek Senior Scientist	Silicon Crystallization and Growth	May, 1978
4. Jerry M. Olson Senior Scientist	Silicon Purification	June 1978
5. Ralph C. Kerns Staff Scientist	Amorphous Materials	July 1978
6. Alex Zunger Senior Scientist	Semiconductor and Device Theory	September, 1978
7. Philip J. Ireland Associate Scientist	Surfaces and Interfaces	May 1978
8. Stephen J. Hogan Associate Scientist	Thick Film Technology; National Measurements Facility	June 1978
9. Jeffery L. Hurd Associate Scientist	Silicon Crystallization and Growth	September, 1978
10. Neil W. Meyer Associate Scientist	Silicon Purification	August, 1978
11. Peter Sheldon Research Associate (Coop)	Surfaces and Interfaces	June 1978
12. David Burleigh Research Associate	Multicrystalline Silicon Characterization Ellipsometry	May 1978
13. Frank S. Barnes Consultant	Measurement Development	June 1978

---

THIS PAGE INTENTIONALLY LEFT BLANK

APPENDIX B  
FY78 CONTRACTED FACILITIES/RESEARCH

---

Experiment/Project	SERI STAFF in Charge	University Staff
Assembly of crystal growth apparatus	T.F. Ciszek	Colorado School of Mines
Preliminary crystal growth heat source	T.F. Ciszek	Colorado School of Mines
Silicon characterization (part of Research Services agreement)	T.F. Ciszek	Colorado School of Mines
SEM, TEM, X-ray analysis of polycrystalline thin-film GaAs	L.L. Kazmerski	Denver Research Institute
Fabrication and characterization of Schottky barrier test diodes on polycrystalline silicon	J.M. Olson	University of Colorado
Electrical characterization of thin semiconductor films	S. Hogan	University of Colorado
Generation of pure and doped amorphous silicon thin films, investigations of their characteristics, and fabrication of devices from the film	R. Kerns	University of Colorado
Molecular beam epitaxy of ternary semiconductors	L.L. Kazmerski	University of Maine
Computer facility	A. Zunger	University of California at Berkeley

---

THIS PAGE INTENTIONALLY LEFT BLANK

## DISTRIBUTION LIST

<u>No. of Copies</u>	<u>Distribution</u>
1	Department of Energy DOE, SERI Site Office Contracting Officer Attn: C. M. Skinner
1	Chicago Operations Office Interim Program Division Attn: M. E. Jackson
1	Division of Solar Technology Office of Asst. Director for Administration Attn: R. H. Annan
2	Office of Asst. Secretary for Conservation & Solar Applications Attn: R. Scott
1	Office of Solar, Geothermal, Electric & Storage Programs Attn: H. H. Marvin
2	Division of Energy Technology Administration Attn: S. Hansen
1	Division of Distributed Solar Technology Office of the Director Attn: R. San Martin
1	Division of Central Solar Technology Office of the Director Attn: H. Coleman
1	Division of Energy Storage Systems Office of the Director Attn: G. Pezdirtz
1	Division of Planning & Energy Transfer Office of the Director Attn: M. Adams